2009

VISIBLE WAVELENGTH MALDI STUDY

Chunyan Yang
Western University

VISIBLE WAVELENGTH MALDI STUDY

(Thesis format: Monograph)

By

Chunyan Yang

Graduate Program in Chemistry

A thesis submitted in partial fulfillment
of the requirements for the degree of
Master of Science

SGPS
The University of Western Ontario
London, Ontario, Canada

THE UNIVERSITY OF WESTERN ONTARIO
SCHOOL OF GRADUATE AND POSTDOCTORAL STUDIES

CERTIFICATE OF EXAMINATION

Supervisor	Examiners
Dr. Robert H. Lipson	
Supervisory Committee	Dr. David M. Wardlaw
Dr. John F. Corrigan	Dr. Lars Konermann
Dr. J. Peter Guthrie	Dr. Gilles Lajoie

The thesis by

Chunyan Yang

entitled:

Exploring Visible Wavelength MALDI Study
is accepted in partial fulfillment of the
requirements for the degree of
Master of Science

Date_____

_____
Chair of the Thesis Examination Board

Abstract

Since its inception over two decades ago matrix-assisted laser/desorption ionization (MALDI) mass spectrometry (MS) using either ultraviolet (UV) or infrared (IR) lasers, has become an important tool for the analysis of molecules of chemical and biological interest. Primarily, this is because MALDI-MS is a relatively "soft" methodology which allows the ionization and detection of intact analytes with minimal fragmentation. Although MALDI mass spectrometry using visible wavelength lasers has been less studied it is expected to have several advantages over UV-MALDI and IR-MALDI. Many macromolecules of interest absorb UV-light but are transparent at visible wavelengths. In principle, visible-MALDI should be softer than UV-MALDI. Like UV-MALDI, visible-MALDI is also expected to require lower pulse energies than IR-MALDI. Furthermore, readily available pulsed visible laser sources such as the solid-state frequency-doubled Nd:YAG laser (532 nm output) are becoming relatively inexpensive and have longer operational lifetimes compared to standard UV devices.

This thesis describes an exploration of possible organic molecules that can absorb 532 nm laser light and serve as matrices. Two classes of compounds considered: pyrromethene and Rhodamine laser dyes. The experiments carried out established that the Rhodamine (R) 610 laser dye is relatively stable; that is, it exhibits minimal fragmentation under 532 nm laser irradiation, and can ionize a selection of analytes. The chloride salt of R610 yielded the cleanest spectra making it a particularly good MALDI matrix candidate for detecting small molecular weight analytes.

R575, a neutral laser dye, was found to be an effective absorber in binary matrices. Analyte ionization was achieved by combining this specific laser dye with

either a proton donor (HCl or CHCA), proton acceptor (NaOH), or alkali donor (NaTFA). A detection sensitivity as low as ~12 femtomole was determined using R575 as a component of an acidic or basic binary matrix.

Key words: Visible Matrix-assisted Laser Desorption/Ionization (Visible MALDI), mass spectrometer (MS), 532nm laser, laser dyes.

To my mother, Shuhong Gao, my husband, Xueyuan Zhang, and my whole family

ACKNOWLEDGEMENTS

I would first like to extend my sincere thanks to my supervisor, Professor Robert Lipson, for his guidance, support, encourage and assistance throughout my graduate studies at the University of Western Ontario. I would also like to express my thanks to Dr. Xiaokun Hu for his invaluable help and interesting discussions during the course of this work. Thanks are also extended to Alexander Loboda of MDS-Analytical Technologies for his long-term support to this project. In addition I'd like to thank my members: Weiping Shi, Cheng Lu, Jin Li, Stamen Dimov for their friendship and help that inspired me to work hard. Finally, I would like to extend my warmest thanks to all who have contributed to this thesis and to all those who have assisted me during these study years, such as Prof. Corrigan, Prof. Workentin and his group, the manager of undergraduate laboratories, Ron Maslen and his coworkers, and especially Prof. Konermann who is my instructor of graduate course, Mass Spectrometry.

This work was supported by the Natural Sciences and Engineering Research Council of Canada (NSERC), the Ontario Center of Excellences (OCE), and the University of Western Ontario.

Finally, I am grateful for endless support and love from my family, especially my mother and my husband.

TABLE OF CONTENTS

List of Figures

Chapter 1: Theoretical Background

1.1. Overview

Mass spectrometry (MS) measures the mass-to-charge ratio of ions. This information has made this technique an extremely important analytical method. MS is characterized by high sensitivity, low detection limits and has found application in many diverse fields and for many analytes. It is most generally used to identify unknown compounds by their mass or by the mass of any species that are generated from the parent molecule by fragmentation. All mass spectrometers consist of three basic parts: an ion source, a mass analyzer, and a detection system. Neutral analytes are first ionized in an ion source, which differs depending on the type of instrument used. The generated ions are then transferred into a mass analyzer. Mass analyzers separate the ions according to their mass-to-charge ratios. The ion beam is subsequently monitored by a detector which transforms the ion signal into an electrical signal that can be recorded (see Figure 1.1)

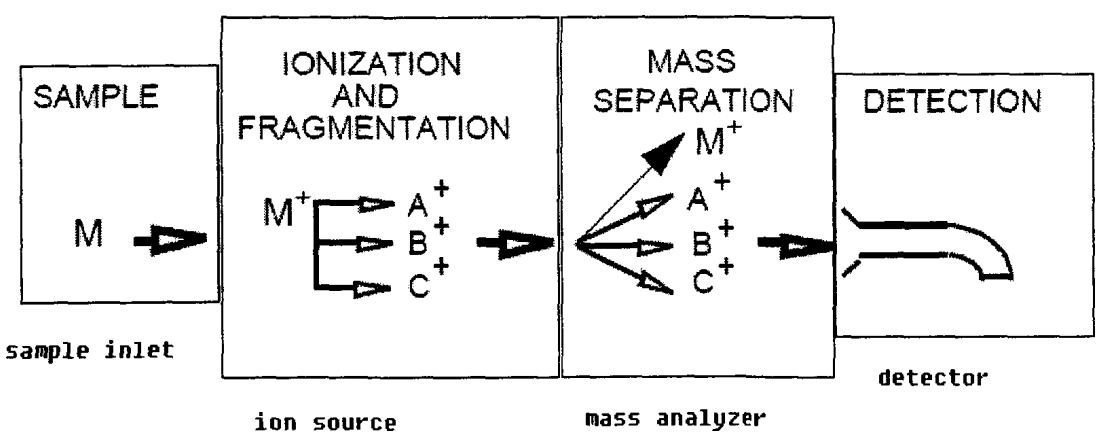

Figure 1.1: Basic block diagram of a mass spectrometer and the function of each component. M is the neutral molecule (analyte) while M^+, A^+, B^+, and C^+ are the parent and possible fragment ions.

Many different ionization techniques have been developed to meet different requirements. Loosely speaking they can be classified as either traditional or soft ionization schemes. Traditional ionization techniques such as electron ionization (EI) or chemical ionization (CI) involve evaporating analytes before they are ionized. For example, in EI, a beam of high kinetic energy electrons collides with the gas-phase molecules to produce ions. In CI, a beam of charged reagent gas molecules (ions) produced by EI react with neutral gas phase analyte molecules to form ions that can be detected. Both methods usually lead to extensive fragmentation because they involve collisions, although CI is softer than EI in this regard. In both cases the parent ion may not necessarily be the dominant ion peak in the mass spectra. These methods are also only suitable for small molecules since the analyte must be in the gas phase. This excludes non-volatile and/or fragile macro- or biomolecules where heating easily pyrolyzes the sample, leading to extensive fragmentation and extremely complicated mass spectra.

A breakthrough emerged ~ 20 years ago with the development of Matrix-Assisted Laser Desorption/Ionization (MALDI) MS and Electrospary Ionization (ESI), as soft ionization techniques. Soft ionization methods are able to generate molecular ions with minimal fragmentation. In 2002, Tanaka[1] and Fenn [2] were awarded Nobel Prize for the development of these techniques.

MALDI MS has two outstanding features. First, it is a laser-based soft ionization technique, and second, its ion source for solid sample makes it particularly amenable for macromolecules such as peptides, proteins, oligonucleotides, carbohydrates, natural products and lipids, and for synthetic polymers. Unlike EI and CI, MALDI produces few

fragments. Typically, the dominant peak is either the protonated (cationic) form or deprotonated (anionic) form of the parent neutral. Therefore, MALDI MS has emerged as the analytical tool of choice for the detection of fragile proteins and synthetic macromolecules. It should be noted that in this very first "MALDI" study ultrafine cobalt powder was used as the "matrix" [1]. Nowadays, however, organic matrix compounds are nearly exclusively used. The latter approach was developed by Franz Hillenkamp and Michael Karas in Germany in 1988 [3].

1.2. MALDI Mass Spectrometry

1.2.1. Overview

MALDI MS analysis is achieved in two steps. The first is sample preparation, and the second is laser desorption and ionization. In the first step, a solid solution of analyte-doped matrix crystals is produced. The second step involves ablation of this solid solution by an intense pulsed laser for a short duration. The irradiation by the laser causes the crystals to rapidly heat by absorption in the condensed phase through photoexcitation of the matrix molecules. The rapid heating causes the matrix molecules to sublime and expand into the gas phase, entraining intact analyte in the process. Ionization reactions can occur at any time during this expansion but the origin of ions produced in MALDI is still not fully understood[4].

1.2.2. Sample Preparation

Sample preparation is often considered to be the most important step in MALDI[5, 6, 7]. The quality of the sample preparation has a direct impact on the quality of MALDI

mass spectra because ion production by MALDI depends on the generation of a suitable solid solution containing a mixture of matrix and analyte compounds. The compound to be analyzed is first dissolved in a solvent containing a high concentration of an organic species, hereafter called the matrix, which has a strong absorption at the wavelength of the laser used in the MALDI process. The mixture is dried on a sample tip before analysis and any liquid solvents used in preparation of the solution are removed by evaporation. The result is a solid deposit of analyte-doped matrix crystals, where the analyte molecules are separated from one another by dilution within the matrix. A schematic of a sample preparation is shown in Fig. 1.2.

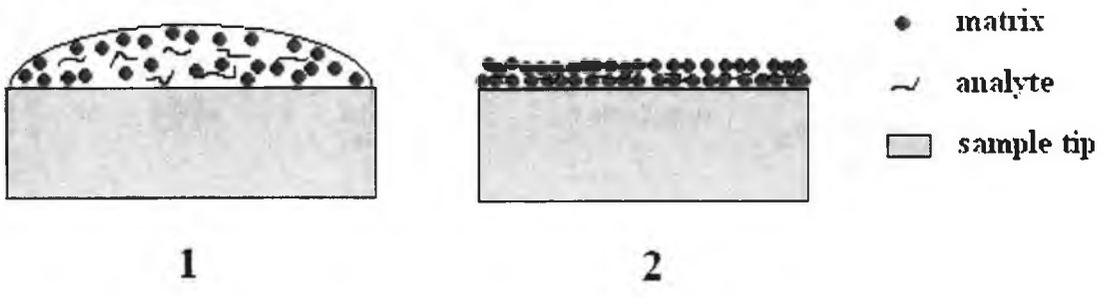

Figure 1.2: A schematic diagram showing the steps involved in MALDI sample preparation. 1) A liquid drop containing matrix compound and analyte sitting on the sample tip. 2) A dried sample on the sample tip after the solvent has been removed by evaporation.

The oldest and most widely used sample preparation method in MALDI is called the Dried-Droplet method[8]. In this procedure, a drop of the mixed matrix and analyte solution is placed onto the sample probe, dried, and then introduced into the mass spectrometer for analysis. This method tolerates the presence of salts and buffers very

well, and is a good choice for samples containing more than one protein or peptide component. Nevertheless, this approach has some disadvantages. First, the matrix and analyte solutions need to be miscible with each other. Second, the solid samples produced in this way often contain many "sweet spots" where MALDI signal intensities are large; namely, the samples made using this method are not homogenous, making the results less reproducible. Despite those disadvantages, it is still widely used due to its simplicity.

1.2.3. Desorption and Ionization Mechanism for MALDI MS

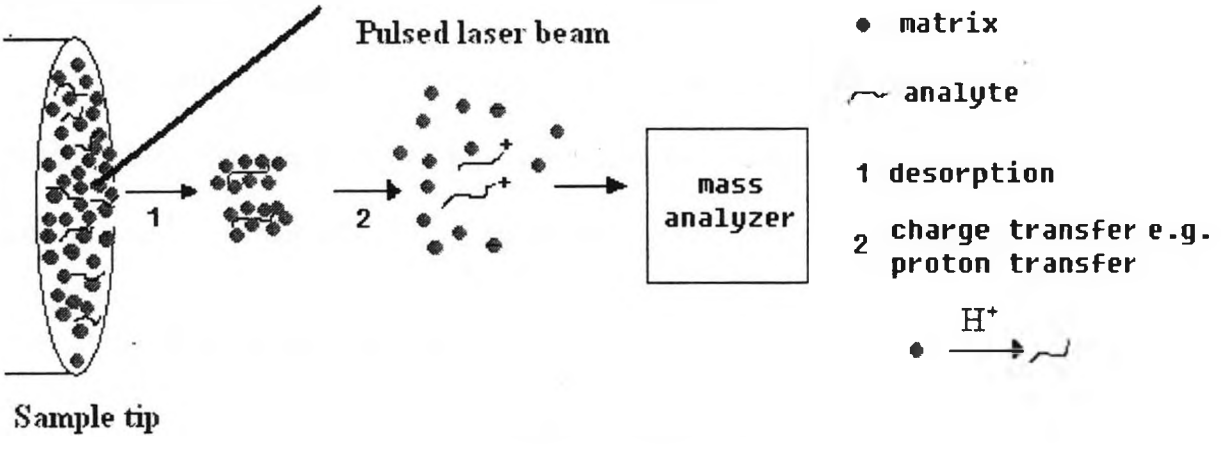

Figure 1.3: A schematic of MALDI desorption and ionization.

1.2.3.1. Desorption process

Analyte desorption is initiated using laser pulses that are focused onto the sample surface at a fixed repetition rate. Although the actual mechanism leading to analyte ionization remains controversial it is generally accepted that the role of the matrix compound is to absorb the laser light which leads to a rapid rise in the local temperature of the sample. When the local temperature exceeds the sublimation temperature of the

matrix, the solid sample desorbs explosively into the gas phase as a plume which entrains the analyte within. Strictly speaking, the process of desorption includes the excitation of the matrix, the subsequent phase change from solid to gas, and the dynamics of the material plume expansion. The desorption step will not induce significant analyte fragmentation, provided the analyte does not absorb the incident laser light. The composition of the expanding plume includes monomers, clusters and fragments of the matrix all surrounding single analyte molecules. In a more comprehensive picture, the presence of alkali ions, protons and electrons may also have an impact on the chemistry taking place in the plume.

Ionization reactions can occur at any time during the plume expansion but as noted above, the origin of the ions generated by the MALDI process is still not fully understood [4]. A schematic of MALDI desorption and ionization is shown in Fig.1.3.

1.2.3.2. MALDI plume imaging

The processes of desorption and of matrix and analyte ionization are closely related to each other in MALDI. Leisner *et al.* [9]studied a MALDI plume. The plume was generated using an Er:YAG (doped ion: Erbium and host material: Yttrium aluminium garnet) infrared (IR) laser with an ~ 100 nsec pulse duration and an Optical Parametric Oscillator (OPO) having a 2.94 μm output of 6 ns pulses. A liquid matrix of glycerol was used instead of solid samples for better sample homogeneity and reproducible plume formation.

Figure 1.4 Figure 1.5 Figure 1.6

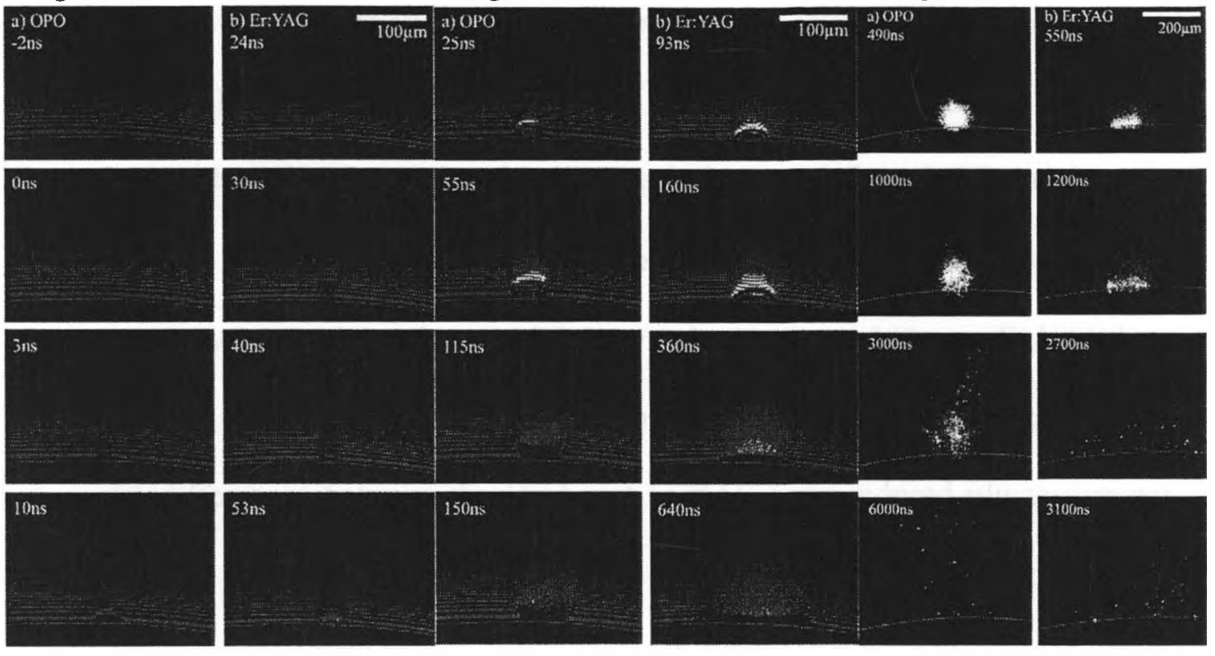

Figure 1.4: The initial phase of the plume expansion (from ref.9)

Figure 1.5: Intermediate phase of the plume expansion (from ref.9)

Figure 1.6: The late phase of the plume expansion (from ref.9)

The initial, intermediate and later phases of the plume development are shown in Figs. 1.4, 1.5 and 1.6, respectively. Initially there appears to be little difference between the plumes generated by the 6 and ~100 ns IR pulses (Fig. 1.4). Upon closer inspection at intermediate times, the plume generated by the Er:YAG laser plume exhibits a forward moving cloud of material about the size of the laser focus with a pronounced radial density gradient compared to that obtained using the OPO (Fig. 1.5). At later times both lasers were scattered from distinct particles in the plume and/or the products of their disintegrations (Fig.1.6). This process however was detected earlier when using Er:YAG irradiation.

The difference in the plume dynamics for the two lasers was attributed to energy confinement. Menzel *et al* [10, 11] determined that formation of ions took place ~ 300 ns after Er: YAG laser irradiation even when the pulse durations were 6, 100 and 185 nsec, respectively. They also found that this time scale is shorter than that found for material ejection (~100 μs). In addition, identical mass spectra of typical peptides and proteins were obtained whether using 6 nsec OPO laser pulses and or a 100 nsec Er:YAG laser. It was concluded therefore, that ion generation occurs early on in the plume evolution where the differences between the OPO and Er:YAG laser-induced plumes are not yet pronounced.

Similar experiments were carried out on a nitrobenzyl alcohol liquid matrix using a UV laser operating at 266 nm[11]. The results from UV-MALDI are similar as those obtained by IR-MALDI, except that the time course of material ejection is shorter compared to the IR-MALDI, because the IR laser photons penetrate deeper into the sample.

It is believed that even though these imaging experiments were conducted on liquid samples, they still reflect the situation for crystalline solid samples[11].

1.2.3.3. Ionization

The mechanisms which lead to the formation of matrix and analyte ions in the MALDI process are even less well understood than the desorption process. Two major models have been developed to explain UV-MALDI ionization: the energy pooling model[12, 13] and the cluster model or "lucky survivor" model[14]. Although both models invoke a two-step framework, their first steps are quite different.

(1) Energy pooling model

In this model [4, 12, 13, 15] the first primary ionization step (matrix ion generation) takes place during or shortly after laser desorption. Secondary ionization reactions, that is, ion-molecule reactions then occur in the ensuing plume. The separation of primary and secondary ion generation takes into account the different time scales involved. The time scale for the deposition of laser energy into the matrix is short, on the order of the laser pulse duration; typically < 10 nsec if using the 337 nm UV output of a N_2 laser or the 355 nm of a frequency-tripled Nd:YAG laser. Conversely, the time required for the plume to expand from its initial high density small volume gaseous state to a collision-free low density plume is much longer, on the order of microseconds [16]. Secondary ion-molecule reactions will take place as long as there are collisions. Most importantly, the gas-phase matrix molecules become electronically excited which enhances the cross section of the secondary reactions. A schematic illustration of the time scales in MALDI is shown in Fig.1.7 [4]

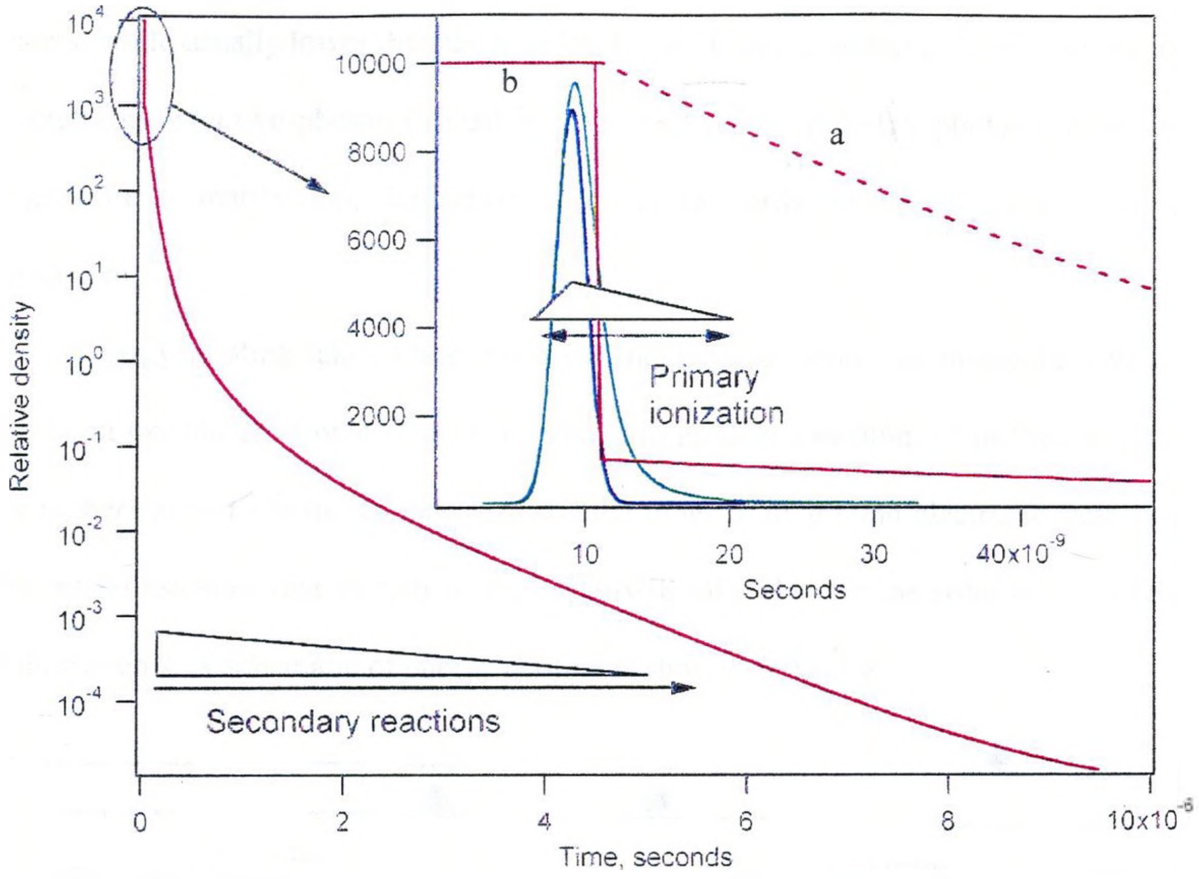

Figure 1.7: The red curve is a plot of the relative density of the MALDI plume to that of a gas at 1atm, as a function of time. The blue curve in the inset represents the time profile of a typical UV laser pulse, while the green curve shows the evolution of the matrix excited state population as a function of time. The dashed line (a) is the time profile for the plume expansion while the full line (b) is the time profile for desorption. (from ref.4)

Primary ionization:

There is general agreement that a UV-MALDI matrix absorbs UV-light efficiently. It is also highly probable that the high intensity of the laser beam used in MALDI can cause the matrix to undergo a two-photon absorption. A two-photon absorption corresponds to the process where two photons are simultaneously absorbed by a ground state matrix molecule in S_0 (subject to quantum mechanical selection rules) to an excited state S_1. Typically, two-photon absorption using a N_2 laser (7.4 eV) or a Nd:YAG laser (7 eV) will not directly ionize a free matrix molecule[17, 18] since the

ionization potentials (IPs) of nearly all MALDI matrices lie > 9 eV. The IPs of matrix clusters, while usually lower than those of the isolated matrix molecule[15], are also usually too high for direct two-photon ionization [17]. Generally, 3 or more UV photons are needed to generate a matrix ion. Ionization is therefore attributed to an energy pooling mechanism.

Energy pooling takes place when two neighboring atoms or molecular entities, both in an excited electronic state (S_1), interact to produce one atom or molecular entity in a higher excited electronic state (S_n) and the other in its ground electronic state (S_0). This model assumes that monomer ionization will take place in the solid by sequential pooling events. A schematic of energy pooling is shown in Fig. 1.8.

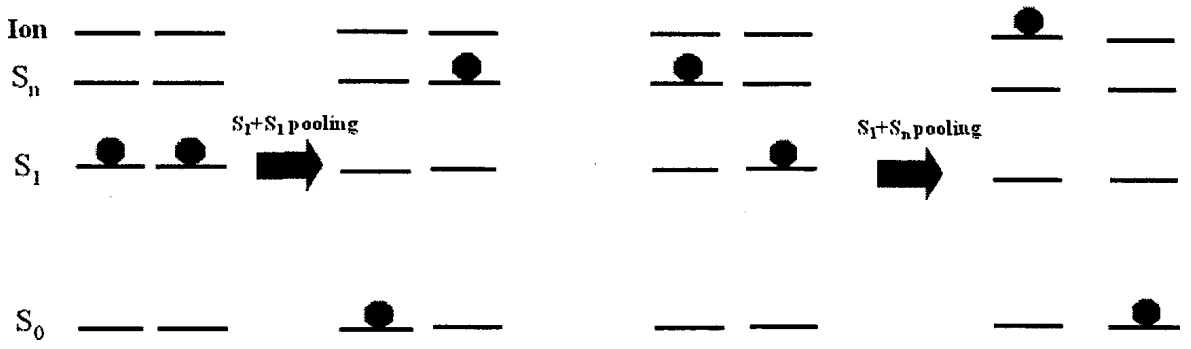

Figure 1.8: A schematic showing the mechanism of energy pooling. An S_1+S_1 pooling event is not expected to generate ions, but S_1+S_n pooling is energetically sufficient for primary ionization.

This model neglects S_n+S_n pooling as a means of generating ions because S_n populations are expected to be very small. Evidence exists in the literature for S_1+S_1[19], and S_1+S_n pooling[20].

In summary, the mechanism of primary ion generation by S_1+S_1 pooling and S_1+S_n pooling can be respectively expressed by reactions (1) and (2):

$$(1) M^*(S_1) + M^*(S_1) \rightarrow M(S_0) + M^{**}(S_n)$$
$$(2) M^{**}(S_n) + M^*(S_1) \rightarrow M^{+\bullet}(ion) + M(S_0)$$

Analyte ions are created in the expanding plume via secondary reactions involving the matrix and the analyte. Typical ionization reactions include proton transfer, electron transfer, and cation transfer. Several types of matrix ions are expected to be present in the plume including $[M+H]^+$, $[M-H]^-$ and $[M+Na]^+$ which are generated after the $M^{+\cdot}$ primary ions are formed.

Secondary reaction:

Denoting the analyte as A, the dominant secondary reactions can be written as:

1. Proton transfer reactions: $MH^+ + A \rightleftharpoons M + AH^+$ and $[M-H]^- + A \rightleftharpoons M + [A-H]^-$

2. Electron transfer reactions: $M^{+\cdot} + A \rightleftharpoons M + A^{+\cdot}$ and $M^{-\cdot} + A \rightleftharpoons M + A^{-\cdot}$

3. Cation transfer: reactions such as $MNa^+ + A \rightleftharpoons M + ANa^+$

The importance of secondary reactions was proven by the observation of a Matrix Suppression Effect (MSE) [21] where the matrix ion signals were completely suppressed through these reactions provided enough analyte was present in a MALDI sample (Fig.1.9).

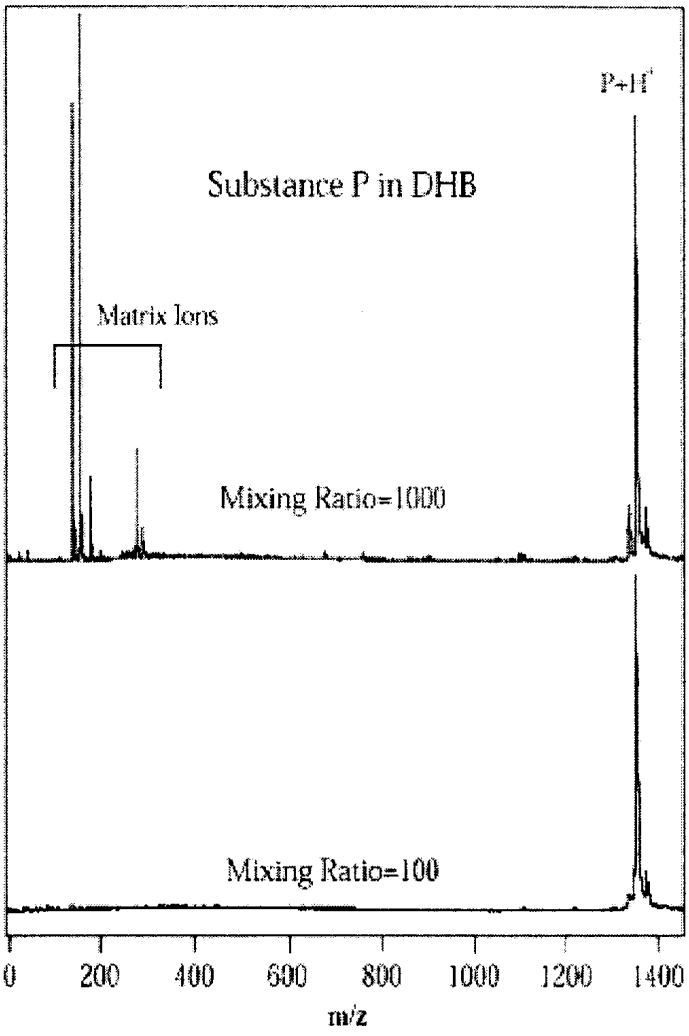

Figure 1.9: Matrix Suppression Effect in the UV-MALDI spectra of a peptide P in the matrix 2,5-dihydroxybenzoic acid (DHB). At a higher analyte concentration (mixing ratio; that is, the matrix to analyze mole ratio = 100), all the low-mass matrix signals have been suppressed through secondary reactions with the analyte (from ref. 21).

One characteristic of MALDI MS is that the spectra are dominated by singly charged species. In the energy pooling model highly charged small to medium sized ions formed in secondary ionization reactions can always be reduced to the +1 state by reaction with the neutral matrix. However, as the analyte becomes larger, the charges can

be sufficiently separated and behave more or less independently. In these cases, multiply charged ions can be detected in MALDI [13].

(2) Cluster or "lucky survivor" model

In this model[14] photoionization of individual gas-phase matrix neutrals is considered to be very unlikely because it requires more than two photons. However, it is assumed that energy pooling will take place more easily in a matrix cluster composed of a high number of excited molecules. Therefore, in the cluster model, the analyte ions and some matrix ions are considered to be largely preformed in the solid solution, and the matrix molecules are mainly viewed as a desorption vehicle. During laser irradiation, desorption takes place due to strong photoabsorption by the matrix molecules. Preformed ions surrounded by matrix molecules are desorbed as clusters from the initial solid material. In the plume, the initial singly and multiply charged analyte ions can be liberated from clusters through desolvation of matrix molecules. On the other hand, if the gas–phase analyte is neutral, charges may be transferred to the analyte via secondary reactions, such as proton and cation transfer, etc.

As noted above, experimental results indicate that singly charged ions are the majority species in the plume. In the cluster model, multiply charged ions in the plume generated by UV-MALDI are believed to undergo extensive neutralization mostly by electrons stemming from matrix photoionization resulting from energy pooling in the matrix clusters. In IR-MALDI, strong material ablation is thought to result in low-charge states and neutral clusters. The singly charged ions that are detected can then be viewed as "lucky survivors". A sketch of cluster model is shown in Fig. 1.10.

The main direct evidence for this mechanism was the preparation of MALDI samples with pH sensor dyes as analytes, from solutions of different pH. The color change of those pH sensor dyes in dried sample directly indicated their (de) protonation state. There the MALDI signal intensities changed with differing pH sensor analytes[22].

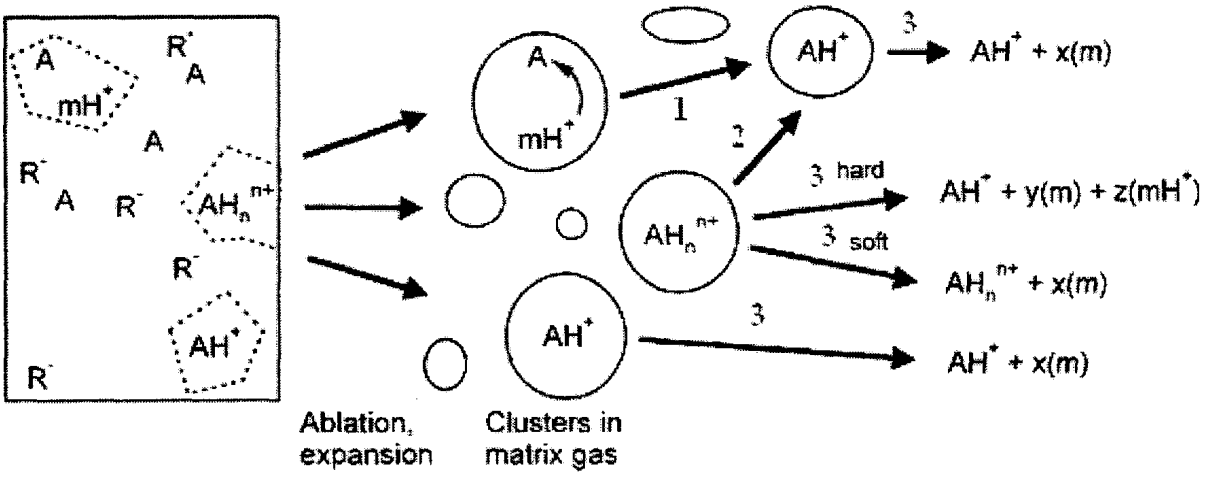

Figure 1.10: Sketch of the major processes proposed in the cluster model of MALDI ionization (modified from ref. 4). m = matrix, A = analyte, R^- = generic counter ion. AHn^{n+} and AH^+ stand for preformed ions. 1. Intra-cluster charge transfer from the matrix to the analyte; 2. Electron neutralization; 3. Desolvation through which excited clusters containing excess energy absorbed by the matrix in solid phase, "evaporate" surrounding matrix molecules into gas phase; clusters having less/more excess energy undergo soft/hard desolvation.

(3) A comparison of the models

In summary, the primary matrix ions formed in the energy pooling model are believed to be created by laser photoionization, while in the cluster model the initial ions including analyte and matrix ions are liberated upon laser irradiation. While both models agree that secondary ion-molecule reactions take place, this is believed to be the main mechanism of analyte ionization in the energy pooling scheme. In other words, the energy pooling model assumes that nearly all the analyte ions are created by ion-

molecule secondary reactions, even if a few preformed analyte ions exist initially in the solid matrix.

Conversely, the cluster model accepts that some neutral analyte molecules may be ionized by secondary ion-molecule reactions, but this is not the only ionization pathway. Instead, a large number of analyte ions are already preformed in the solid matrix. Therefore the main on-going debate concerns the origin of the the majority of analyte ions. Although the MALDI mechanism remains controversial, these two major models have formed the foundation of many fundamental studies probing this question. Regardless of how analyte ions are formed, the ratio of ions to neutrals in the MALDI plume is very low, between 10^{-4} and 10^{-7} [23]. Fortunately, MS is very sensitive and so MALDI MS has become a standard analysis technique in many fields including chemistry, biochemistry, and the pharmaceutical industry. MALDI mass spectrometer sales are in the muti-million dollar range per year.

1.2.4. Conventional laser wavelengths and matrices used in MALDI MS

1.2.4.1. Lasers

A variety of gas and solid-state lasers have been successfully used for MALDI-MS. Pulsed lasers for MALDI are essential because the energy necessary for desorption and ionization must be transferred to the matrix in a time shorter than that required for thermal diffusion. The method is called UV-MALDI or IR-MALDI if an ultraviolet (UV) laser or infrared (IR) laser is used, respectively. The most common UV laser used for MALDI is the N_2 laser having an output at λ = 337 nm. Frequency tripled and quadrupled Nd: YAG lasers (λ = 355 nm or 266 nm, respectively) have also been used.

Er: YAG (λ = 2,940 nm) and CO_2 (λ = 10,600 nm) are the most common lasers used for IR-MALDI.

Interestingly, the MALDI mass spectra obtained using UV and IR lasers are essentially identical[14, 24, 25], even though the former involves exciting electronic transitions while the latter pumps vibrational modes of the matrix. This has prompted many to suggest that the final ions detected in both cases arise from common secondary ion-molecule reactions.

IR-MALDI has been shown to generate less fragment ions than UV-MALDI in the analysis of fragile biological macromolecules such as DNA and RNA[26], because the energy of an IR photon is much smaller than that of a UV photon. Consequently, IR-MALDI is generally regarded as a softer desorption method. Since IR excitation excites vibrational motions, IR-MALDI can apply a wider array of possible matrix compounds, including liquids. Liquid matrices are attractive because they can mimic the physiological environment of a bio-analyte. Moreover, liquid matrices can be exhibit better sample homogeneity and yield more reproducible results, even though they are less sensitive than solid matrices[27]. On the other hand IR-MALDI is not as sensitive as UV-MALDI, although the ions it generates are a bit "cooler"; that is, they have lower internal energies.

UV-MALDI setups are more common than those working with IR sources because they are easier to operate and the UV lasers are relatively cheaper.

1.2.4.2. Matrices

MALDI matrices can be divided into two groups; those which are effective for UV-MALDI and the others which readily absorb light from the common IR lasers. Currently most UV-MALDI matrices are chosen from a relatively small number of

established compounds such as benzoic or cinnamic acid derivatives. An example of the former is 2,5-Dihydroxybenzoic acid (DHB)[28], and of the latter, 3-methoxy-4-hydroxycinnamic acid, 3,5-dimethoxy-4-hydroxycinnamic acid (sinapic acid)[29], and α-cyano-4-hydroxycinnamic acid (CHCA)[30]. The feature in common with these compounds is that each one has an aromatic ring.

Compounds such as urea, carboxylic acids, alcohols and even water have been used as IR matrices. One widely used IR-MALDI matrix is glycerol [26, 31].

In general, an effective matrix is believed to have some essential functions. First it must separate analyte molecules by dilution to prevent analyte aggregation during sample preparation. Second, the matrix must absorb the laser energy by either electronic excitation in UV-MALDI or by vibrational excitation in IR-MALDI. Third, matrix desorption must take place by rapid sublimation without fragmenting the embedded analyte molecules. Although the matrix must sublime rapidly upon laser irradiation, it should also sublime very slowly at room temperature and in the vacuum system without laser irradiation. Fourth, it is considered very important that matrix can serve as a proton donor or receptor to ionize the analyte. Lastly, the compound should be chemically inert to the analyte and solvent used during sample preparation.

Even if a compound meets all these requirements, there is no guarantee that it will be a good matrix, because it may not lead to effective MALDI ionization. For this reason most matrices must be empirically examined. Although numerous matrix candidates have been tested, only a few are commercially available.

1.2.5. Research goals of this thesis

Numerous MALDI studies using UV and IR lasers have been carried out since the MALDI was first developed in 1987 [3]. However, relatively few studies have been carried out using visible lasers (400 nm - 750 nm) and visible laser absorbing matrix molecules. MALDI MS using visible wavelength lasers is expected to have some advantages. For example, many macromolecules of interest have UV light absorbing chromophores but remain transparent at visible wavelengths. They would be expected to be more stable against fragmentation using visible-MALDI MS[32, 33]. Furthermore, coherent radiation in the green portion of the visible spectrum at 532 nm can be easily generated by frequency doubling the IR output of a Nd:YAG laser. Nd: YAG lasers are commercially available solid state devices which are relatively inexpensive, have intense outputs, and can be operated for many years, compared to the most common laser used in UV-MALDI: the N_2 gas laser.

Despite these potential advantages, visible-MALDI has not been extensively explored. Early studies were published on the potential of Rhodamine B, Rhodamine 6 G [33, 34], Neutral Red [35] and 2-amino-3-nitrophenol which were regularly used as UV-matrices [36] as possible matrices for visible MALDI. More recently, Au-assisted visible laser MALDI has emerged [37] as a new analysis technique. There, an analyte-doped UV-absorbing MALDI matrix was coated by a thin film of Au. It was found that after a few initial higher fluence laser shots, analyte and matrix-related ions could be created at even lower laser fluences. This suggested the photo-excitation and ionization of matrix molecules by the visible laser are probably assisted by the gold nanoparticles and nanostructures formed by the higher energy pulses. The key problem for visible-MALDI

is that good matrices that work using 532 nm sources have not yet been found. Our group studied visible-MALDI using Coumarin laser dyes as MALDI matrices using the 480 nm output of an optical parametric oscillator[38]. OPOs however are not considered to be convenient light sources because they are expensive.

Laser dyes (organic molecules used in dye laser operation) are natural candidates as visible-MALDI matrices because they absorb visible light with extremely high efficiency. They can also serve as a laser absorber in a binary matrix, where two molecular components fulfill different functions in the MALDI mechanism[34]. There are several commerically available laser dye families that cover the entire spectral region from UV to near-IR. The research in this thesis is focused on those dyes which can absorb radiation at 532 nm. To this end, several pyrromethene dyes and Rhodamine derivatives were studied for the first time to assess their viability as matrices for visible-MALDI.

Chapter 2: Experimental and Chemical details

2.1. Overview

After preparation, each sample was introduced into the MALDI quadrupole mass spectrometer (MS). The sample probe was rotated at an angular frequency of 0.05 revolutions per second. Consequently, because the laser beam focus was spatially fixed, a typical scan left an observable ablation ring on the sample surface. The area covered by the ablation ring could be measured and used to calculate the average amount of analyte consumed by the laser shots. Quantitative measurements were made by consuming all the sample material within the ablation ring. MALDI ions were generated using the 532 nm output of a frequency-doubled Nd: YAG laser, and detected after the triple quadrupole with a channeltron detector.

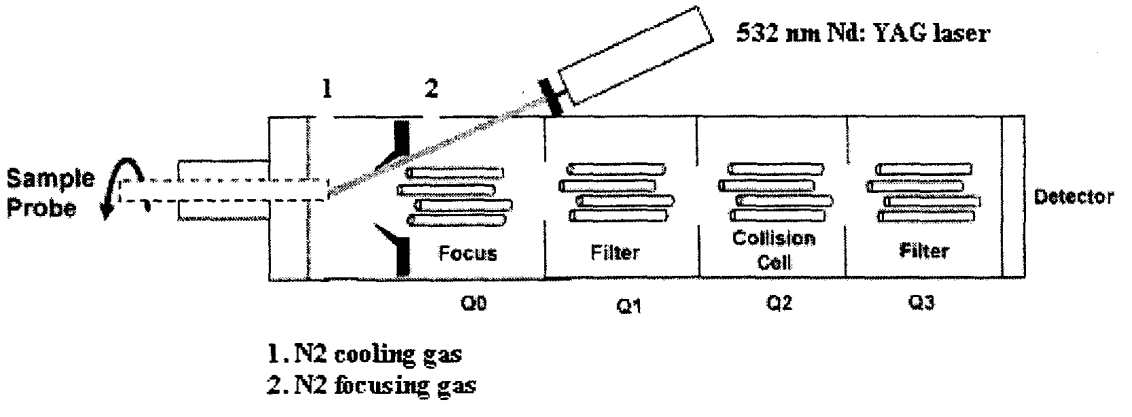

Figure 2.1: Schematic of the experimental apparatus used to obtain MALDI mass spectra

2.2. Experimental details

1. Sample preparation

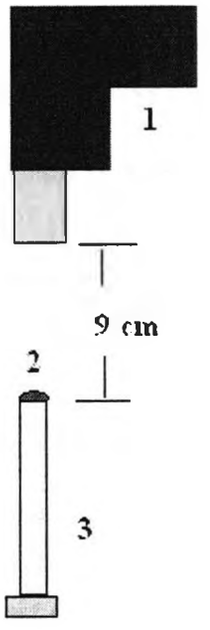

Figure 2.2: Sample preparation. 1. Hair dryer; 2. Liquid sample; 3. Sample probe

In this project, samples were prepared using the standard Dried Droplet method[39]. Matrix (the proton donor) and analyte solution were premixed in small plastic vials. The combined solution was then transferred onto a sample probe tip using a micropipette and quickly dried using heat from a hair dryer maintained at a fixed position over the sample probe

2. Mass Spectrometer

Briefly, the MALDI mass spectrometer was built by replacing the front end of an Applied Biosystems/MDS Sciex API-365 LC/MS/MS triple quadrupole (QqQ) mass spectrometer originally configured for electrospray ionization (ESI) with a home-made MALDI ion source. In this work, mass spectra were obtained by scanning the first quadrupole (Q_1) across the mass range of 30 to ~2200 Da, averaged over multiple laser shots. MALDI ions were detected with a channeltron electron multiplier (Burle Industries). The remaining quadrupoles: Q0, Q2 and Q3 served as ion bridges to transmit the ions through the mass analyzer Q1 and onto the detector. During these experiments,

the pressure of N_2 gas, set to 10 mTorr, was divided into two gas flows. One was introduced into the ion source to cool the ions, and the other into Q_0, to help focus the ions within the spectrometer. Empirically, analyte dimer peaks were found to increase in intensity with increasing N_2 gas pressure, while fragmentation peaks decreased. The optimum N_2 gas pressure had to be established independently for each analyte. Although the mass range of a quadrupole instrument is smaller than that of a time-of-flight (TOF) mass spectrometer, the former has the advantage of allowing only the ions of interest to be transmitted for detection, thereby limiting matrix signal interferences.

3. The visible laser operating at 532 nm

In this work a 532 nm laser operating at a 10 Hz repetition rate was generated by frequency doubling the output of a Q-switched Nd: YAG laser (Quanta-Ray GCR-4; λ = 1064 nm) in a potassium dideuterium phosphate (KDP) nonlinear crystal. The 532 nm laser beam was introduced into a 100 μm diameter optical fiber using a 5 cm focal length lens and directed towards the MALDI sample at the front end of the mass spectrometer. The radiation was focused onto the rotating sample surface of ~0.01 mm^2 by two parallel f =10 cm lenses. The typical laser intensity at the output of the optical fiber of ~17 uJ/s was controlled by a half-wave plate and polarizer combination, and measured with a power meter (Ophir Electronics, model NOVA).

2.3. Chemical details

2.3.1. Matrix candidates

There are several commerically available laser dye families that covering the entire spectral region from UV to near-IR. The research in this thesis is focused on those

dyes which can absorb radiation at 532 nm. Pyrromethene and Rhodamine laser dyes meet this requirement, and therefore were chosen for exploration as potential matrix candidates.

1. Pyrromethene 567 (PM 567)[40]

Chemical name: 1,3,5,7,8-pentamethyl-2,6-diethylpyrromethene-difluoroborate.

Chemical formula: $C_{18}H_{25}N_2BF_2$

Molecular weight: 318.22 amu.

$\lambda_{max}^{abs} = 518$ nm in ethanol and 516 nm in methanol

Chemical structure:

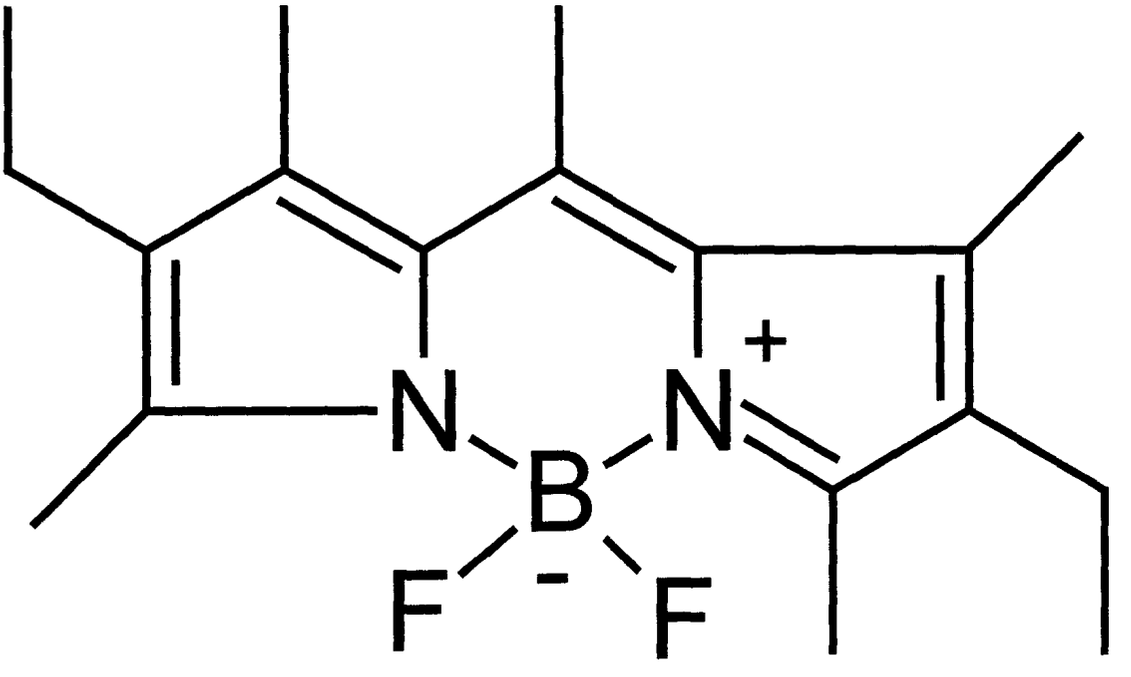

Figure 2.3: Chemical structure of PM 567

2. Pyrromethene 597 (PM 597) [41]

Chemical name: 1,3,5,7,8-pentamethyl-2,6-di-t-butylpyrromethene-difluoroborate.

Chemical formula: $C_{22}H_{33}N_2BF_2$

Molecular weight: 374.32 amu.

$\lambda_{max}^{abs} = 544$ nm in ethanol and 523 nm in methanol.

Chemical structure:

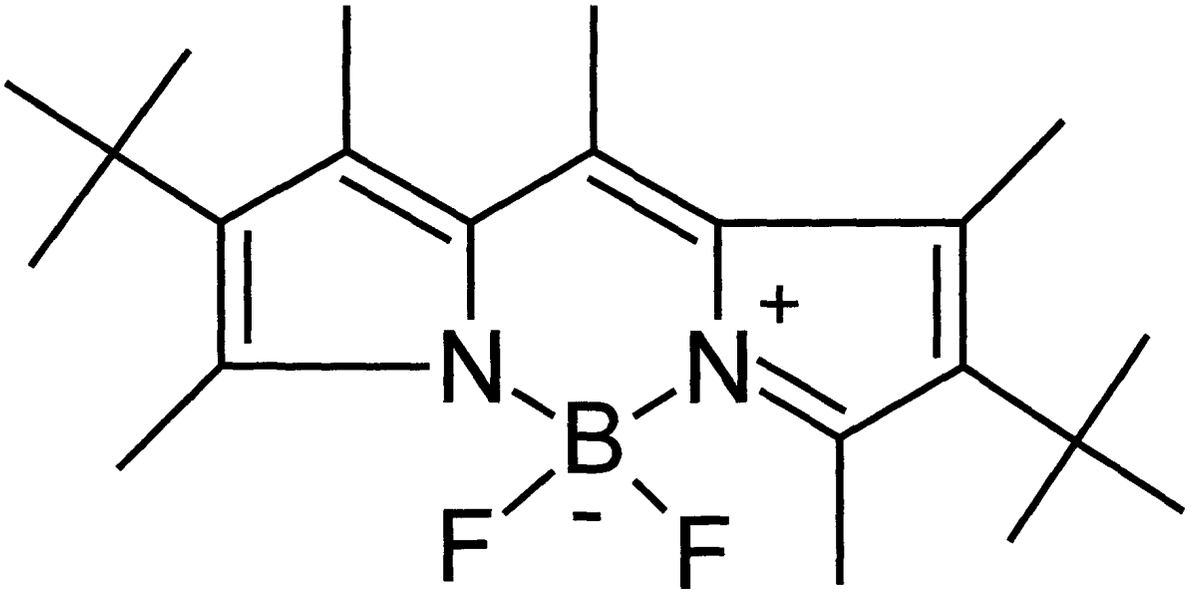

Figure 2.4: Chemical structure of PM 597

3. Rhodamine 610 (Rhodamine B) [42]

Chemical name: N-[9-(2-carboxyphenyl)-6-(diethylamino)-3H-xanthen-3-ylidine]-N-ethyl-ethanaminium chloride or perchlorate or tetrafluoroborate

Chemical formulas and molecular weights:

$C_{28}H_{31}N_2O_3.Cl$ (MW: 479.02 amu)

$C_{28}H_{31}N_2O_3.ClO_4$ (MW: 543.02 amu)

$C_{28}H_{31}N_2O_3.BF_4$ (MW: 530.38 amu)

λ_{max}^{abs} = 552 nm in ethanol and 544 nm in methanol

Chemical structure:

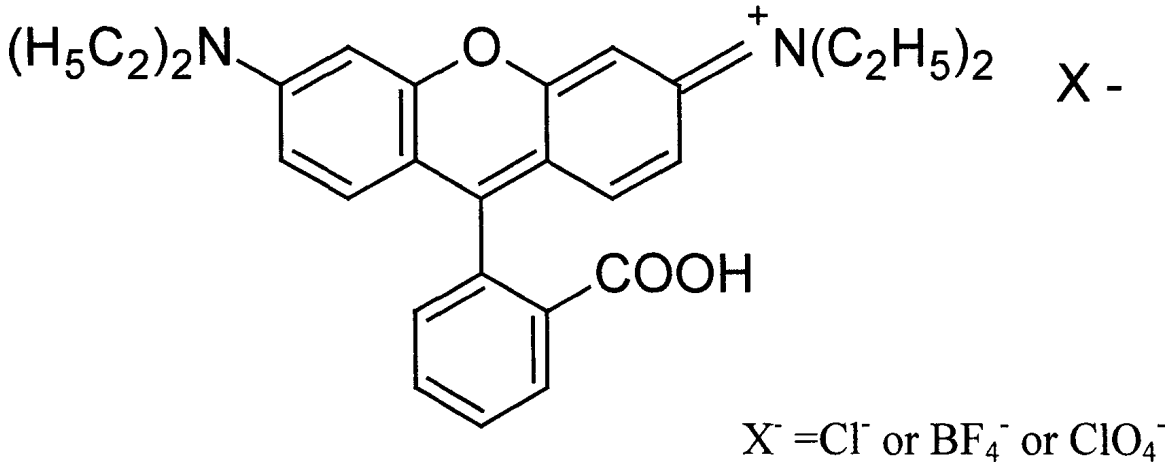

Figure 2.5: Chemical structure of R610

4. Rhodamine 590 (R6G) [43]

Chemical name: 2-[6-(ethylamino)-3-(ethylimino)-2,7-dimethyl-3H-xanthen-9-yl]-benzoic acid, ethyl ester, chloride or tetrafluoroborate or perchlorate

Chemical formulas and molecular weights:

$C_{28}H_{31}N_2O_3.Cl$ (MW: 479.02 amu)

$C_{28}H_{31}N_2O_3.ClO_4$ (MW: 543.02 amu)

$C_{28}H_{31}N_2O_3.BF_4$ (MW: 530.38 amu)

λ_{max}^{abs} = 530 nm in ethanol.

Chemical structure:

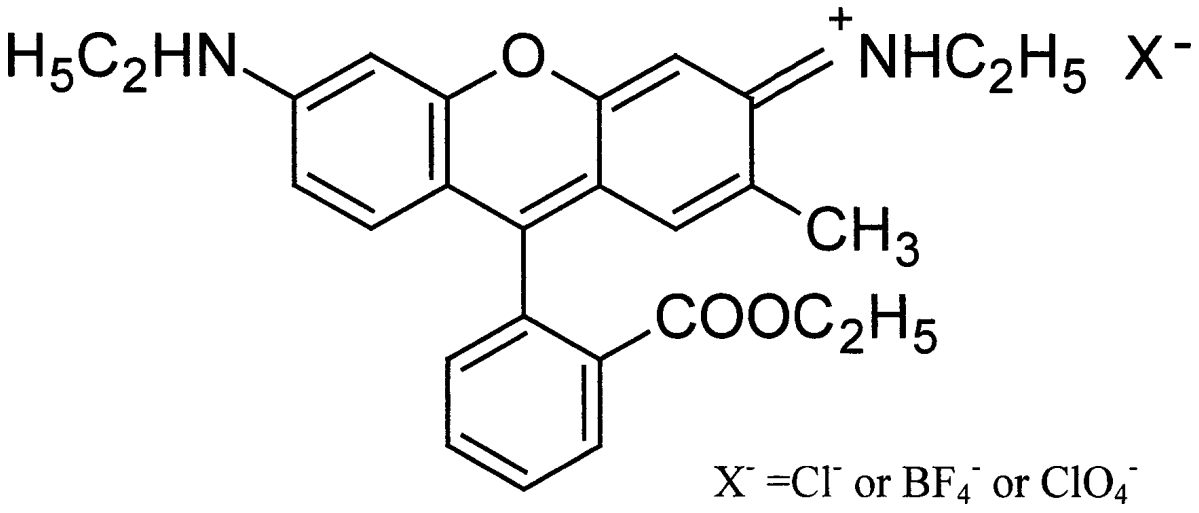

Figure 2.6: Chemical structure of R6G

5. Rhodamine 575 (R575) [44]

Chemical name: 2-[6-(ethylamino)-3-(ethylimino)-2,7-dimethyl-3H-xanthen-9-yl]-benzoic acid.

Chemical formula: $C_{26}H_{26}N_2O_3$

Molecular weight: 414.49 amu

$\lambda_{max}^{abs} = 518$ nm in ethanol and methanol

Chemical structure:

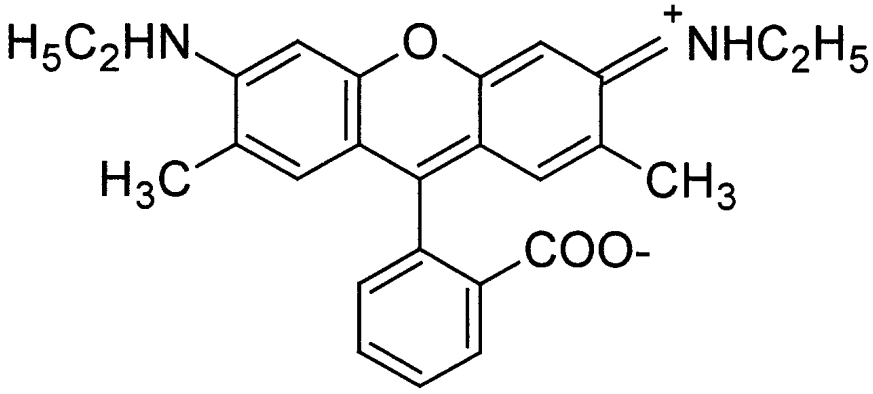

Figure 2.7: Chemical structure of R575

All laser dyes shown above were purchased from Exciton and made into solutions without further purification. Exciton indicated that their R575 was 99% pure, and R610 and , R6G were 97-98% pure. The main impurities in R575 were expected to be trace amounts of R590, R610 and NaOH.

PM laser dyes were dissolved in a mixture of 100% ethanol and cyclohexane (1:1 in volume ratio) to make 2 mM solutions. Each Rhodamine dye was dissolved in 100% ethanol to make 2 mM solutions. All solutions were used within one month after preparation, and alkali metal ion contamination was minimized by storing the dye laser solutions in plastic vials.

2.3.2. Analytes

Several analytes were used to test the utility of the selected dyes as MALDI matrix candidates, including Dalargin, Bradykinin, Bentazon, Erythromycin and Lovastatin. Each analyte except Bentazon was dissolved in a mixture of acetonitrile and deionized water (30:70 or 70:30 (v/v)), for better solubility and rate of evaporation. Bentazone was dissolved in neat ethanol.

1. Dalargin

Chemical formula: $C_{35}H_{51}N_9O_8$

Molecular weight: 725.83 amu

Chemical structure:

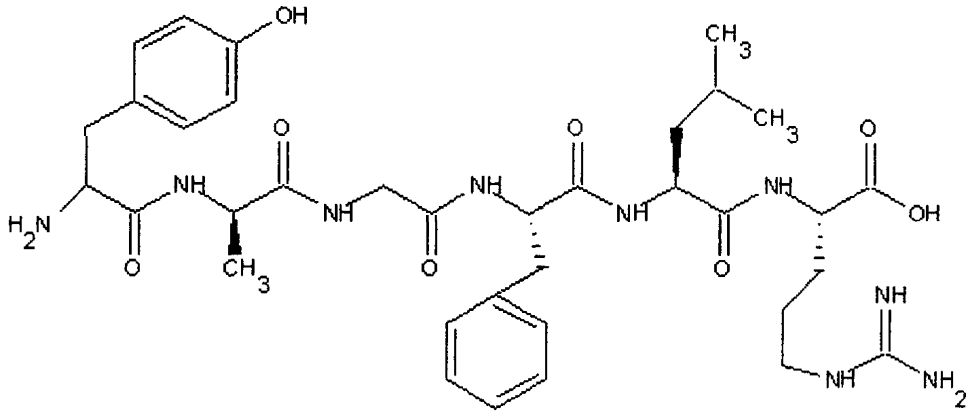

Figure 2.8: Chemical structure of Dalargin

Dalargin, a hexapeptide contains both a weakly acidic (pKa = 3.55 ± 0.21)[45] and a strongly basic (pKa = 13.55 ± 0.70) [45] functional group. This means that this analyte should be readily detected either as a protonated species in positive ion mode or as a deprotonated species in negative ion mode.

2. Bradykinin

Chemical formula: $C_{50}H_{73}N_{15}O_{11}$

Molecular weight: 1060.21 amu

Chemical structure:

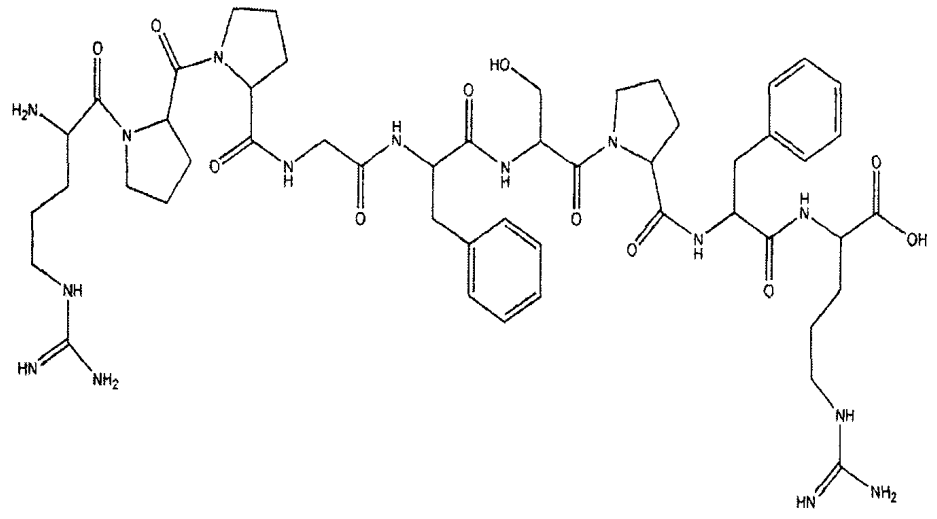

Figure 2.9: Chemical structure of the nonapeptide Bradykinin

3. Bentazone

Chemical formula: $C_{10}H_{12}N_2O_3S$

Molecular weight: 240.28 amu

Chemical structure:

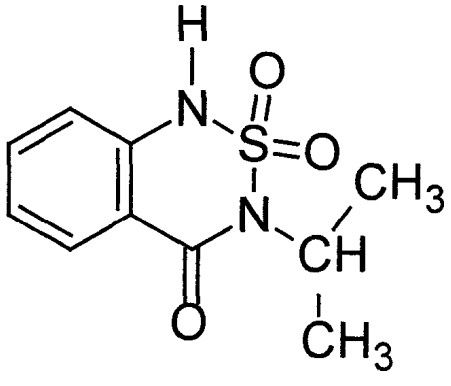

Figure 2.10: Chemical structure of Bentazone

Bentazone is acidic with a pKa value of 3.3 [46]. If the matrix is basic, it should be detected as a deprotonated ion in negative ion mode.

4. Erythromycin

Chemical formula: $C_{37}H_{67}NO_{13}$

Molecular weight: 733.93 amu

Chemical structure:

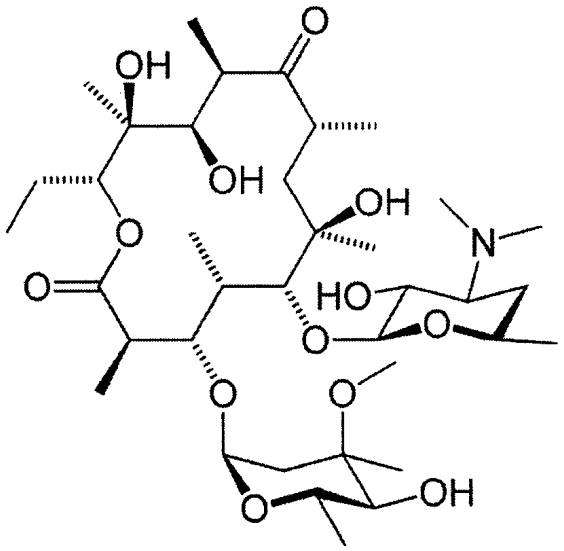

Figure 2.11: Chemical structure of Erythromycin

5. Lovastatin

Chemical formula: $C_{24}H_{36}O_5$

Molecular weight: 404.54 amu

Chemical structure:

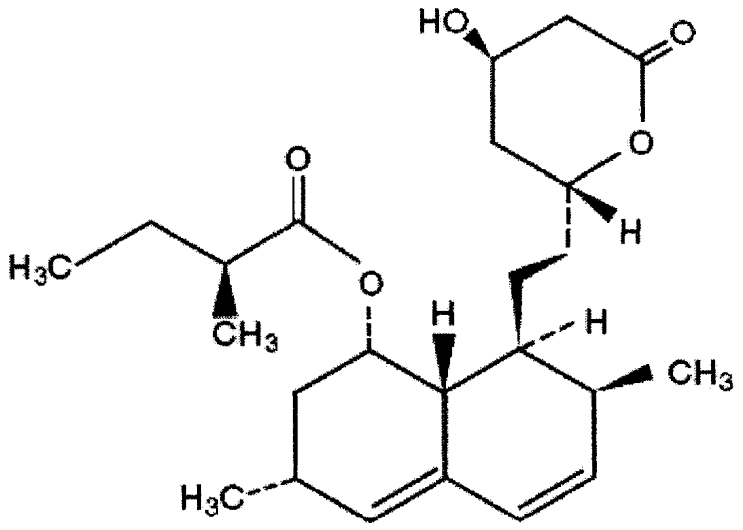

Figure 2.12: Chemical structure of Lovastatin

Erythromycin and Lovastatin have no obvious acidic or basic functional groups. In these cases, it is expected that the only way to ionize them is by cationization using alkali impurities or cation additives.

Chapter 3:Pyrromethene laser dyes as matrix candidates

3.1. Overview

Pyrromethene (PM) dyes strongly absorb 532 nm light and can be used as gain media for dye lasers under 532 nm pumping. The basic structure of a PM dye consists of two pyrrole units linked by methylene (shown in Fig 3.1d) and BF_2 groups, as shown in Fig. 3.1[47]. Two structurally similar PM dyes, PM567and PM597 were chosen for examination as possible matrices. The chemical structures of PM567 and 597 are shown in Chapter 2, Figs. 2.3 and 2.4, respectively.

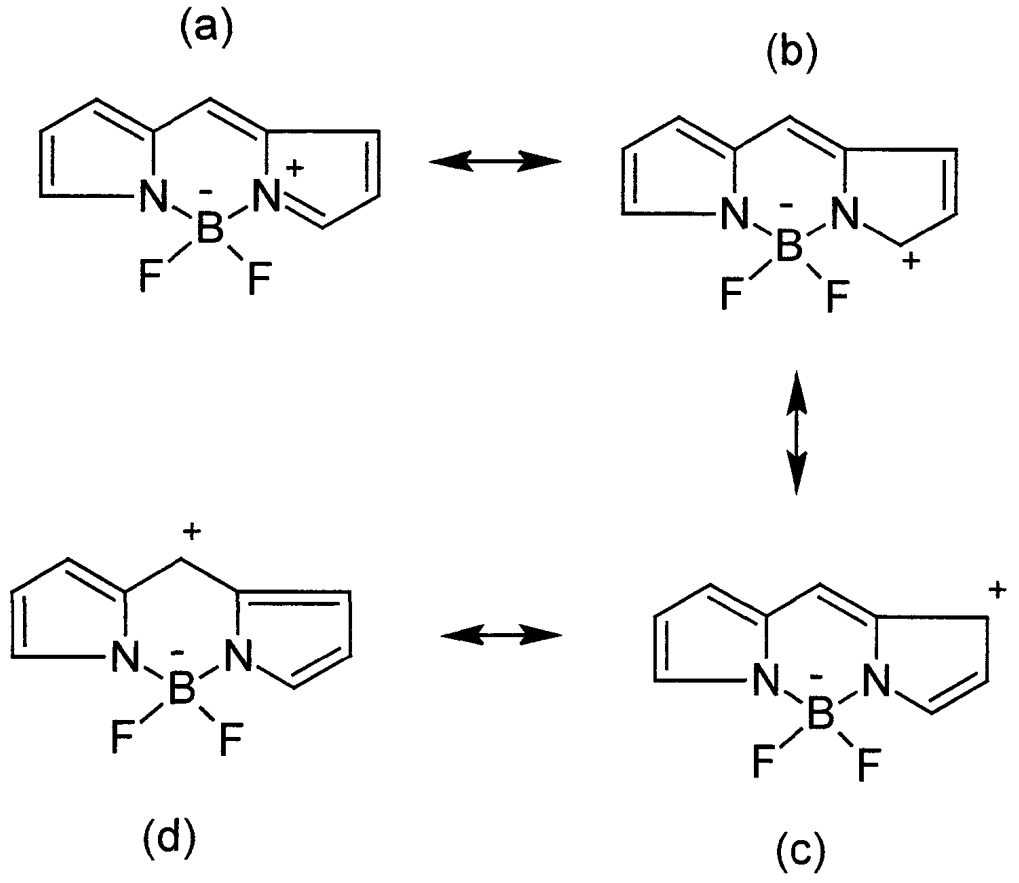

Figure 3.1: Resonance structures of the PM chromophore.

The initial motivation to try PM dyes as matrix candidates was that some of them are moderately good electron donors[48]. If this is indeed the case, then one might expect to observe negatively charged analytes by MALDI mass spectrometry.

3.2. Results and peak assignments [49, 50]

1. Sample 1: PM567 + Dalargin

The sample containing PM567 as the matrix and Dalargin (Dal) as the analyte in a molar ratio of 12:1 was tested. This molar ratio was used to initially test potential matrix candidates. Under such large analyte loadings, the analyte signal would be expected to be intense due to matrix suppression effect (MSE) [21] if the matrix candidate is promising. In such cases, the molar ratio of matrix to analyte would then be increased in subsequent experiments to observe the level of chemical noise caused by the matrix compound. The resultant MALDI mass spectra in positive and negative ion mode obtained using PM567 are shown in Figs. 3.2 and 3.3, respectively. Peak assignments of some of the features due to PM567 in positive ion mode are given in Fig. 3.4.

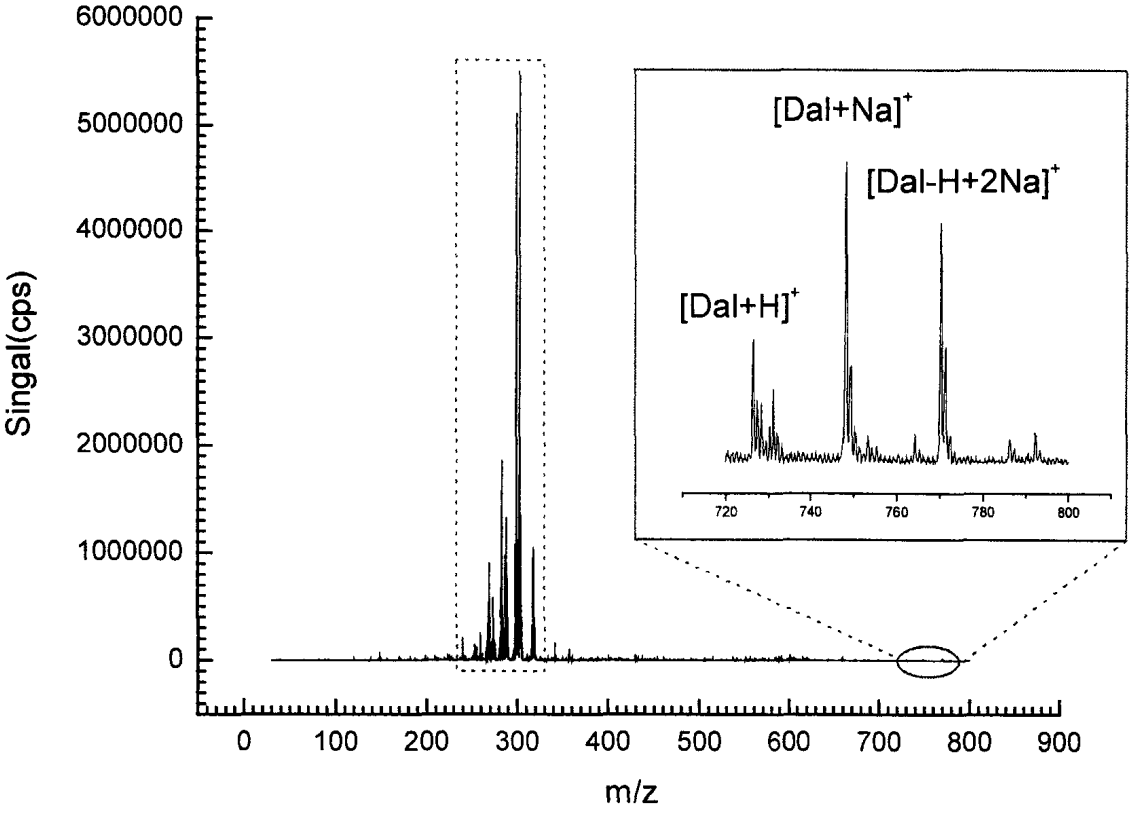

Figure 3.2: Positive ion mode MALDI mass spectrum of PM 567+Dalargin (12:1 in molar ratio). The inset is a close-up the MALDI mass spectrum in the mass region corresponding to the analyte.

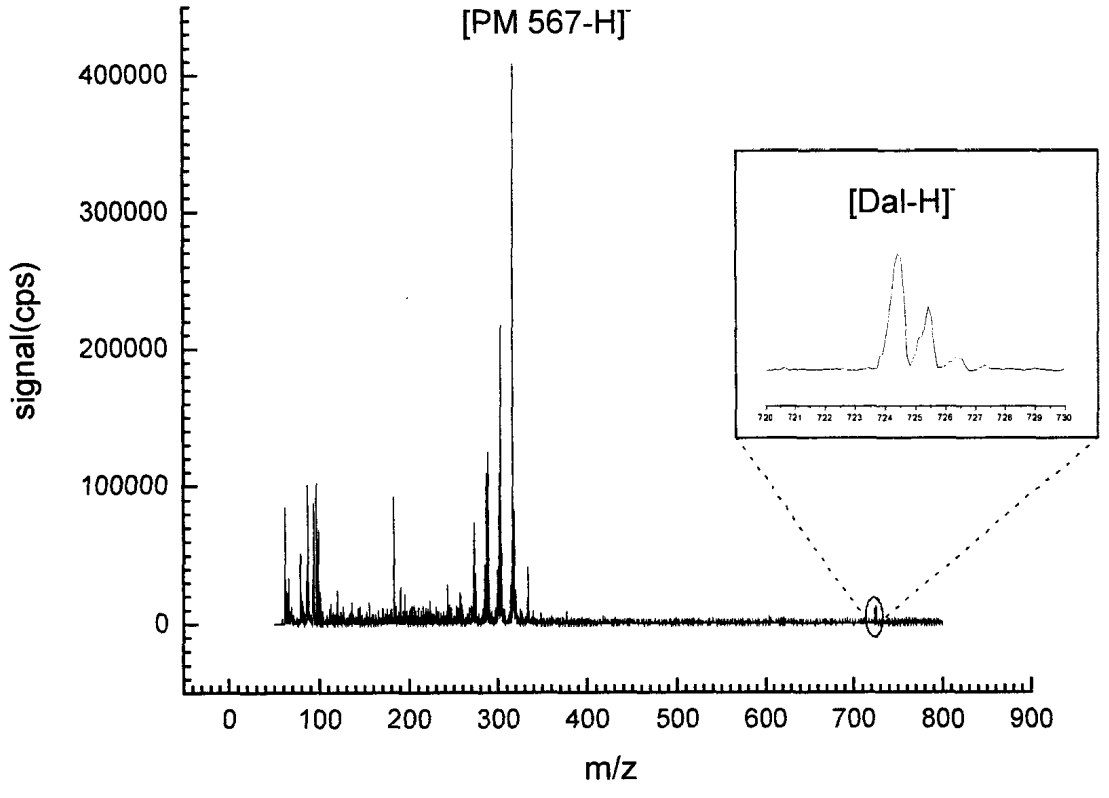

Figure 3.3: Negative ion mode MALDI mass spectrum of PM 567+Dalargin (12:1 in molar ratio). The inset is a close-up the MALDI mass spectrum in the mass region corresponding to the analyte.

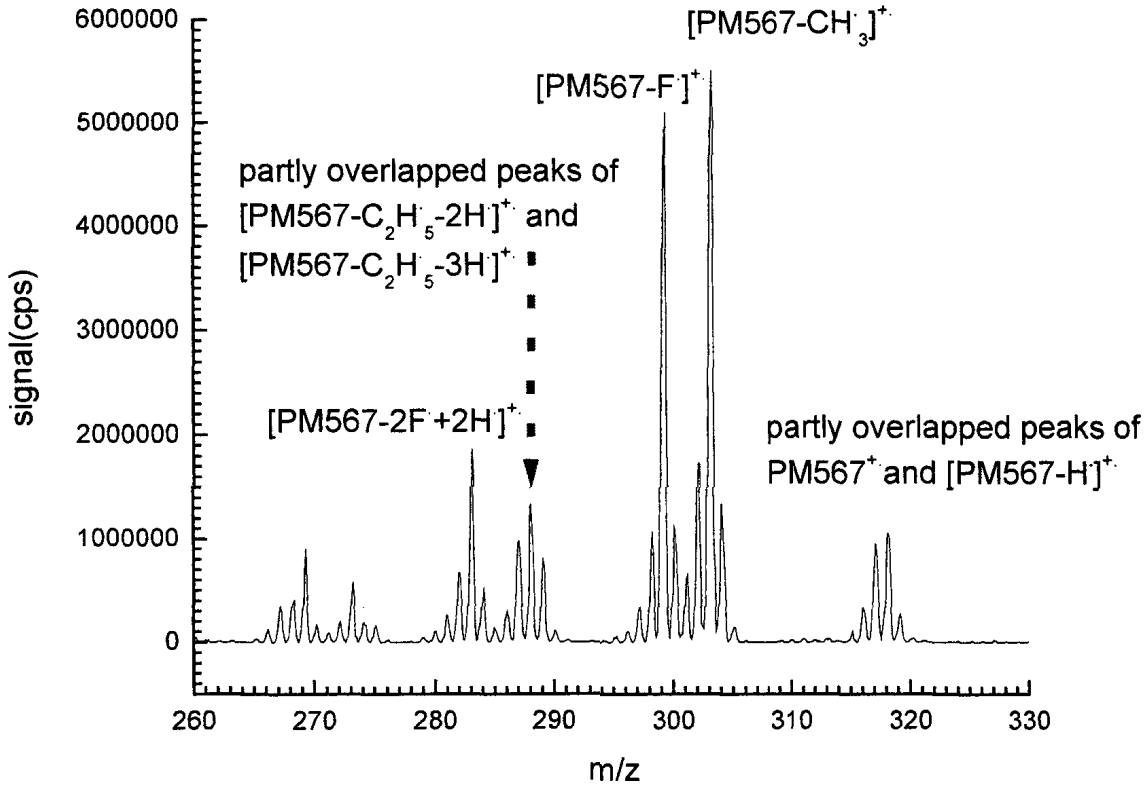

Figure 3.4: Tentative peak assignments of some of the low molecular weight features due to PM567 in the MALDI mass spectrum taken in positive ion mode.

2. Sample 2: PM597 + Dalargin

The sample containing PM597 as the matrix and Dal as the analyte in a molar ratio of 12:1 was tested. The resultant MALDI mass spectra taken in positive and negative ion mode are shown in Figs. 3.5 and 3.6, respectively. Peak assignments of some of the lower molecular weight features due to PM597 in positive ion mode are given in Fig. 3.7.

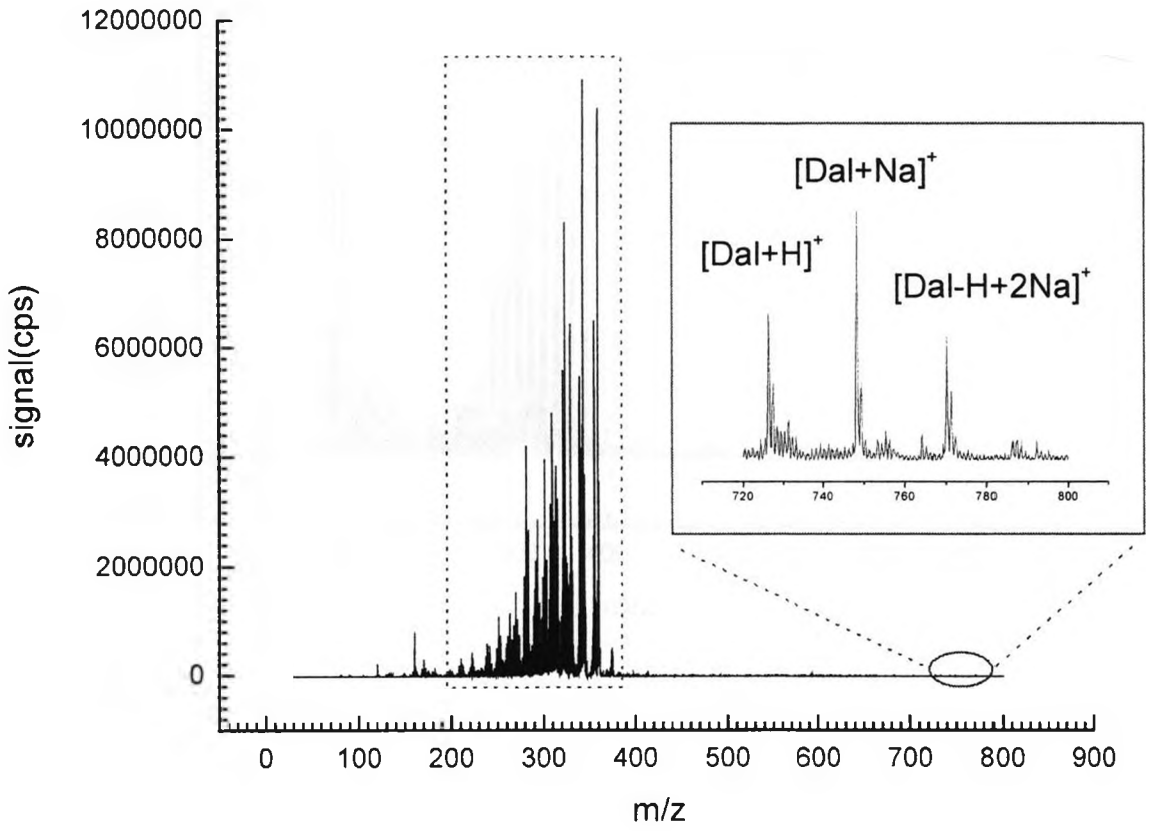

Figure 3.5: Positive ion mode MALDI mass spectrum of PM 597+Dalargin (molar ratio = 12:1). The inset is a close-up the MALDI mass spectrum in the mass region corresponding to the analyte.

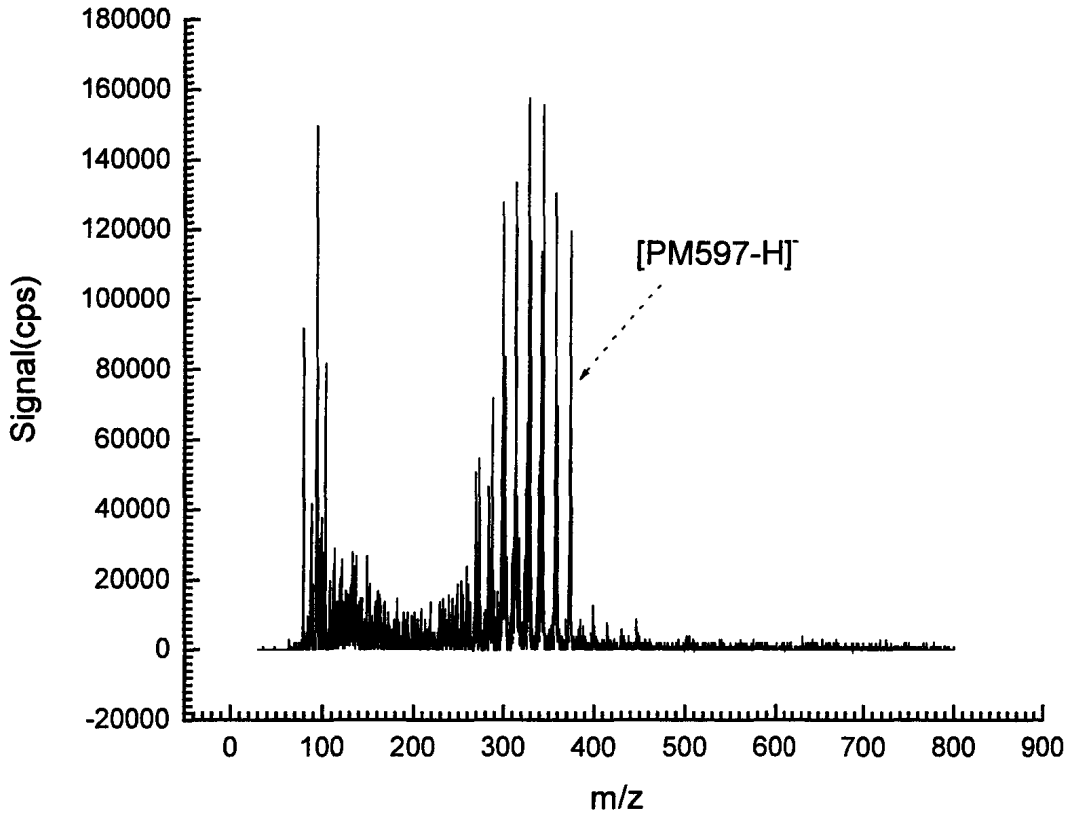

Figure 3.6: Negative ion mode MALDI mass spectrum of PM 567+Dalargin (molar ratio = 12:1). An extremely weak signal of $[Dal-H]^-$ only (not shown) could be observed.

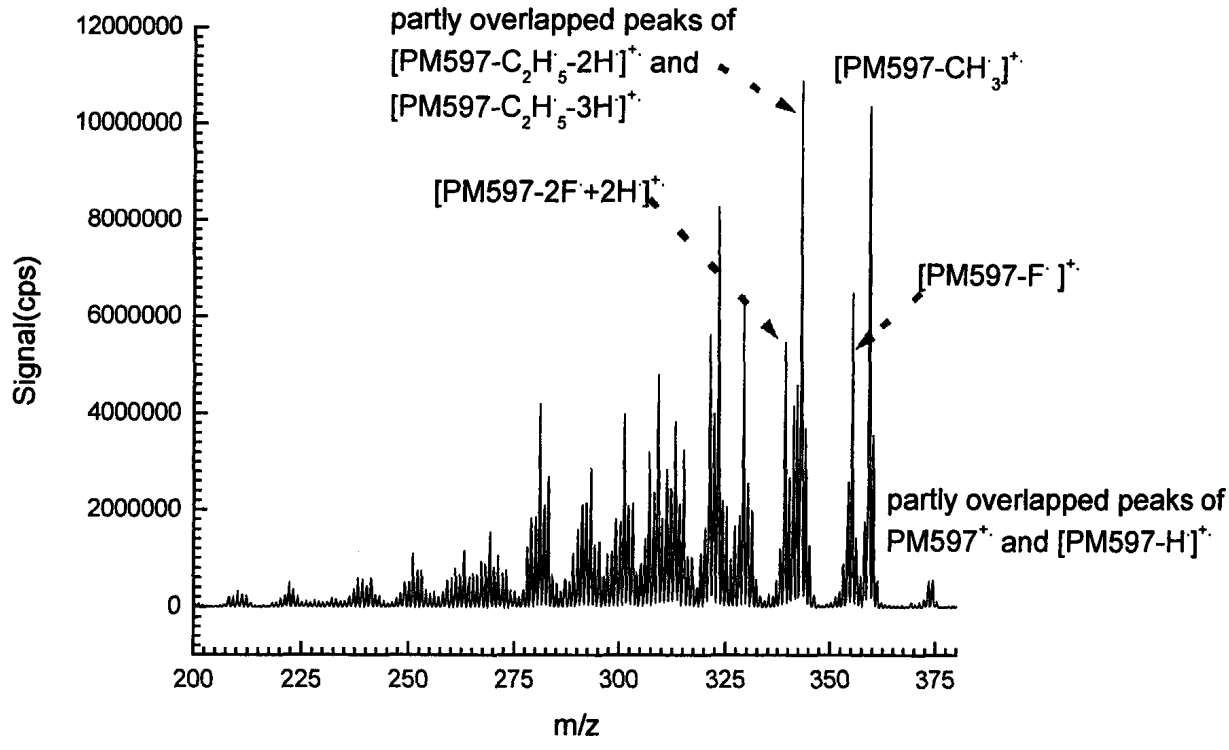

Figure 3.7: Tentative peak assignments of some of the low molecular weight features due to PM597 in the MALDI mass spectrum taken in positive ion mode.

3.3. Discussion

1. Dalargin Ionization

MALDI mass spectra in positive ion mode of samples prepared using PM 567 and 597 as the matrices exhibit signals due to $[Dal+H]^+$, $[Dal+Na]^+$ and $[Dal-H+2Na]^+$. Sodium adduct formation is attributed to sodium impurities found in all glassware. The dye manufacturer, Exciton, was consulted on this matter. They stated that their syntheses of PM567 and PM597 do not involve the use of sodium salts, but that the compounds were in contact with standard glassware. The Dalargin solutions prepared in the lab could also have been contaminated with sodium salts by using glassware prior to being transferred into plastic vials. The presence of MALDI signals due to $[Dal+H]^+$ and $[Dal-H+2Na]^+$ show that both PM567 and PM597 can act as proton donor and acceptor.

Contrary to initial expectations, negative parent ion signals of Dalargin (Dal^-) were not found in negative ion mode, while extremely weak signals of $[Dal-H]^-$ were. The weak signal intensity of $[Dal-H]^-$ is attributed to sodium addition reactions which yield the $[Dal-H+2Na]^+$ signal readily observed in positive ion mode.

2. Mechanism of ionization of PM567 and 597

The mass spectra shown in Figs. 3.4 and 3.7 show that both PM567 and PM597 undergo extensive fragmentation under 532 nm laser irradiation. One possible reason for this is that PM dyes are known to be photolytically unstable [51, 52]. Therefore the chemical fragments may originate from the decomposition of excited state PM 567 and 597 in the MALDI plume.

3. Mechanism of ionization of Dalargin

As observed, PM567 and PM597 do protonate and deprotonate Dalargin. However, it may be that some acidic or basic fragment ions generated from the PM dyes also serve as proton donors or acceptors.

3.4. Conclusions

Although samples containing PM567 or PM597 as matrices and Dalargin as the analyte do yield MALDI ion signals in both positive and negative ion mode, both dyes undergo extensive fragmentation. This will limit their utility for detecting low molecular weight drug analytes. As important, the MALDI ion signals were not particularly intense even though a high concentration of Dalargin was used (1mM). It can therefore be concluded that pyrromethene dyes are not promising matrix candidates for visible-MALDI using 532 nm lasers.

Chapter 4: Rhodamine 610 dyes as matrix candidates

4.1. Overview [53, 54]

Many laser dyes used today belong to the class of compounds known as xanthenes whose chromophore structure shown in Fig. 4.1a. Rhodamine dyes, whose chromophore structure is shown in Fig. 4.1 b, are derived from the xanthene family.

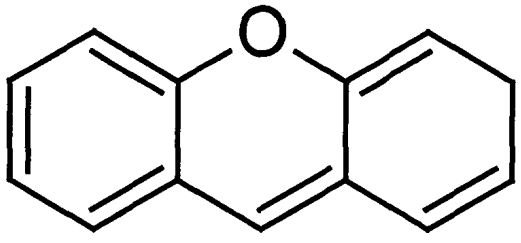

a

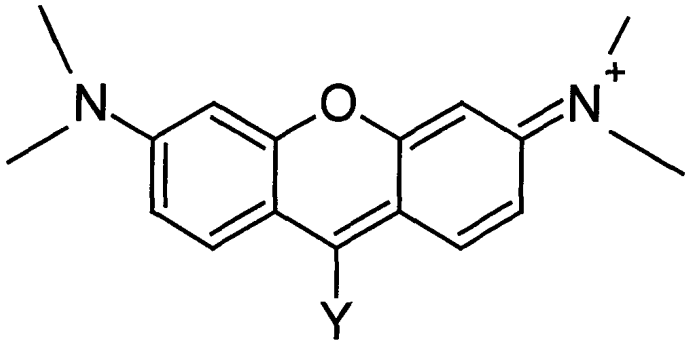

b

Figure 4.1: Structure of the a) xanthene and b) Rhodamine chromophores.

Rhodamine dyes strongly absorb 532 nm light. For example, Rhodamine 6G (R6G) , one of the most common laser dyes in use today. The UV-visible absorption

spectrum of a solution of R6G (structure given in Fig. 2.6), is shown in Fig. 4.2. The peak of the strongest absorption band of a Rhodamine dye is determined mainly by the aromatic ring structure. The Y substituent shown in Fig. 4.1b is not part of the π-system and therefore has only a minor influence on the absorption spectrum.

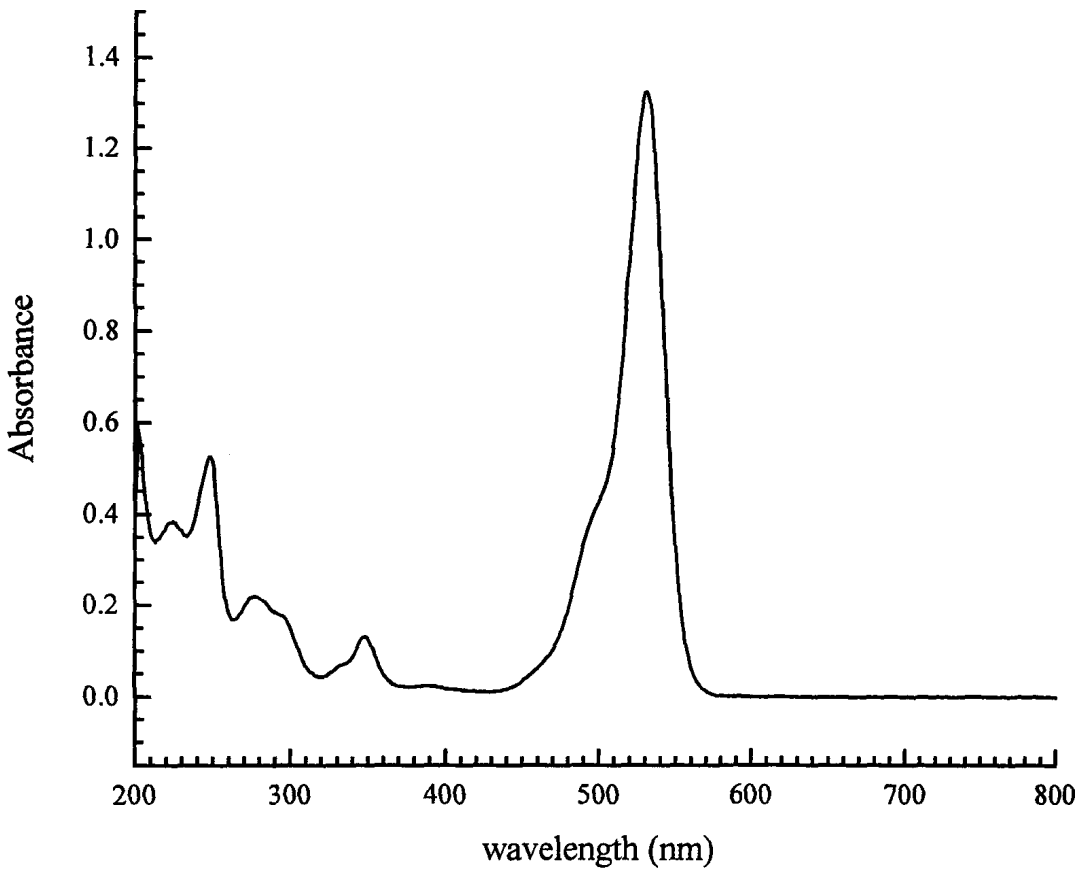

Figure 4.2: UV-visible absorption spectrum of a solution of 0.012mM Rhodamine 6G in ethanol; $\lambda_{max}^{abs} = 530\,nm$.

Our initial motivation to use Rhodamine 610 dyes (also known as Rhodamine B) as matrix candidates is not only due to its strong absorption at 532 nm, but also because the compound has a carboxyphenyl substituent, Y = C_6H_4COOH which could be a good proton donor.

The chemical structure of neutral Rhodamine 610 is shown in Fig. 4.3[55]. Three R610 laser dyes were tested which differ only by the anion making up the salt. They are R610.Cl, R610.ClO_4 and R610.BF_4, whose chemical formula, molecular weights and chemical structures are given as part of Fig. 2.5. The mass to charge ratio, m/z of the cation was calculated by the Isotope Distribution Calculator v. 0.3 (Michael J. MacCoss, University of Washington) to be m/z = 443.23. The cation has an acidic carboxylic acid group which is expected to be a good proton donor.

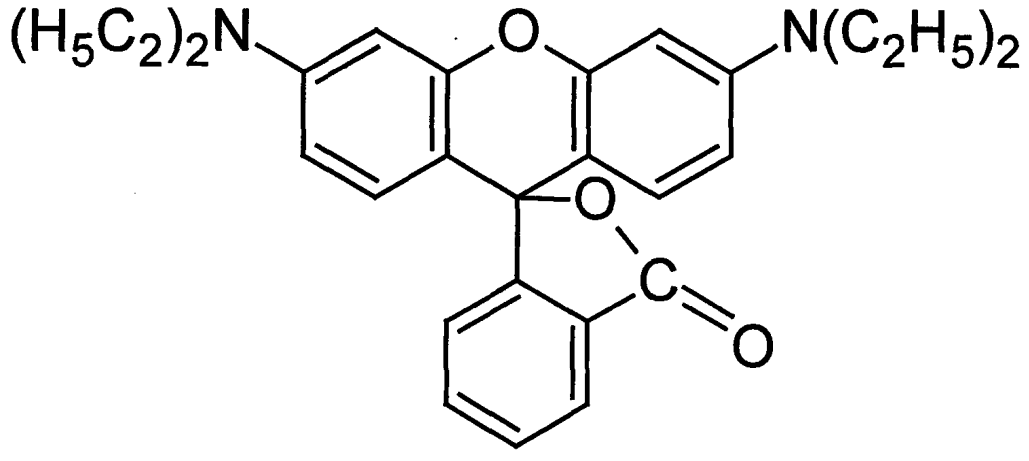

Figure 4.3: Chemical structure of neutral Rhodamine 610 ($C_{28}H_{30}N_2O_3$)

4.2. R610.ClO_4 as a matrix candidate

4.2.1. Results and peak assignments [49, 50]

The MALDI mass spectra of R610.ClO_4 without any co-deposited analyte (sample 1) obtained in this work are shown in Fig. 4.4. The base (strongest) peak in the mass spectrum taken in positive ion mode detection, (Fig. 4.4 a), is a feature at m/z =

433.21 which is attributed to R610 cation: $C_{28}H_{31}N_2O_3^+$. Two isotopic bands could also be assigned. There are many other signals which have not yet been identified but are probably due to chemical fragments. The base peak in the MALDI spectrum recorded in negative ion mode, (Fig. 4.4b) at m/z = 98.89 is assigned to ClO_4^-.

A MALDI mass spectrum taken in positive ion mode of a sample containing R610.ClO_4 as the matrix and Dalargin as the analyte in a molar ratio of 5:1 (sample 2) is shown in Fig. 4.5. Although this molar ratio is small it was found to give the best results as shown in Fig. 4.6. Although the absolute signal strength of $[Dal+H]^+$ at m/z = 726 looks very strong, the signal-to-noise ratio is not particularly good due to background chemical noise. The MALDI mass spectrum of sample 2 taken in negative ion mode is not shown because no signals due $[Dal-H]^-$ were found.

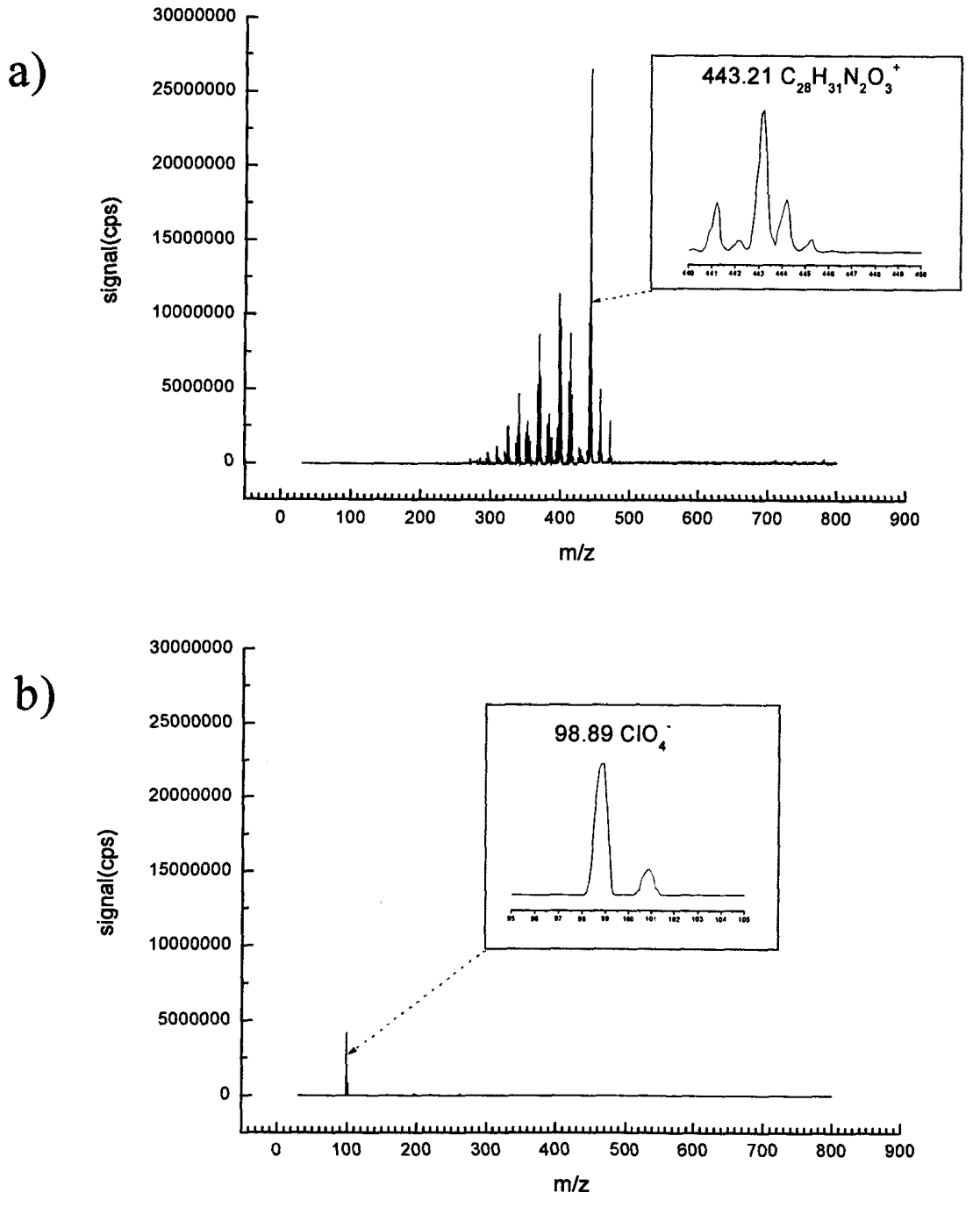

Figure 4.4: MALDI mass spectra of R610.ClO4 without any analyte in a) positive ion mode and b) negative ion mode. The inset in a) is a blowup of the MALDI signal in the mass region corresponding to the cation of R610. The inset in b) is a blowup of the MALDI signal corresponding to ClO_4^-.

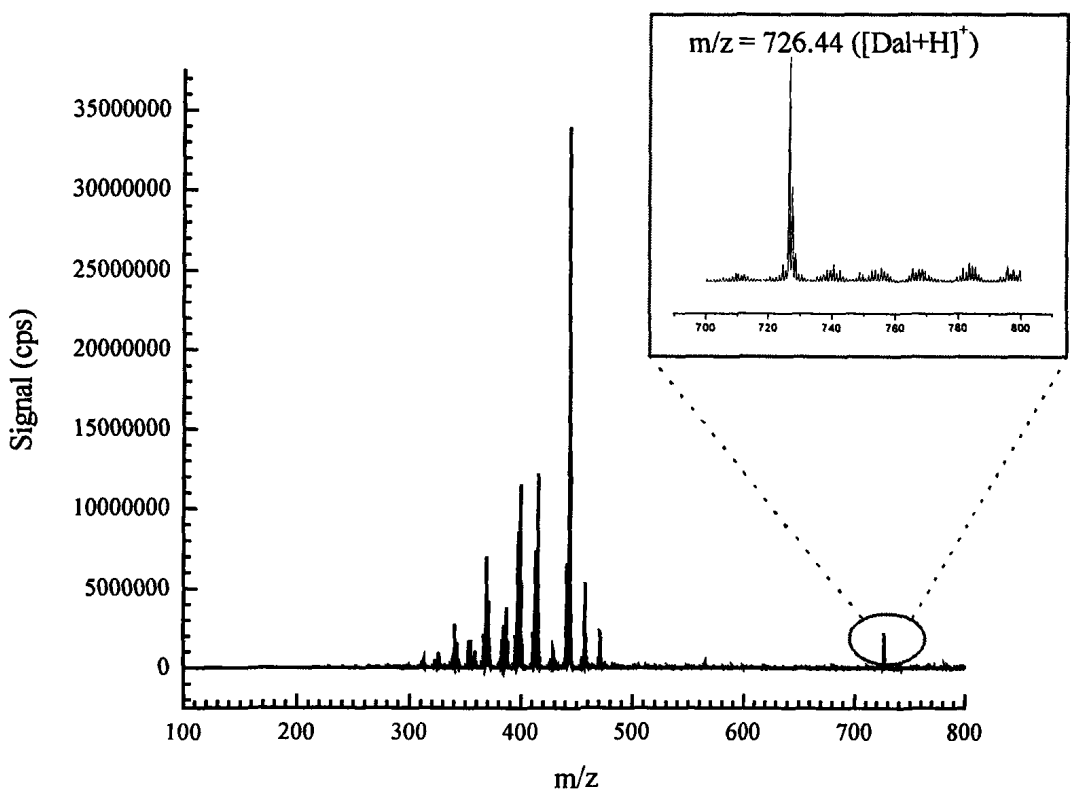

Figure 4.5: MALDI mass spectrum taken in positive ion mode of a sample containing R610.ClO4 and Dalargin in a molar ratio = 5:1. The inset is a blowup of the mass region corresponding to protonated Dalargin.

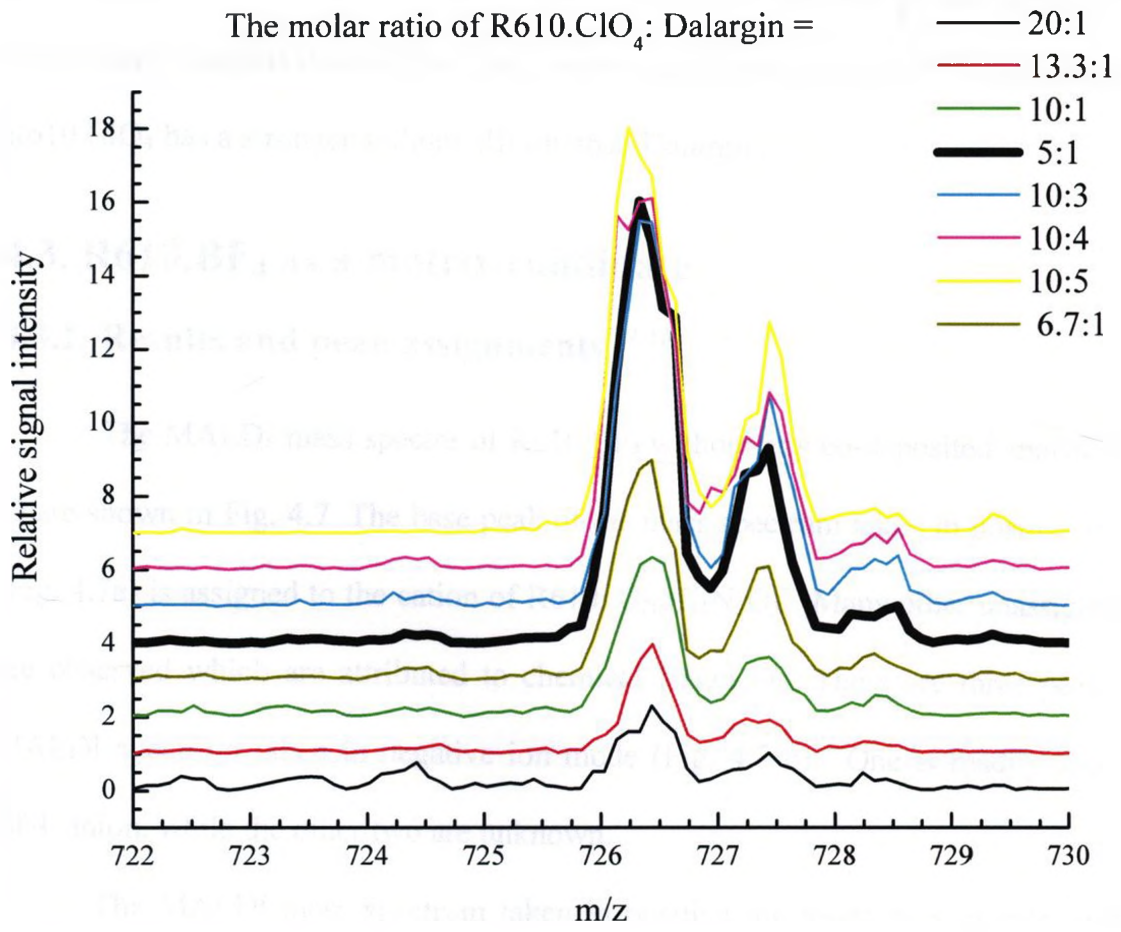

Figure 4.6: A series of MALDI mass spectra taken in positive ion mode in the vicinity of the protonated Dalargin signal at m/z =726 for different molar ratios of R610.ClO4 : Dalargin. The spectrum with the best signal-to-noise ratio is highlighted with a thick black line.

4.2.2. Discussion

R610.ClO_4 has proton donating capability, and therefore produces a very intense signal of $[Dal+H]^+$ when used as a visible MALDI matrix. However, it also generates a significant amount of chemical noise presumably due to fragmentation reactions. It is still

not clear if excited R610.ClO_4, $C_{28}H_{31}N_2O_3^+$ or the generated chemical fragments are the proton donors, or if more than one species actually contribute to the $[Dal+H]^+$ signal. Interestingly, signals due to $[Dal+Na]^+$ were not observed in Fig. 4.5 which suggests that R610.ClO_4 has a stronger sodium affinity than Dalargin.

4.3. R610.BF_4 as a matrix candidate

4.3.1. Results and peak assignments [49, 50]

The MALDI mass spectra of R610.BF_4 without any co-deposited analyte (sample 3) are shown in Fig. 4.7. The base peak of the mass spectrum taken in positive ion mode (Fig. 4.7a) is assigned to the cation of R610: $C_{28}H_{31}N_2O_3^+$. Many other unassigned peaks are observed which are attributed to chemical fragments. There are three peaks in the MALDI spectrum taken in negative ion mode (Fig. 4.7 b). One is readily assigned to $BF4^-$ anion, while the other two are unknown.

The MALDI mass spectrum taken in positive ion mode of a sample containing R610.BF_4 as the matrix and Dalargin as the analyte in a molar ratio is 5:1 (sample 4) is shown in Fig. 4.8. Three features are observed in the mass range between 700 and 800 which can be assigned to $[Dal+H]^+$, $[Dal+Na]^+$ and $[Dal-H+2Na]^+$. The presence of a signal due to $[Dal-H+2Na]^+$ suggests the matrix or a fragment of the matrix has some proton-accepting capability.

4.3.2. Discussion

R610.BF_4 as a visible MALDI matrix not only has proton-donating ability, producing the signal of $[Dal+H]^+$, but also weak proton-accepting ability as evidenced by the signal due to $[Dal-H+2Na]^+$.

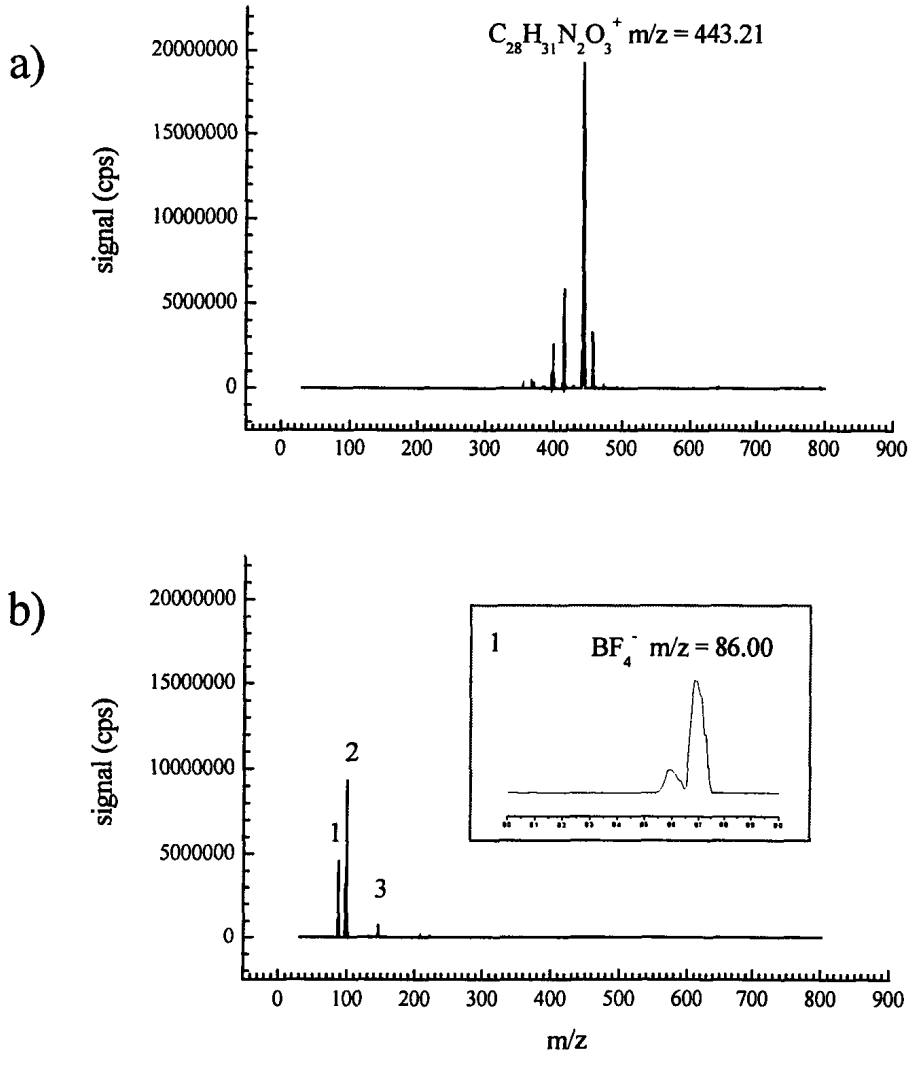

Figure 4.7: MALDI mass spectra of R610.BF_4 without any co-deposited analyte in a) positive ion mode and b) negative ion mode. Peak 1 is attributed to BF_4^-, while peaks 2 and 3 remain unassigned. The inset in b) is a blowup of the MALDI spectrum in the mass region corresponding to BF_4^-.

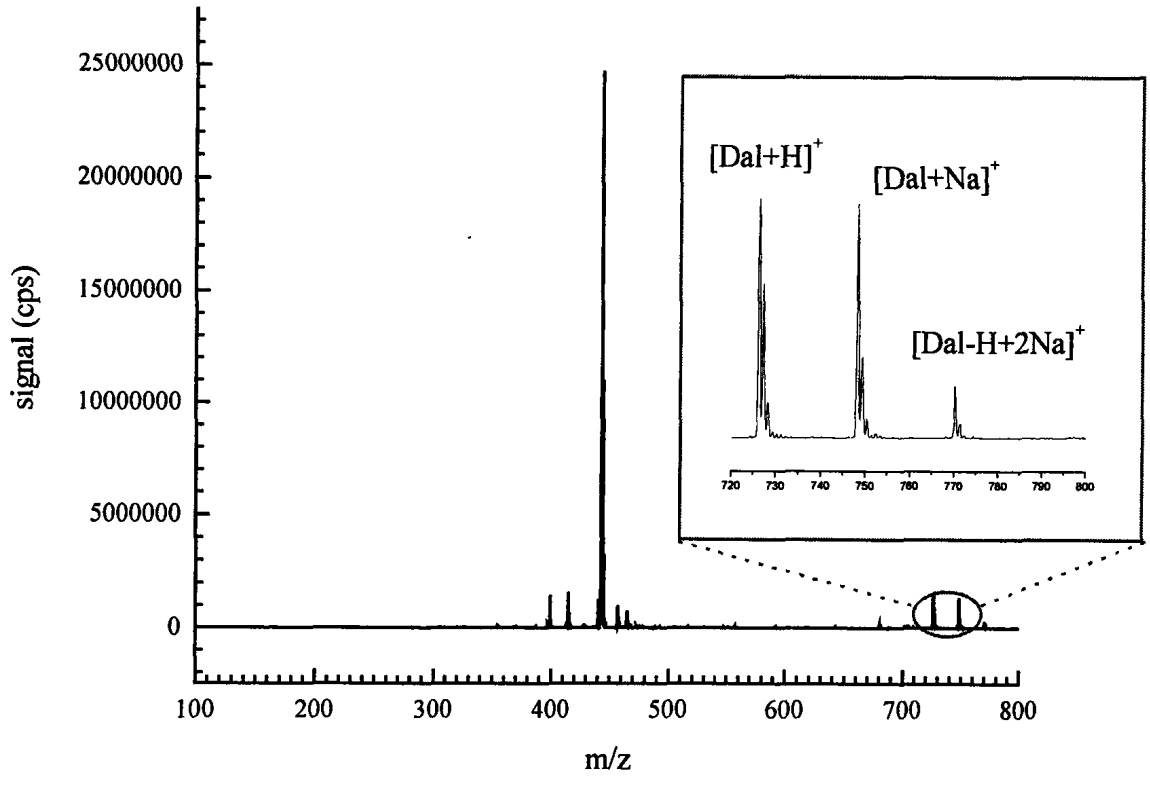

Figure 4.8: MALDI mass spectrum of the sample containing R610.BF4 and Dalargin in a molar ratio of 5:1, taken in positive ion mode. The inset is a blowup of the mass region corresponding to $[Dal+ H]^+$, $[Dal+ Na]^+$, and $[Dal-H+2Na]^+$.

4.4. R610.Cl as a matrix candidate

4.4.1. Results and peak assignments [49, 50]

MALDI mass spectra of a sample of R610.Cl without any co-deposited analyte (sample 5), are shown in Fig. 4.9. The mass spectrum taken in positive ion mode, Fig.4.9a, is remarkably clean. The only feature at m/z = 443.21 is due to the cation of R610: $C_{28}H_{31}N_2O_3^+$. The mass spectrum taken in negative ion mode, Fig.4.9b, contains some lower molecular mass peaks. From the patterns of isotopic features in the enlargement, the base peak is very likely the $C_2H_2NOCl_3^-$ anion whose chemical structure remains unknown.

The MALDI mass spectrum taken in positive ion mode of a sample containing R610.Cl and Dalargin in a molar ratio of 5:1 (sample 6), is shown in Fig. 4.10. Three features are found in the m/z region between 700 and 800 which are readily assigned to $[Dal+H]^+$, $[Dal+Na]^+$ and $[Dal-H+2Na]^+$. The signal of $[Dal-H+2Na]^+$ suggests that a chemical fragment derived from R610 could be basic, having proton-accepting capability.

4.4.2. Discussion

Of all the R610 salts R610.Cl produces the cleanest mass spectrum in positive ion mode. This results indicates that the chloride species may be a useful visible- MALDI matrix for analyzing small molecular weight compounds. The presence of a $[Dal-H+2Na]^+$ signal suggests that a fragment of R610 generated from R610.Cl can act as a proton acceptor.

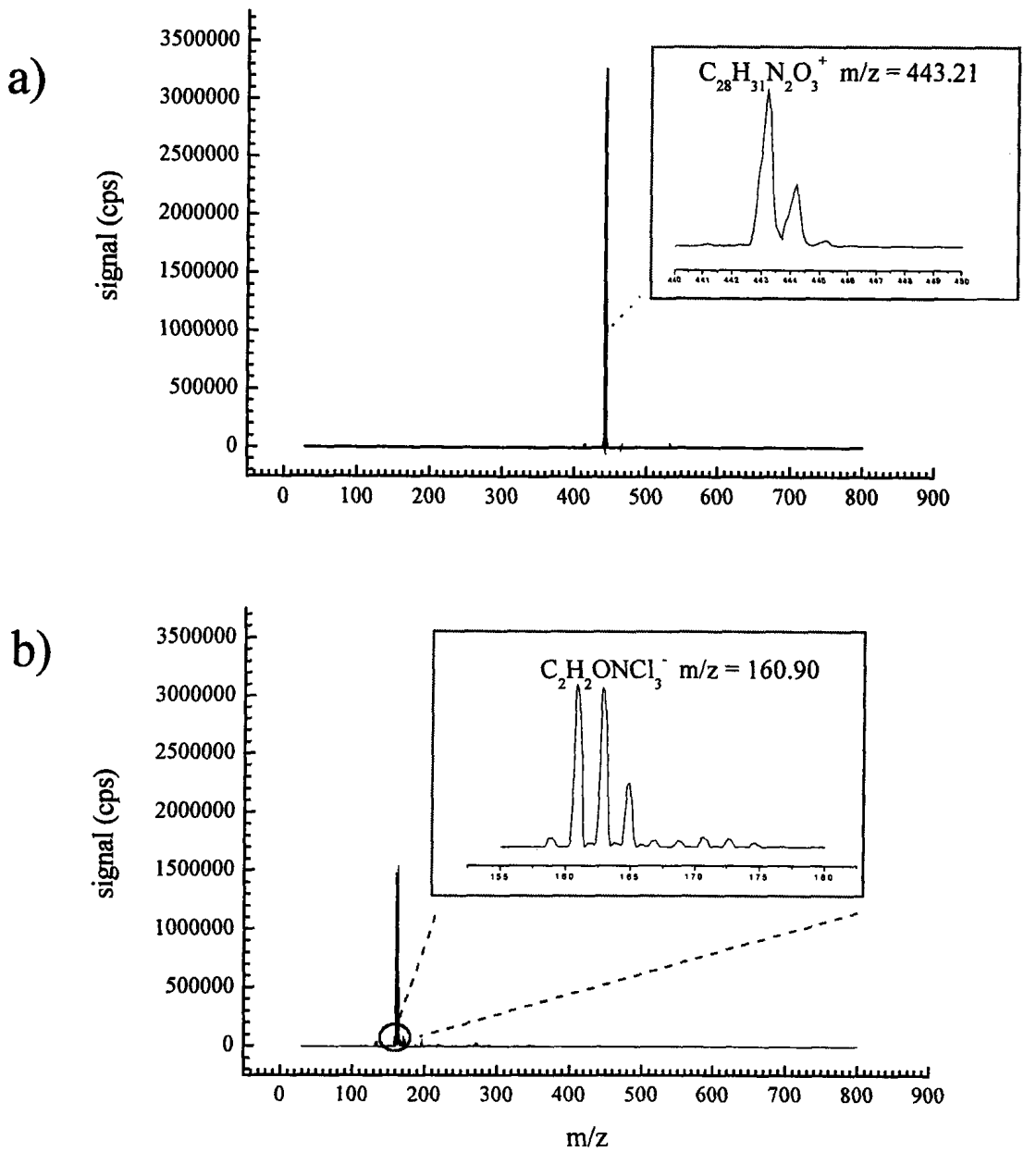

Figure 4.9: MALDI mass spectra of R610.Cl without any co-deposited analyte in a) positive ion mode and b) negative ion mode detection. The inset in a) is a blowup of the mass region corresponding to protonated R610. The inset in b) is a blowup of the mass region corresponding to the $C_2H_2NOCl_3^-$ anion.

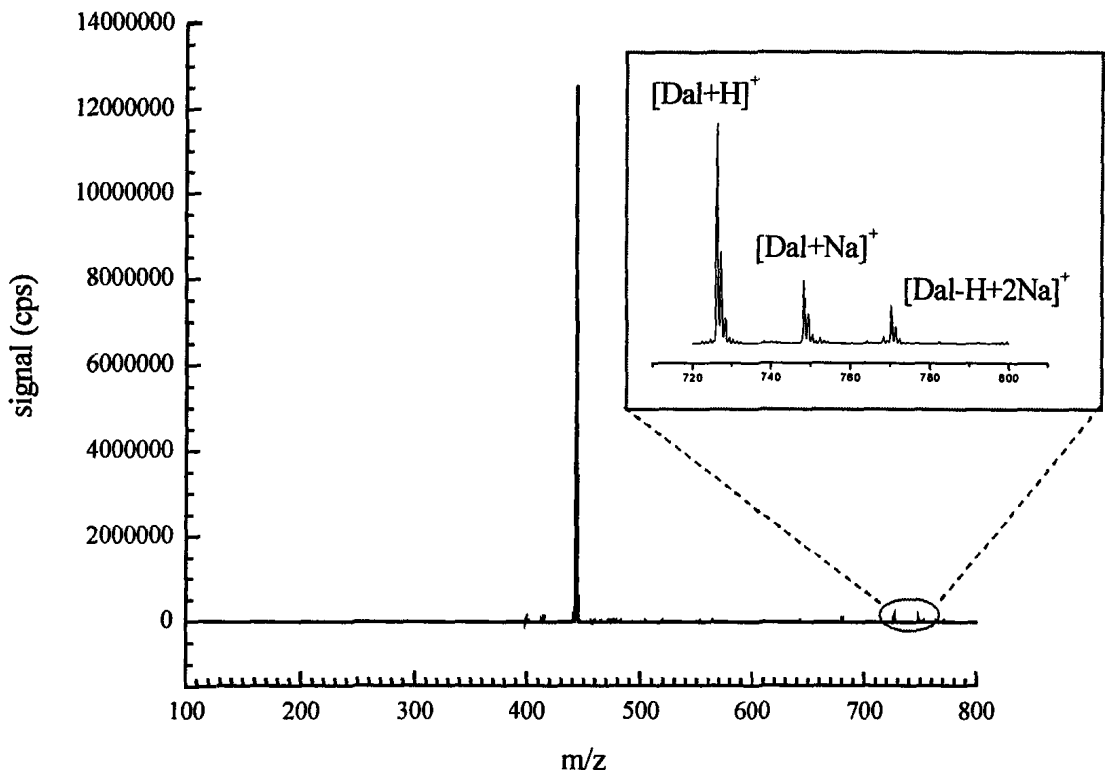

Figure 4.10: MALDI mass spectrum taken in positive ion mode of a sample containing R610.Cl and Dalargin in a molar ratio of 5:1. The inset is a blowup of the mass region corresponding to $[Dal+ H]^+$, $[Dal+ Na]^+$, and $[Dal-H+2Na]^+$.

4.5. A comparison of R610.ClO_4, R610.Cl and R610.BF_4

Results

R610.ClO_4, R610.Cl and R610.BF_4 samples containing equal amounts of the analyte Dalargin in a molar ratio of matrix: analyte of 500:1, were tested under identical experimental conditions of concentration, sample preparation and laser power. The results are shown in Fig. 4.11.

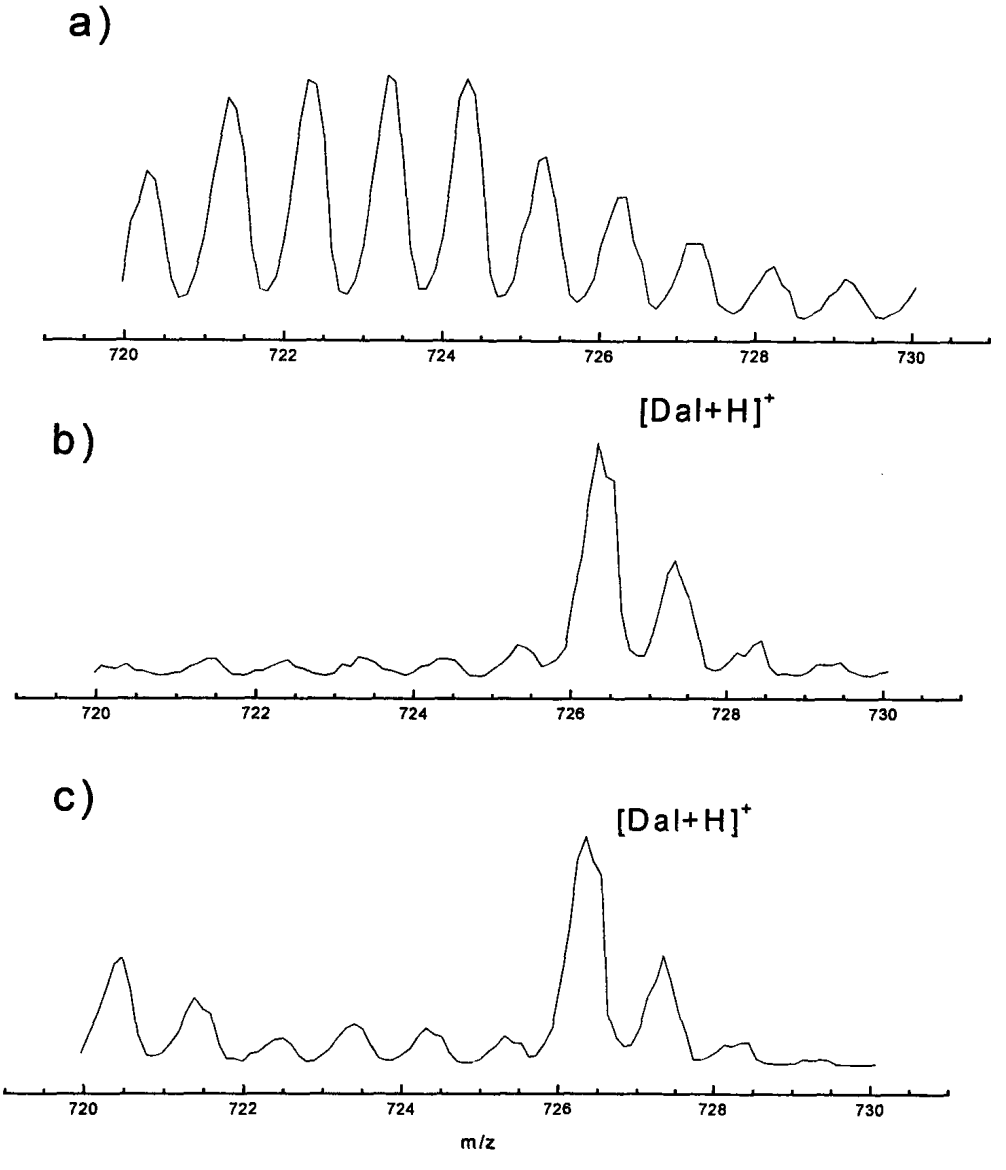

Figure 4.11: Visible-MALDI mass spectra near m/z =726.21 of samples containing matrix: analyte molar ratio of 500:1. a) R610.ClO_4 + Dalargin, b) R610.Cl + Dalargin and c) R610.BF_4 + Dalargin.

Fig. 4.11a shows the protonated Dalargin signal is strongly overlapped by chemical noise when using R610.ClO_4. This is not too surprising given that the overview

spectrum shows that this salt undergoes extensive fragmentation under 532 nm laser irradiation. Conversely, the cleanest signal of Dalargin (Fig. 4.11b) is obtained using R610.Cl as the matrix, which does not undergo extensive fragmentation under 532 nm irradiation. The signal of Dalargin (Fig. 4.11c) is clearly discernible when using $R610.BF_4$ as the matrix, producing fewer fragments than $R610.ClO_4$ but more than R610.Cl under identical experimental conditions

Conclusions

These experiments show that R610.Cl is a relatively "clean" matrix compared to other two, exhibiting significantly less fragmentation under 532 nm irradiation. This does not mean however that $R610.ClO_4$ and $R610.BF_4$ could not be useful as visible MALDI matrices. They may be acceptable if one is detecting heavier molecules than the chemical fragments generated by the laser irradiation.

4.6. The effect of the choice of salt anion on the fragmentation of the R610 matrix

4.6.1. Results

Although the three dye salts, R610.ClO_4, R610.Cl and R610.BF_4, have the same cation, $C_{28}H_{31}N_2O_3^+$, they fragment differently under identical experimental conditions of concentration, sample preparation and laser power. It would appear therefore that the anion has a strong influence on the MALDI behavior of these salts. In order to investigate this further, three other laser dyes: R6G.ClO_4, R6G.Cl and R6G.BF_4, whose chemical structures are shown in Fig. 2.6, were tested and compared. The mass spectra obtained for R610.ClO_4 and R6G.ClO_4; R610.Cl and R6G.Cl; R610.BF_4 and R6G.BF_4 can be compared by examining Figs. 4.12 – 4.17.

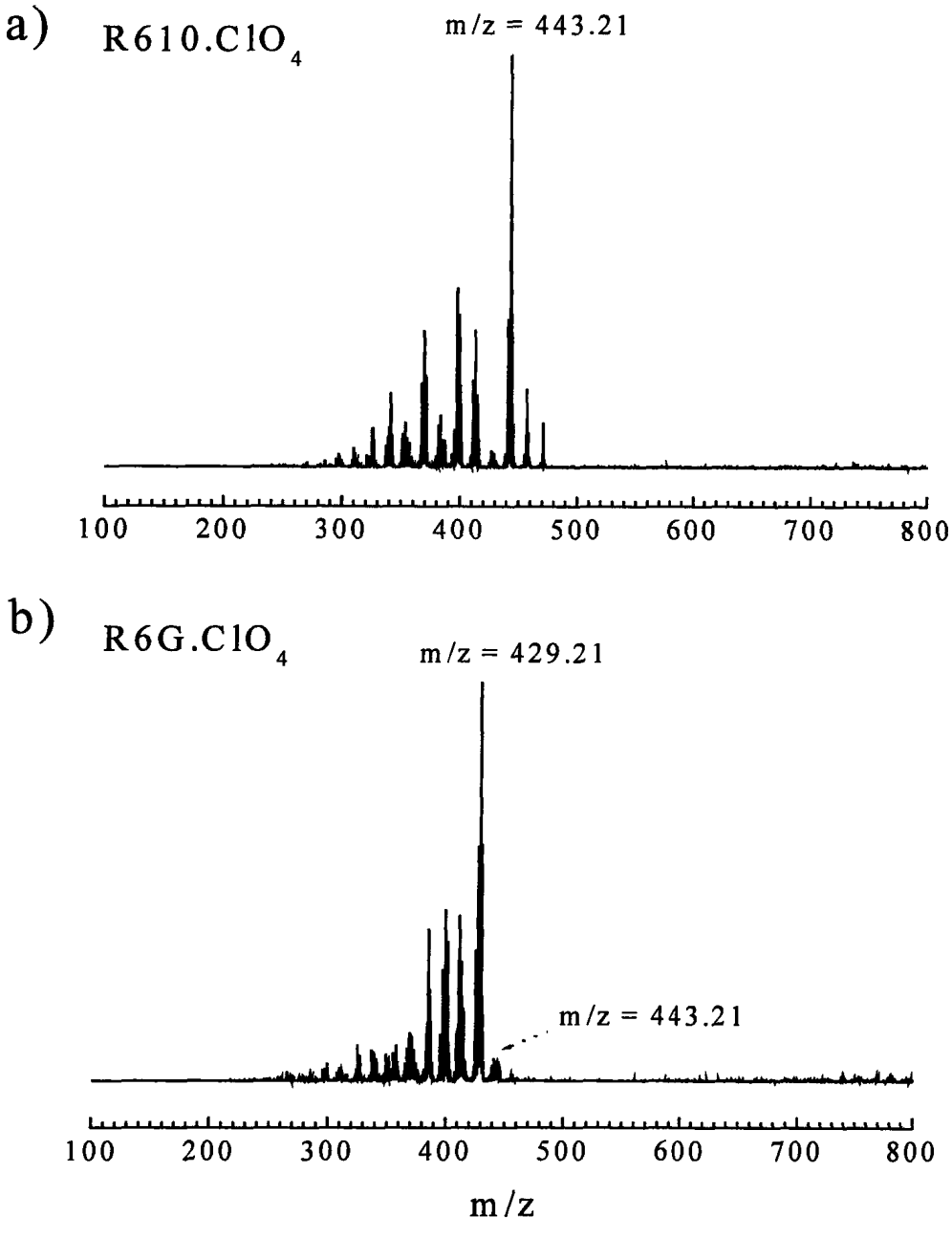

Figure 4.12: Visible-MALDI mass spectra taken in positive ion mode for a) R610.ClO_4 and b) R6G. ClO_4, between m/z = 30 and 800.

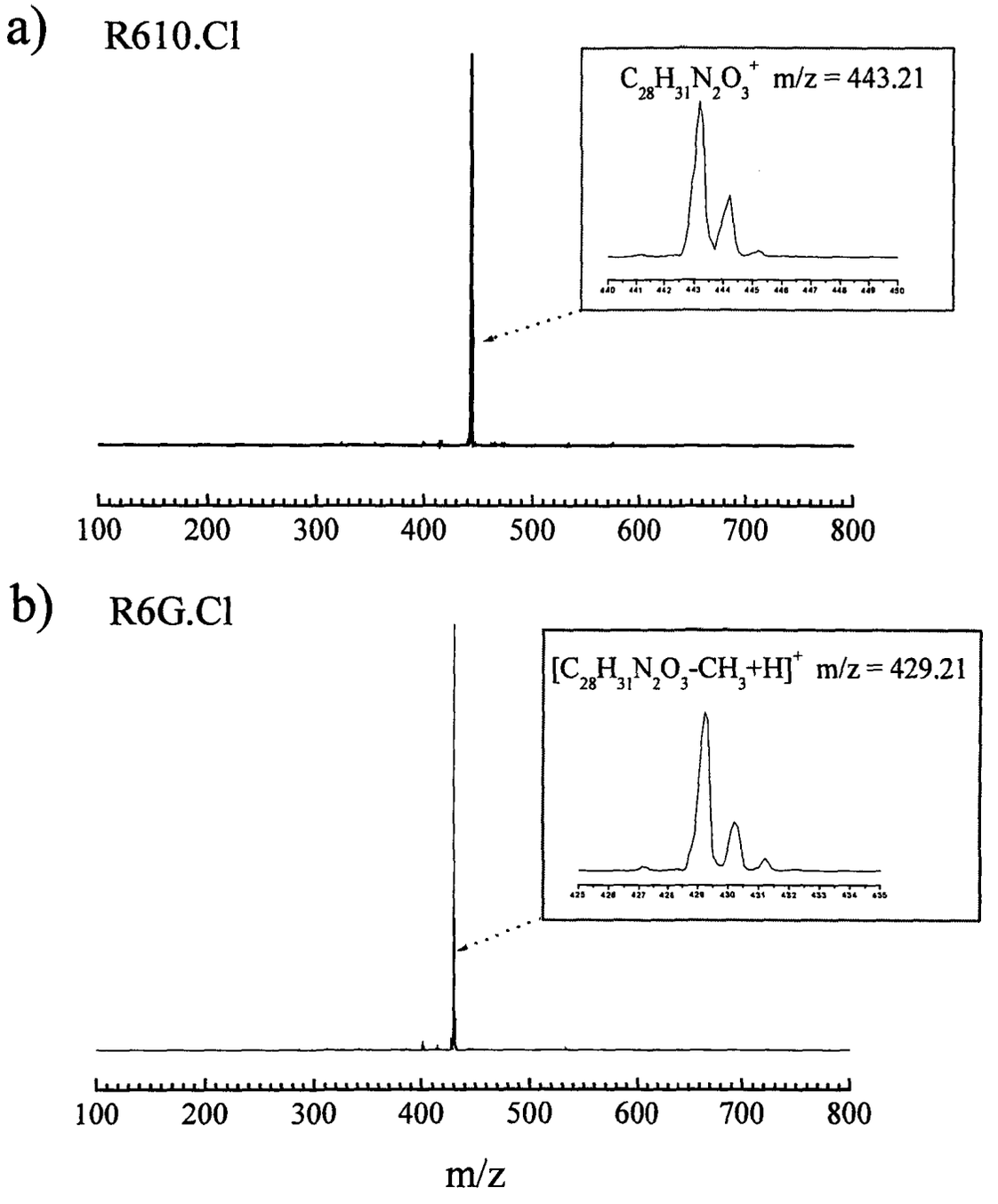

Figure 4.13: Visible-MALDI mass spectra taken in positive ion mode for a) R610.Cl and b) R6G.Cl, between m/z = 30 and 800.

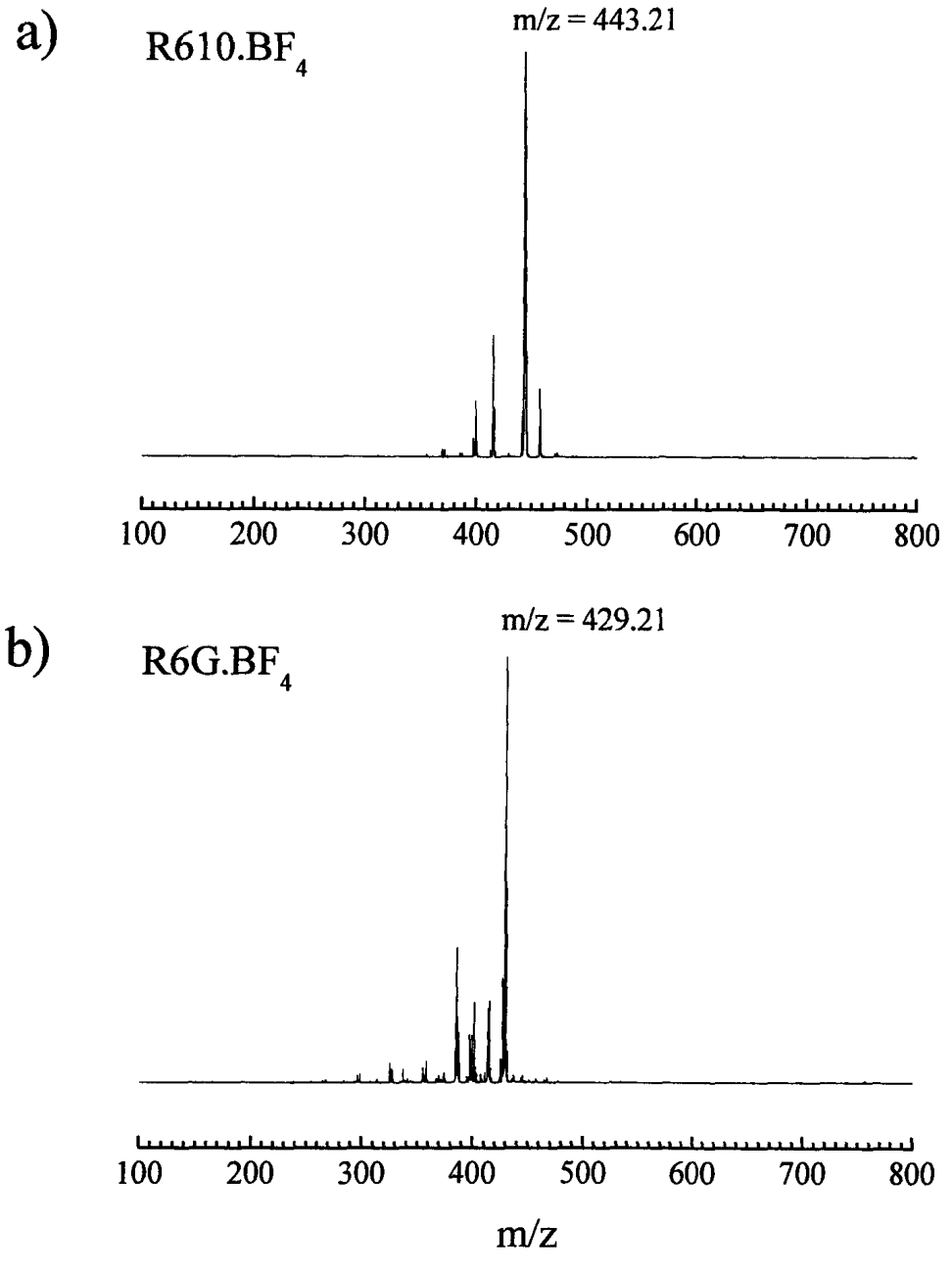

Figure 4.14: Visible-MALDI mass spectra taken in positive ion mode for a) $R610.BF_4$ and b) $R6G.BF_4$ between m/z = 30 and 800.

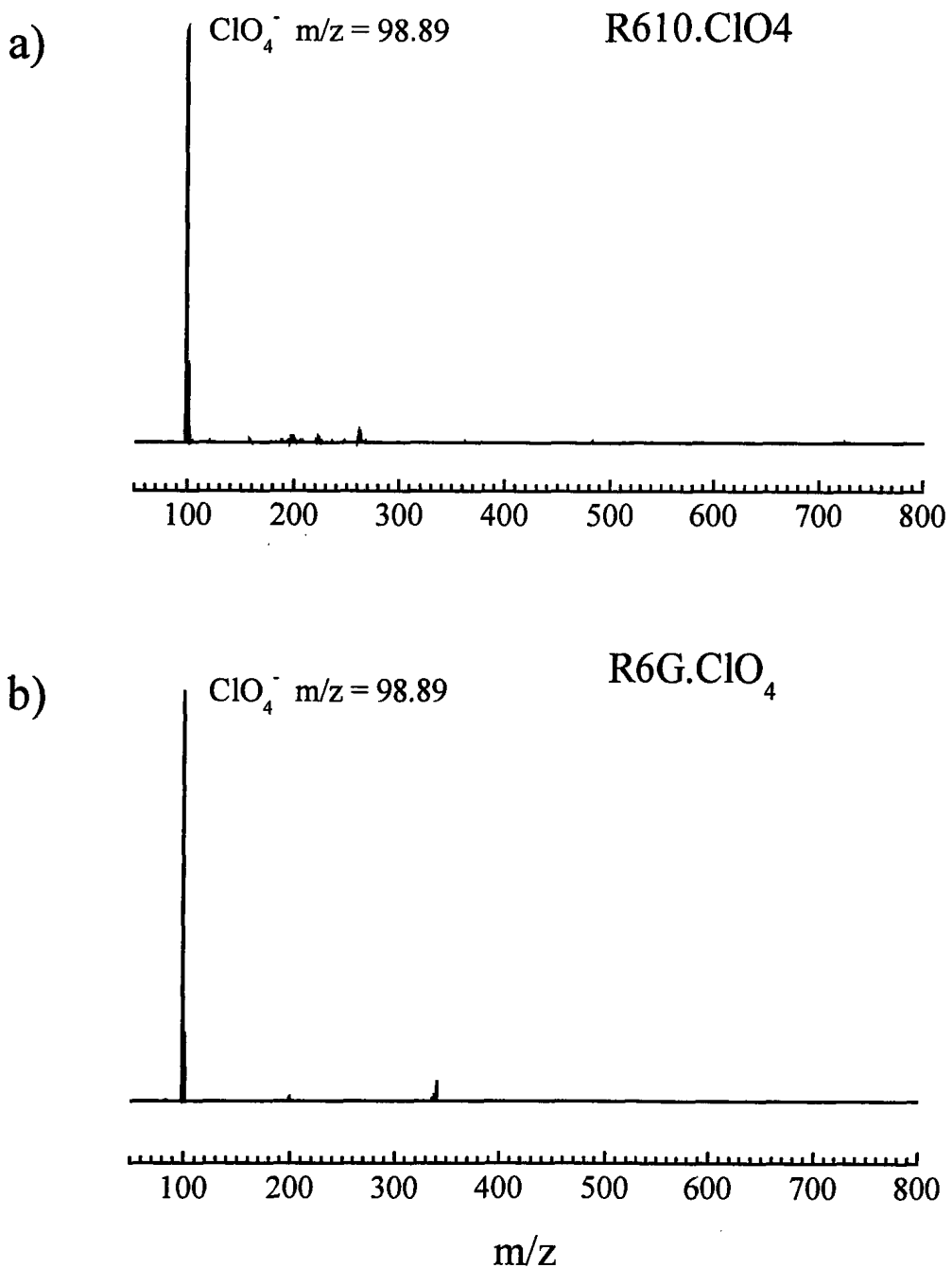

Figure 4.15: Visible-MALDI mass spectra taken in negative ion mode for a) R610.ClO4 and b) R6G.ClO4 between m/z = 30 and 800.

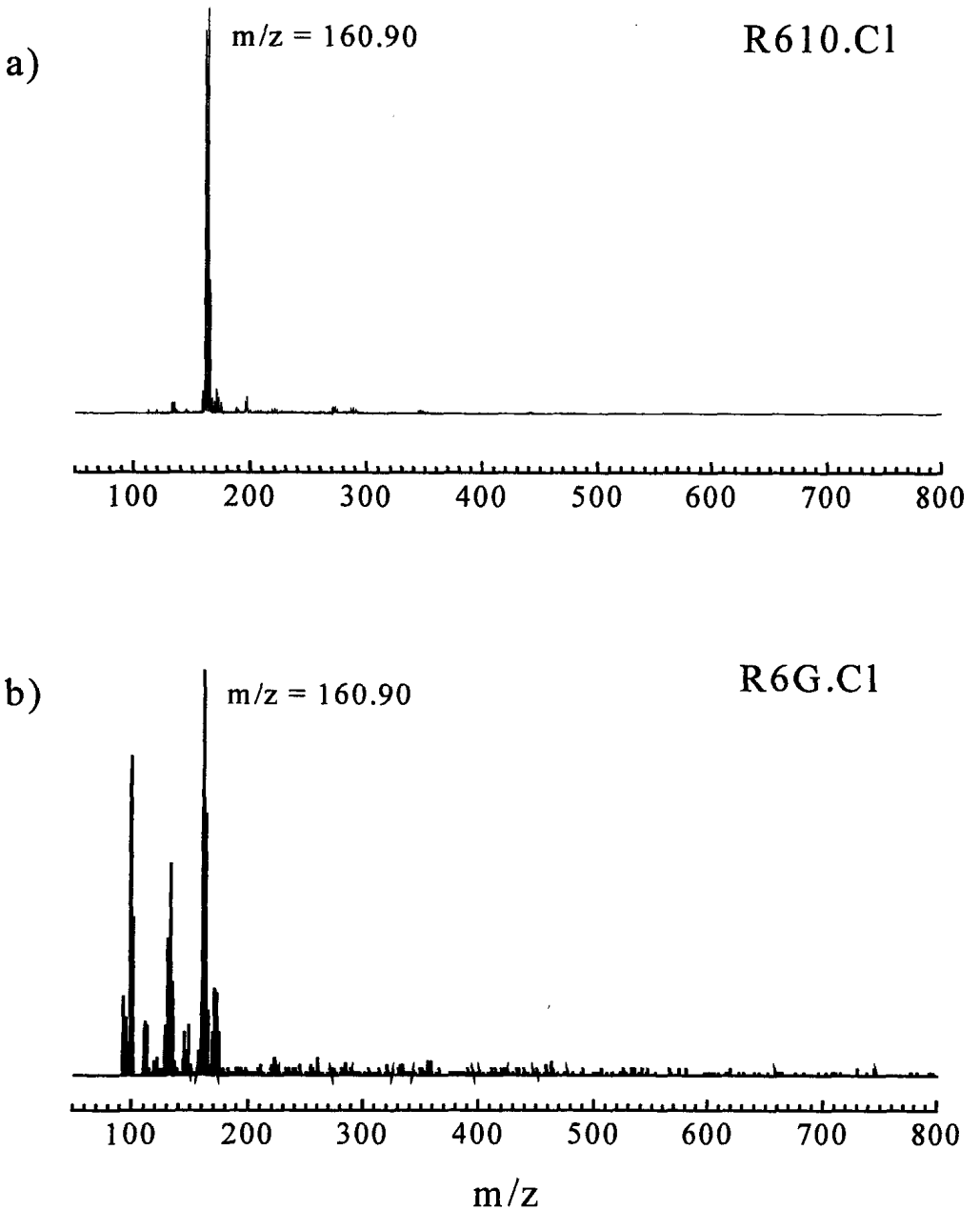

Figure 4.16: Visible-MALDI mass spectra taken in negative ion mode for a) R610.Cl and b) R6G.Cl between m/z = 30 and 800.

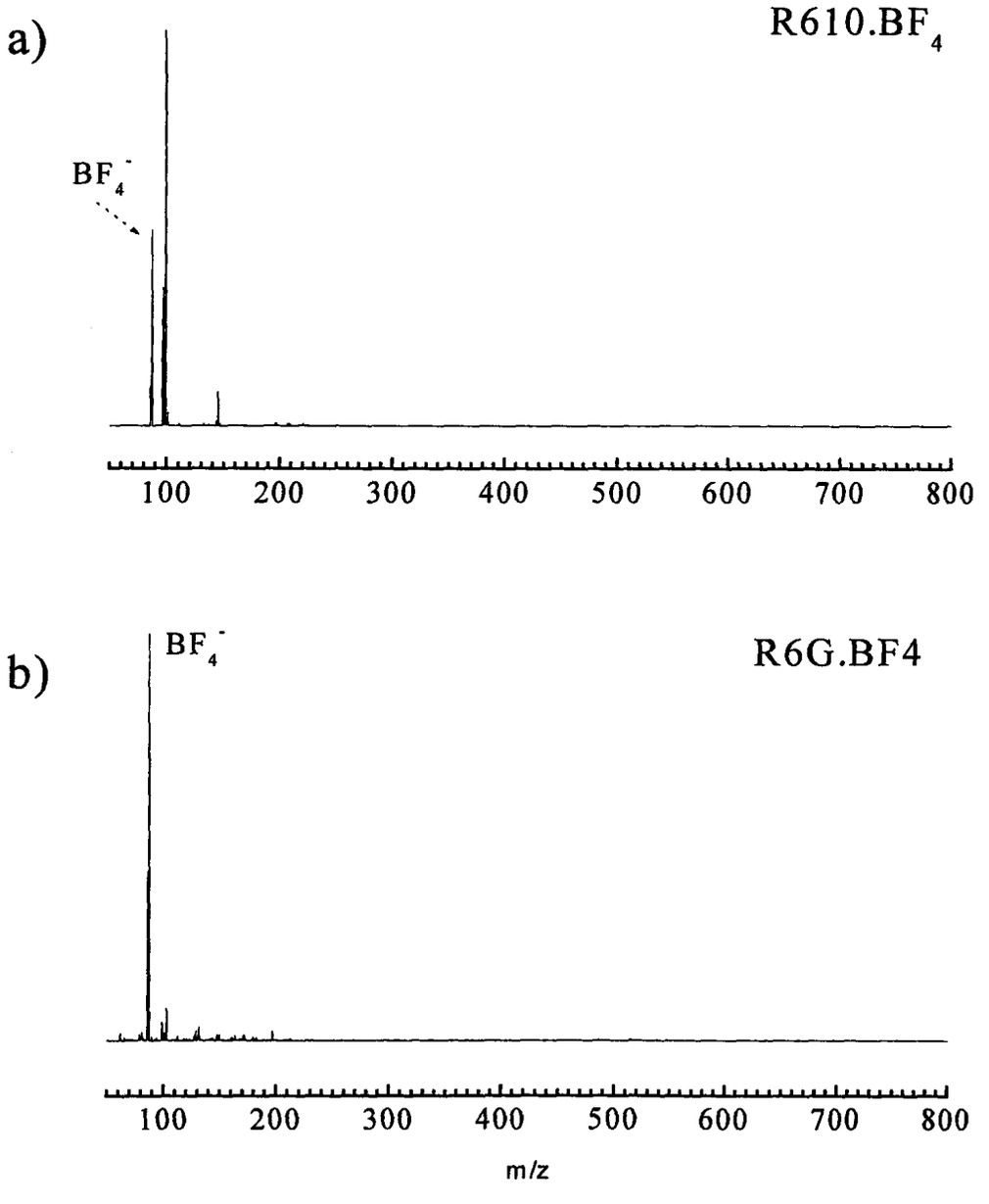

Figure 4.17: Visible-MALDI mass spectra taken in negative ion mode for a) R610.BF_4 and b) R6G.BF_4 between m/z = 30 and 800.

4.6.2. Discussion

It is very clear that the similarities between the MALDI mass spectra of R610.X and R6G.X (X = Cl^-, ClO_4^-, and BF_4^-), under 532 nm illumination must be due to the anion making up the dye salt. This is an interesting effect which merits further examination. It is unclear why the choice anion has such an important influence on the fragmentation patterns. It may have important implications if the effect is related to the structure and morphology of the matrix, where some anions favor the formation of preformed ions in the solid state as a prerequisite for MALDI activity.

4.6.3. Conclusions

Rhodamine dyes appear to be photolytically more stable than PM dyes, and of the Rhodamine dyes tested, the chloride salts yield the cleanest visible MALDI mass spectra in positive ion mode under 532 nm laser irradiation. R610.Cl has potential as a matrix for small molecular weight analytes. Due to extensive fragmentation, the other R610 salts may be better for heavier analytes. All three compounds need to be tested with a time-of-flight instrument to establish the upper mass range of those analytes that can be desorbed and ionized using 532 nm laser excitation.

Chapter 5: Rhodamine 575 as a matrix candidate

5.1. Overview

R575 is a neutral laser dye whose chemical structure as given by the dye manufacturer Exciton is shown in Fig. 2.7 [44]. The structure shown in Fig. 5.1 is the one described in reference 55. In these experiments, the laser dye was dissolved in a solvent to make solutions, so the chemical structure presented in Fig. 2,7 is more realistic.

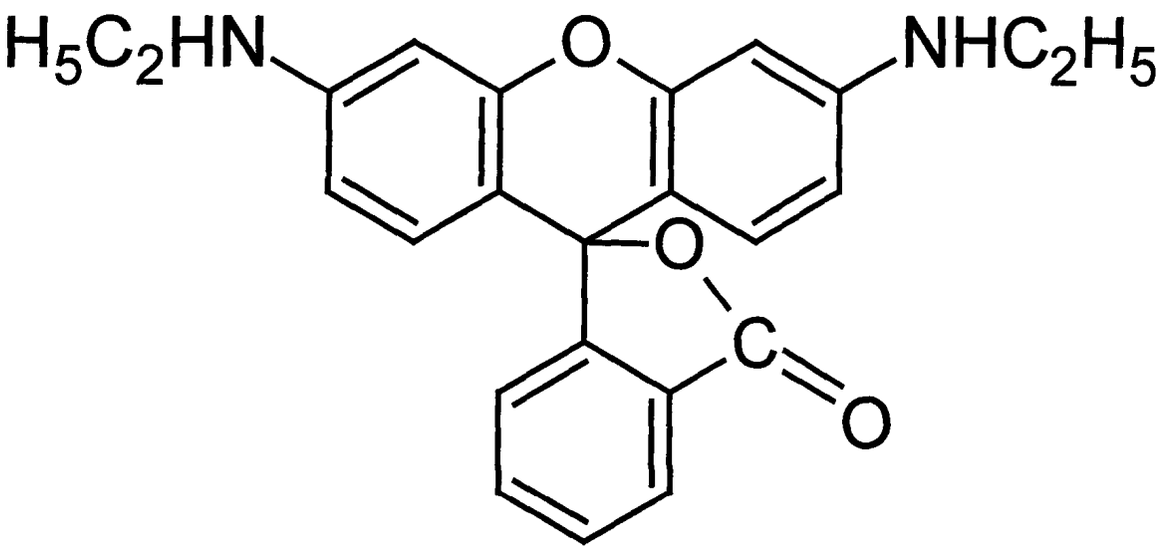

Figure 5.1: The chemical structure of R575 according to reference 55.

5.2. R575 as a matrix candidate

1. MALDI mass spectra of R575 without any co-deposited analyte

MALDI mass spectra of solid R575 are shown in Fig. 5.2. In positive ion mode (trace a)), the base peak of the mass spectrum is attributed to $[R575+H]^+$ at m/z = 415.012. Two isotopic features are also readily observed. Peaks due to $[R575+Na]^+$ and

$[R575+K]^+$ could also be readily assigned. The lower molecular weight peaks are most likely due to chemical fragmentation of the R575 molecule. For example, peaks 1, 2 and 3 are tentatively assigned to $[R575\text{-}CO_2\text{-}CH_3]^+$, $[R575\text{-}CO_2+H]^+$ and $[R575\text{-}2CH_3+3H]^+$. No signals could be readily detected in negative ion mode (trace b).

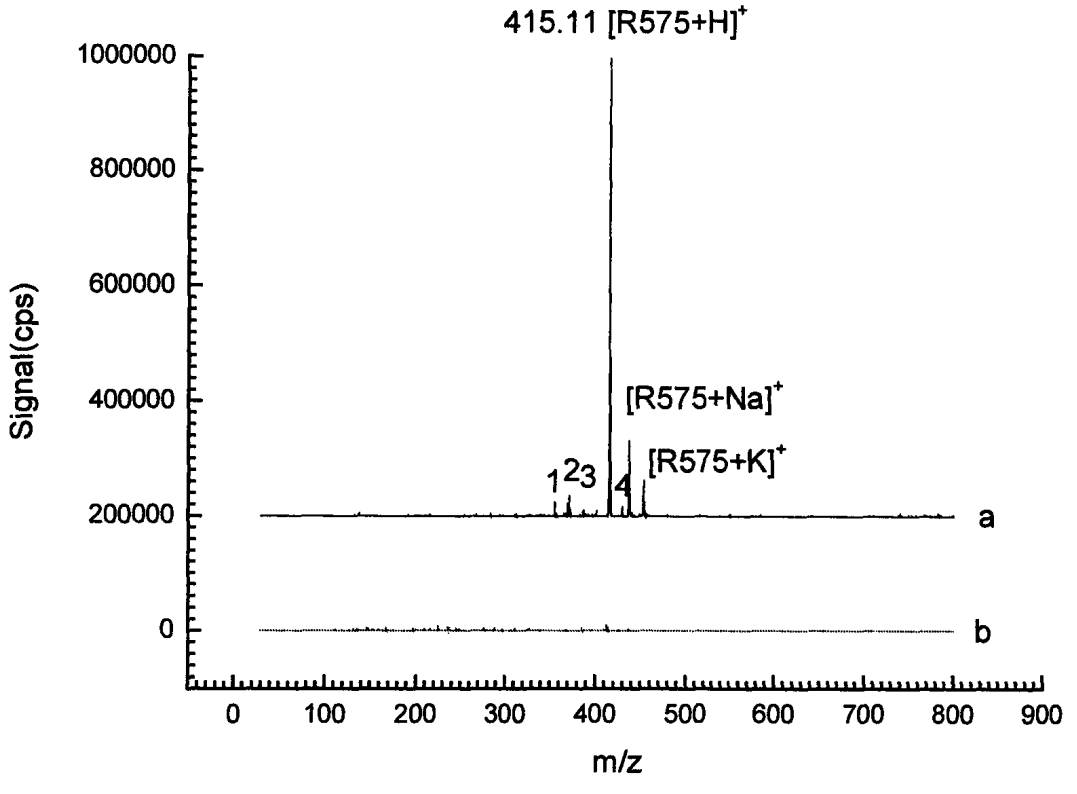

Figure 5.2: Mass spectra of solid R575 without any co-deposited analyte under 532 nm illumination between m/z = 30 and 800. Spectrum a), was acquired in positive ion mode. Peak 1, 2 and 3 are attributed to $[R575\text{-}CO_2\text{-}CH_3]^+$, $[R575\text{-}CO_2+H]^+$ and $[R575\text{-}2CH_3+3H]^+$, respectively, while peak 4 at m/z = 429 may be an R6G impurity. Spectrum b) was taken in negative ion mode.

2. R575 as a laser absorber in a binary matrix

(1) Positive ion mode

Protonated Dalargin (Dal) signals, $[Dal+H]^+$, were observed to be very weak when R575 and Dal were co-deposited in a molar ratio of 1000:1 as the matrix and analyte, respectively (spectrum 2 in Fig. 5.3). Under acidic conditions R575 is expected to be a weak conjugate acid: $R{=}NHC_2H_5^+$, with proton-donating capability. R575 efficiently absorbs light at 532 nm. It is also absorbs efficiently at this wavelength under acidic and basic conditions. Thus a series of experiments were carried out to improve the analyte signal by forming a binary matrix of R575 and different acidic compounds to enhance its proton-donating capabilities.

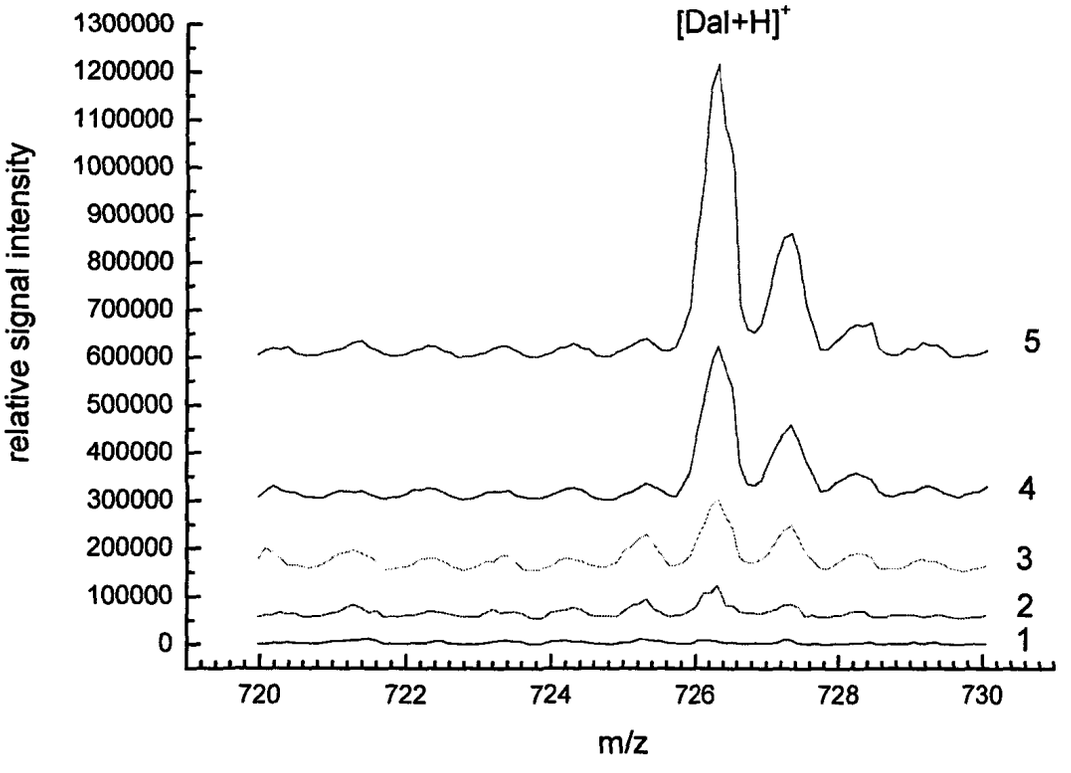

Figure 5.3: Trace 1: MALDI mass spectrum of R575 only in the mass region corresponding to protonated Dalargin; trace 2) molar ratio of R575: Dalargin = 1000:1; trace 3: molar ratio of R575: TFA: Dalargin= 1000:508:1; trace 4) molar ratio of R575: CHCA: Dalargin = 1000:537:1 and trace 5: molar ratio of R575: HCl: Dalargin = 1000:500:1.

As noted in Chapter 4, the chloride salt of the Rhodamine dyes produced the cleanest mass spectra in positive ion mode. Therefore, one of the proton donors considered was hydrochloric acid (HCl). Other proton donors tried were trifluoroacetic acid (TFA, pKa=0.52) [56] and α-cyano-4-hydroxycinnamic acid (CHCA, pKa=1.17 ± 0.31)[57]. As shown in Fig.5.4 these acids, when combined with R575, did not create additional chemical fragments in positive ion mode, or inhibit the formation of $[R575+Na]^+$ and $[R575+K]^+$. In each case, the resultant MALDI mass spectrum in positive ion mode detection was found to be very clean; that is, with minimal

fragmentation. Fig. 5.3 shows that under identical conditions of acidity before mixing, HCl was the most effective proton donor, followed by CHCA and TFA. Furthermore, HCl increases the solubility of R575 in ethanol.

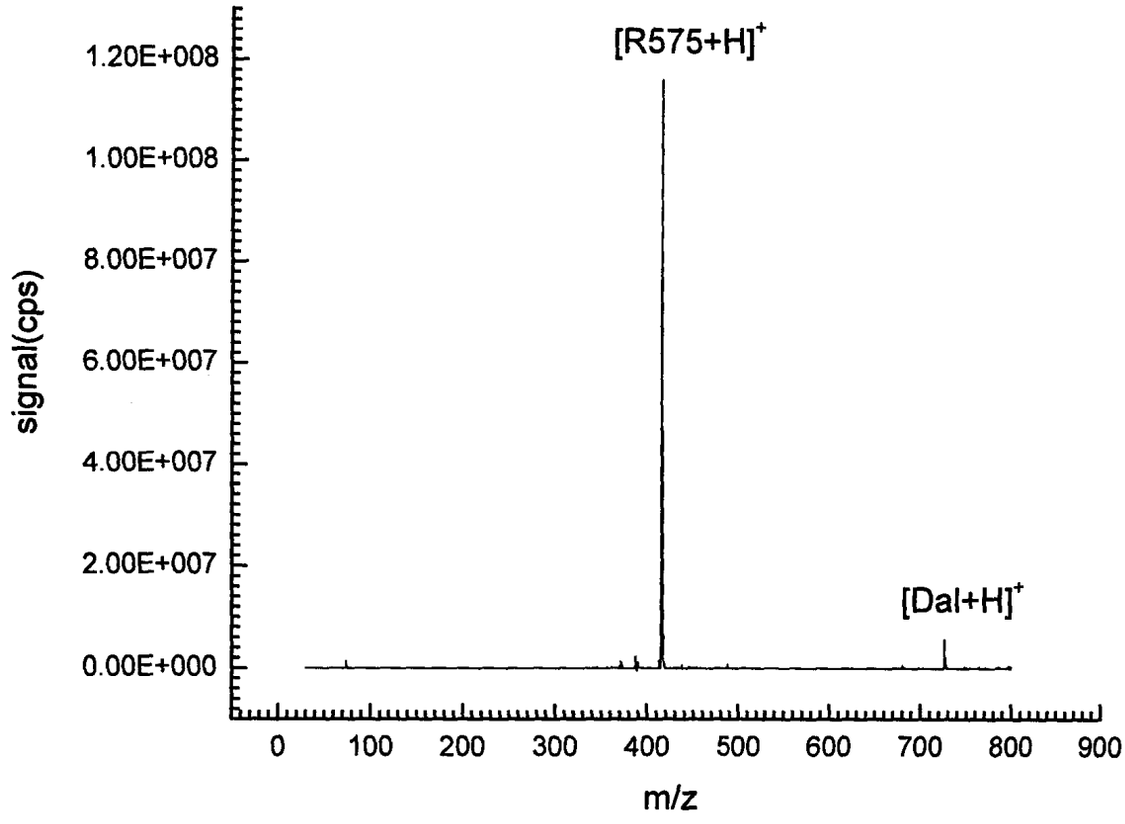

Figure 5.4: Positive ion mode mass spectrum from m/z = 30 to 800 of the sample containing R575+HCl+Dal (12:6:1 in molar ratio). In this mass spectrum, the signals due to $[R575+Na]^+$ and $[R575+K]^+$ are inhibited by HCl. The positive ion mode mass spectra obtained using CHCA or TFA as proton donors are similar to this spectrum.

The signal-to-noise ratio of the visible-MALDI spectrum of Bradykinin shown in Fig. 5.5 obtained by using a binary matrix R575+HCl (2:1 in molar ratio) is similar to that obtained for Dalargin.

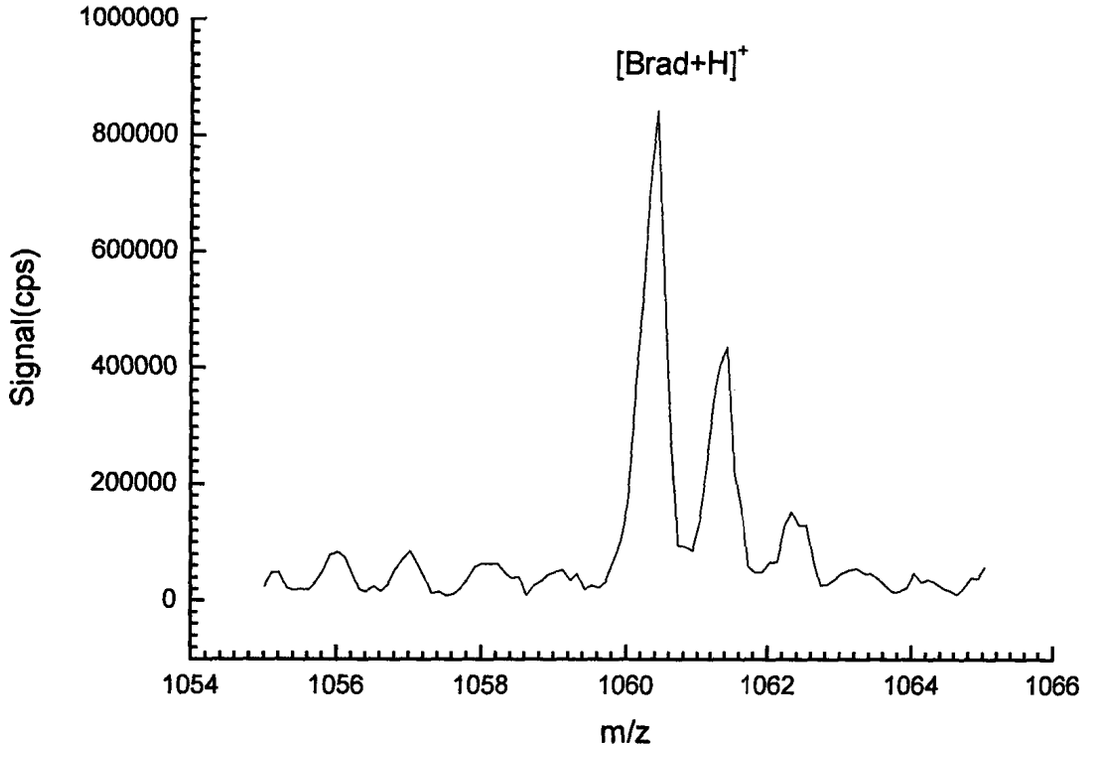

Figure 5.5: Visible-MALDI mass spectrum of protonated Bradykinin, produced by a sample containing R575:HCl:Bradykinin in a molar ratio of 1000:500:1.

A series of spectra containing equal amounts of R575 and Dalargin but different amounts of HCl were recorded. As shown in Fig.5.6a) the S/N of the $[Dal+H]^+$ signal maximized when the R575:HCl:Dal molar ratio was 100:50:1. However, as shown in Fig. 5.6b) the signal of $[R575+H]^+$ increased ~linearly with increasing HCl concentration.

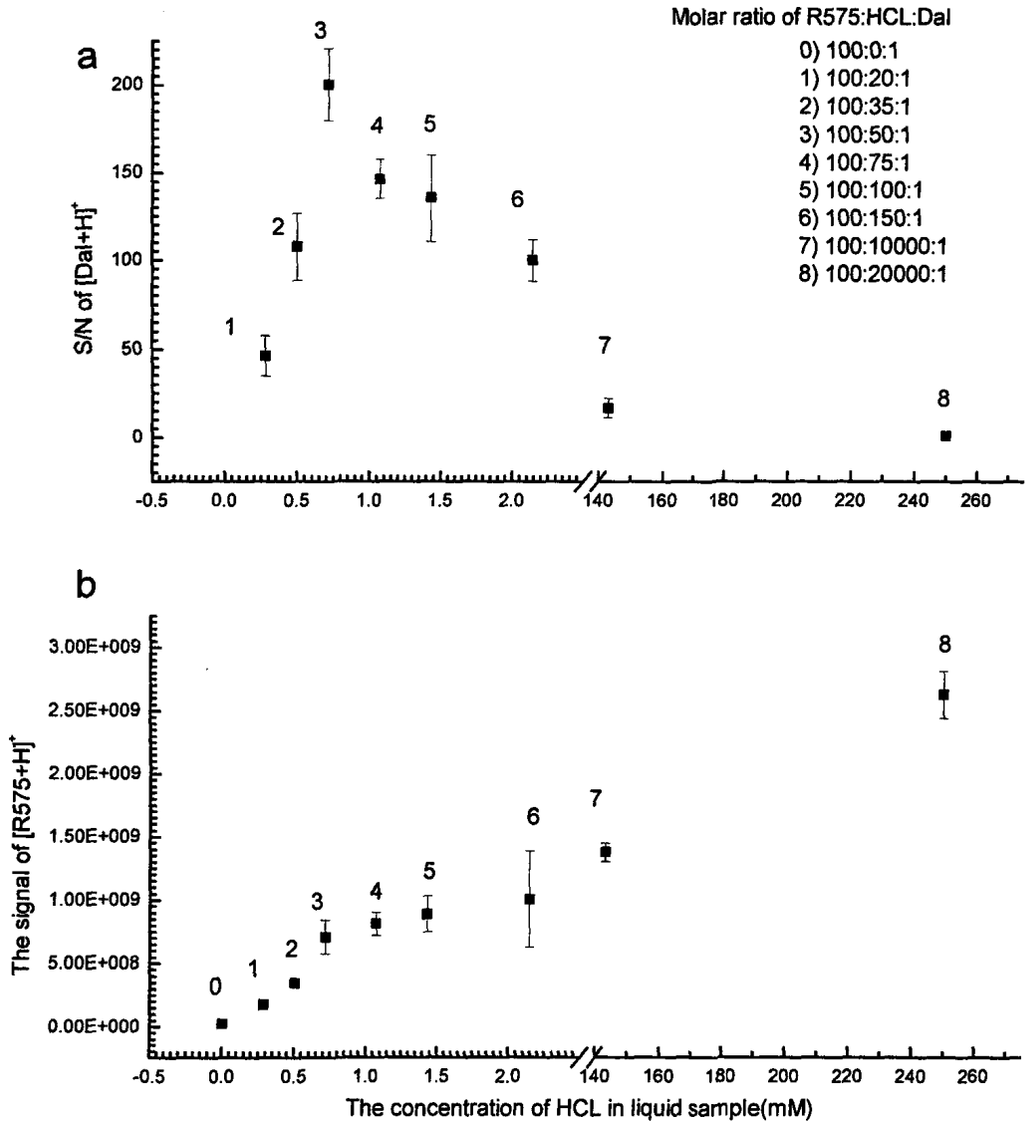

Figure 5.6: a) A plot of the signal-to-noise ration (S/N) of the protonated Dalargin signal as a function of HCl concentration; b) A plot of the protonated matrix signal as a function of HCl concentration.

(2) Detection limit

A detection limit for Dalargin of $(2 \pm 1) \times 10^{-13}$ mol was obtained by extrapolating a plot of signal-to-noise ratio (S/N) versus absolute analyte concentration obtained from a series of samples where the amount of R575 and HCl (molar ratio = 2:1) was held constant but the analyte concentration was changed (Fig. 5.7). A similar detection limit was found for Bradykinin.

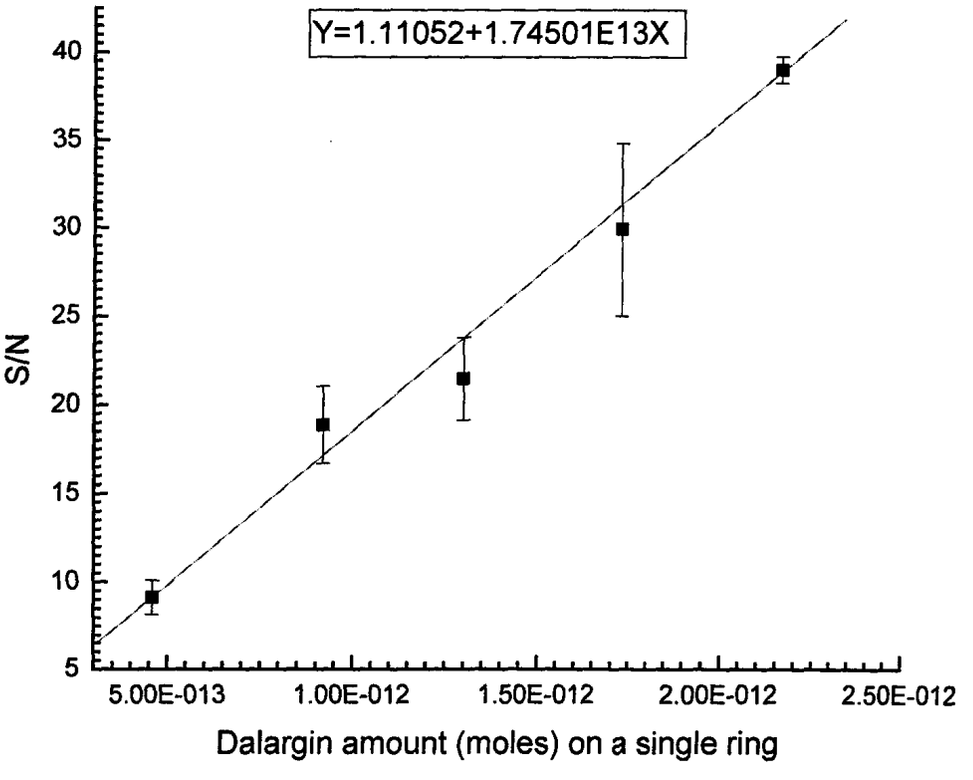

Figure 5.7: A plot of the signal-to-noise ratio versus the amount of Dalargin in the laser ablation ring. The detection limit for Dalargin in the binary matrix of R575+HCl (molar ratio of R575:HCl = 2:1) was determined to be $(2.23 \pm 1) \times 10^{-13}$ mol.

The signal mass peak used to obtain the S/N ratio was that of $[Dal+H]^+$ at m/z = 726.44, while the noise was determined by measuring the background signal in the mass range between m/z =720 and 724. A value of S/N =5 was considered as a minimum value that would allow the peak signal to be clearly differentiated from the noise.

(3) Negative ion mode

Since the $[R575+H]^+$ signal could be enhanced by the addition of a proton donor, it was anticipated that R575 would be a good matrix for detecting acidic analytes in negative ion mode. Indeed, as shown in Fig. 5.8 deprotonated Bentazone was easily detected in negative ion mode using only R575 as the matrix.

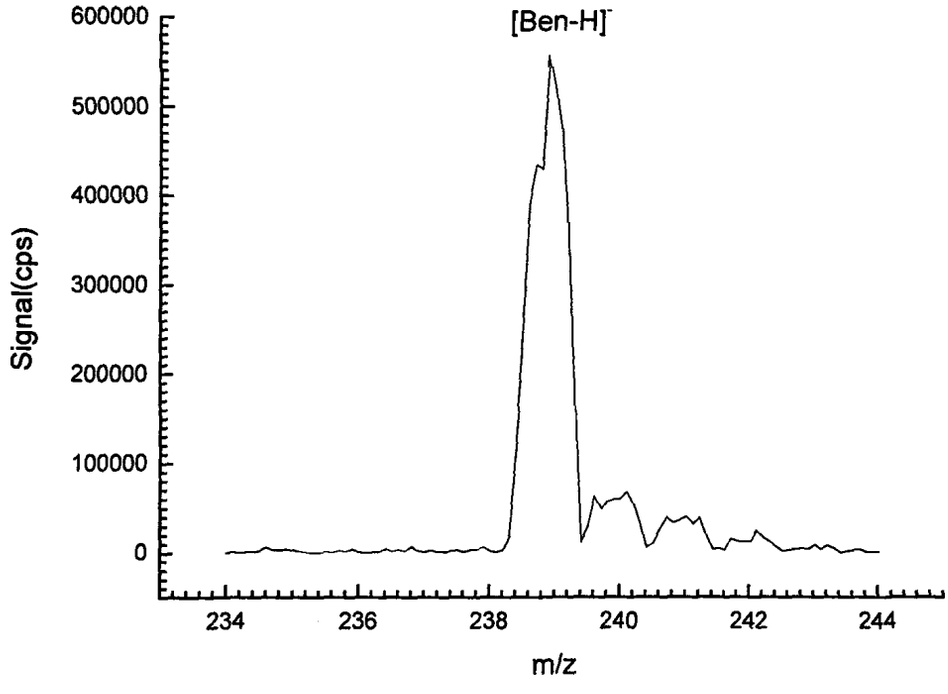

Figure 5.8: Deprotonated Bentazone peak obtained in negative ion mode detection obtained from ~6×10^{-13} mole Bentazone in a matrix containing R575+Bentazone (molar ratio R575:Bantazone = 1200:1)

As shown in Figs.5.9 - 5.11 the deprotonated Bentazone signal intensity could be dramatically increased by adding NaOH into the matrix. A molar ratio of R575: NaOH: Bentazone = 1200:10:1 produced the cleanest spectrum, (Fig. 5.9; sample 3). In this way, analyte amounts as small as 12 fmol could be detected, (Fig.5.12). It is believed that deprotonated Bentazone formation is enhanced by the addition of NaOH because R575 has a higher sodium affinity than proton affinity. Bentazone is acidic and therefore reacts with NaOH to form sodium Bentazone[58] and H_2O. R575 is then sodiated to form $[R575+Na]^+$, thereby enhancing the $[Ben-H]^-$ signal. The $[Ben-H]^-$ signal disappeared however in Fig.5.11 (sample 9) when excess NaOH was used, because this effectively minimized the dominance of the reaction between R575 and sodium Bentazone.

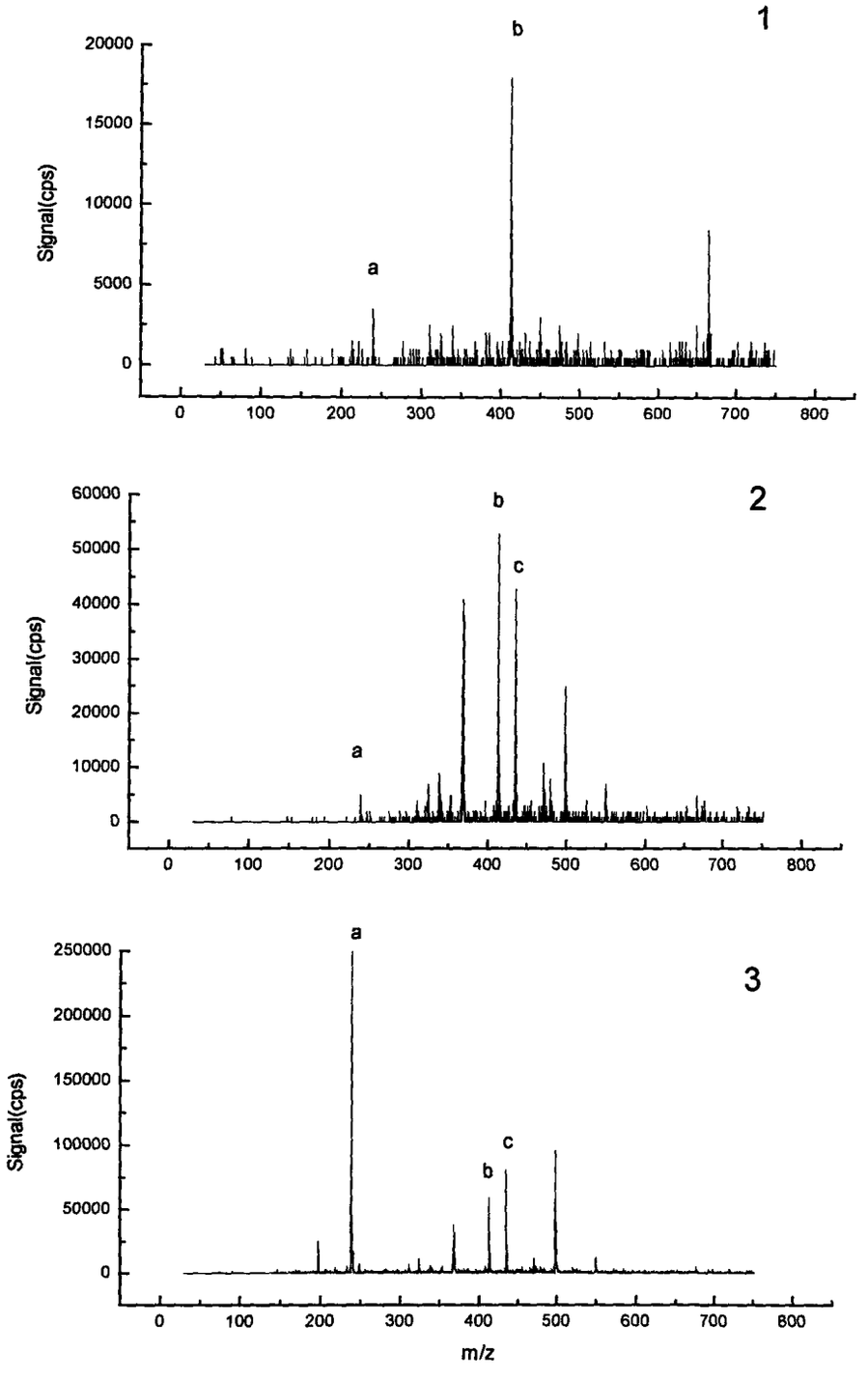

Figure 5.9: Three negative ion mode mass spectra obtained from 1: a sample of R575:Bentazone (molar ratio = 1200:1); 2: a sample R575:NaOH:Bentazone (molar ratio = 1200:5:1); and 3: a sample of R575:NaOH:Bentazone (molar ratio = 1200:10:1). The features labeled a, b and c are attributed to $[Ben-H]^-$, $[R575-H]^-$ and $[R575-2H+Na]^-$, respectively.

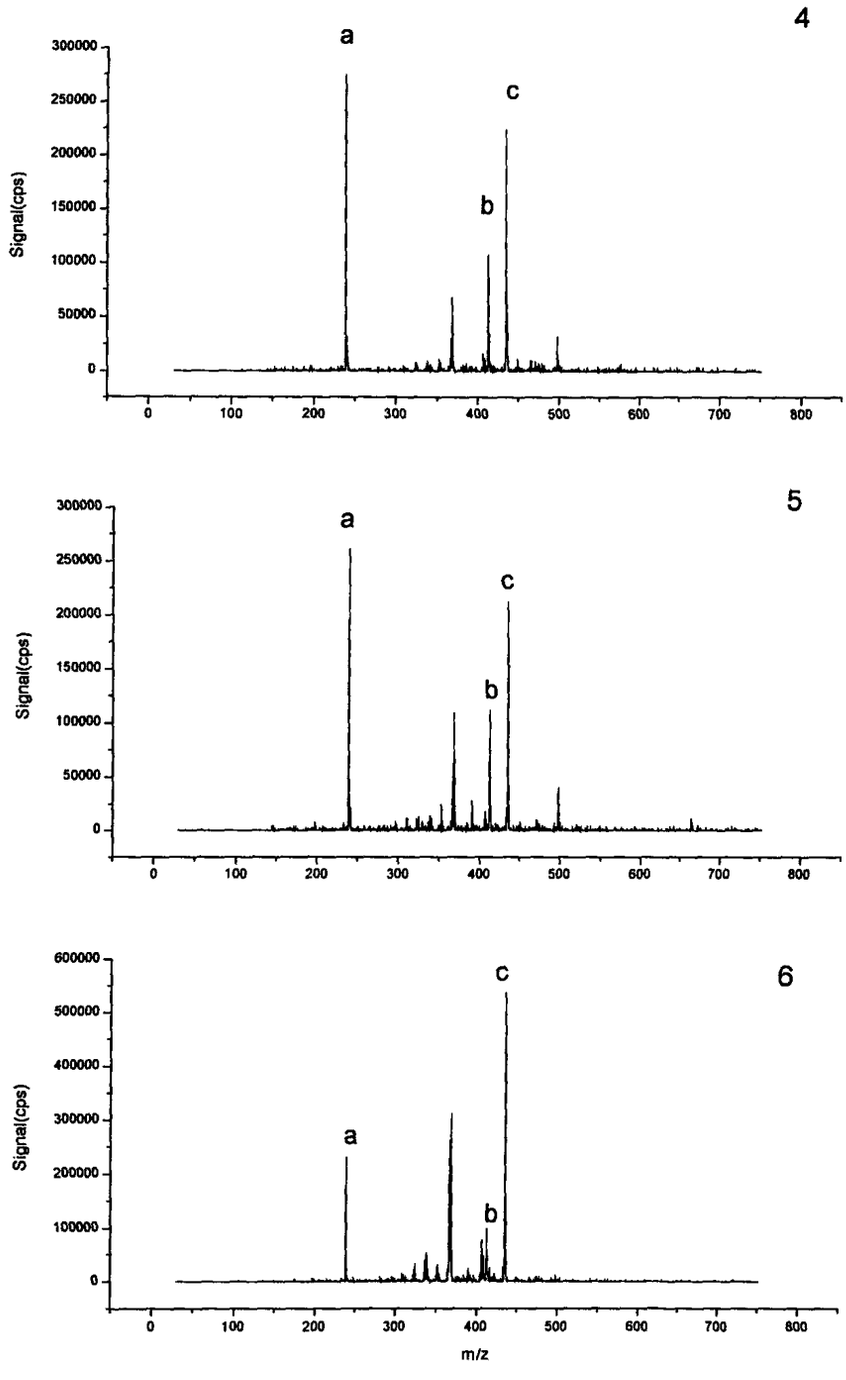

Figure 5.10: Three negative ion mode mass spectra obtained from 4: a sample of R575:NaOH:Bentazone (molar ratio = 1200:15:1); 5: a sample of R575:NaOH:Bentazone (molar ratio = 1200:20:1); and 6: a sample of R575:NaOH:Bentazone (molar ratio = 1200:50:1). The features labeled a, b and c are attributed to $[Ben-H]^-$, $[R575-H]^-$ and $[R575-2H+Na]^-$, respectively.

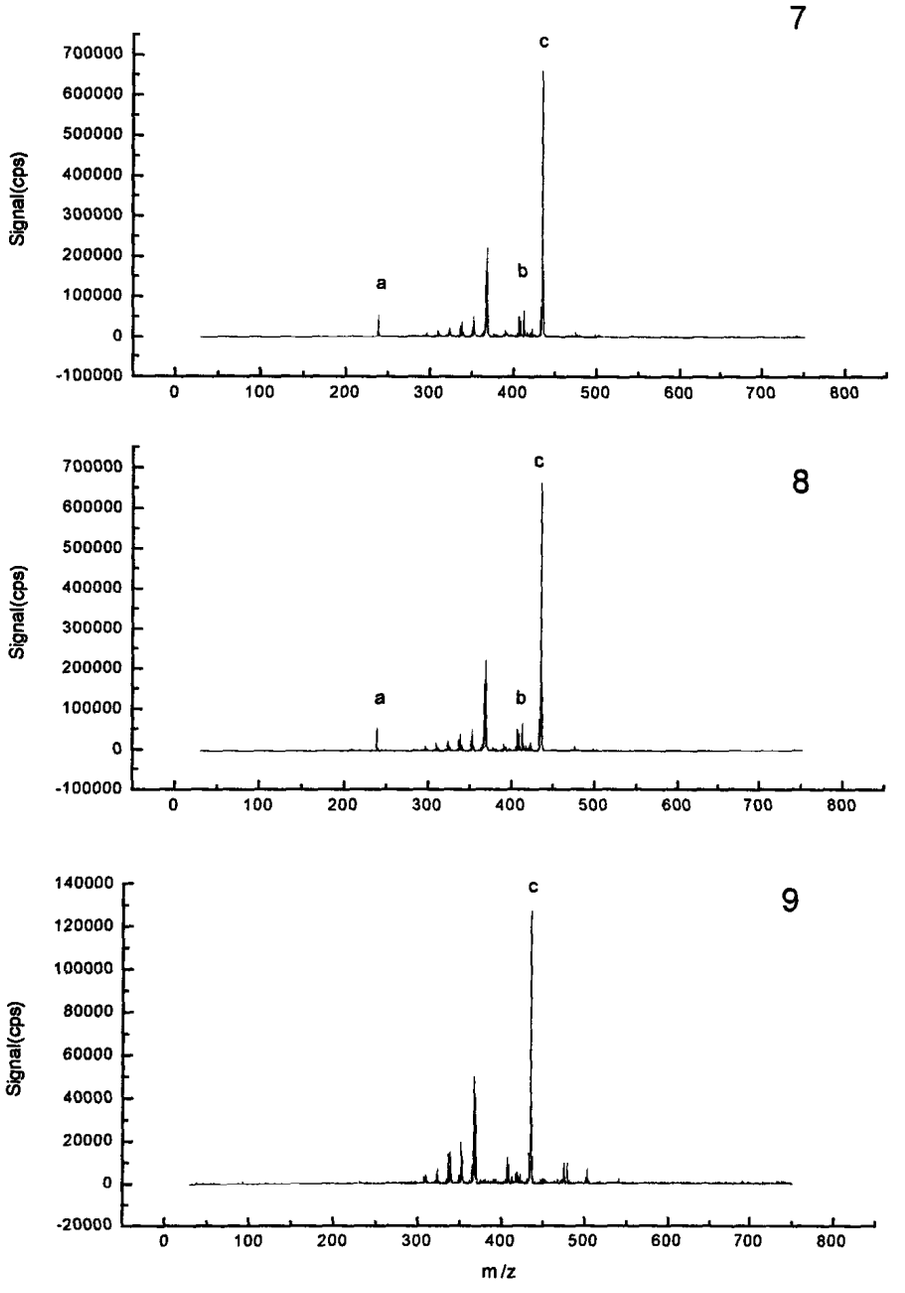

Figure 5.11: Three negative ion mode mass spectra obtained from 7: a sample of R575:NaOH:Bentazone (molar ratio = 1200:100:1); 8: a sample of R575:NaOH:Bentazone (1200:500:1); and 9: a sample of R575:NaOH:Bentazone (molar ratio = 1200:2000:1). The features labeled a, b and c are attributed to $[Ben-H]^-$, $[R575-H]^-$ and $[R575-2H+Na]^-$, respectively.

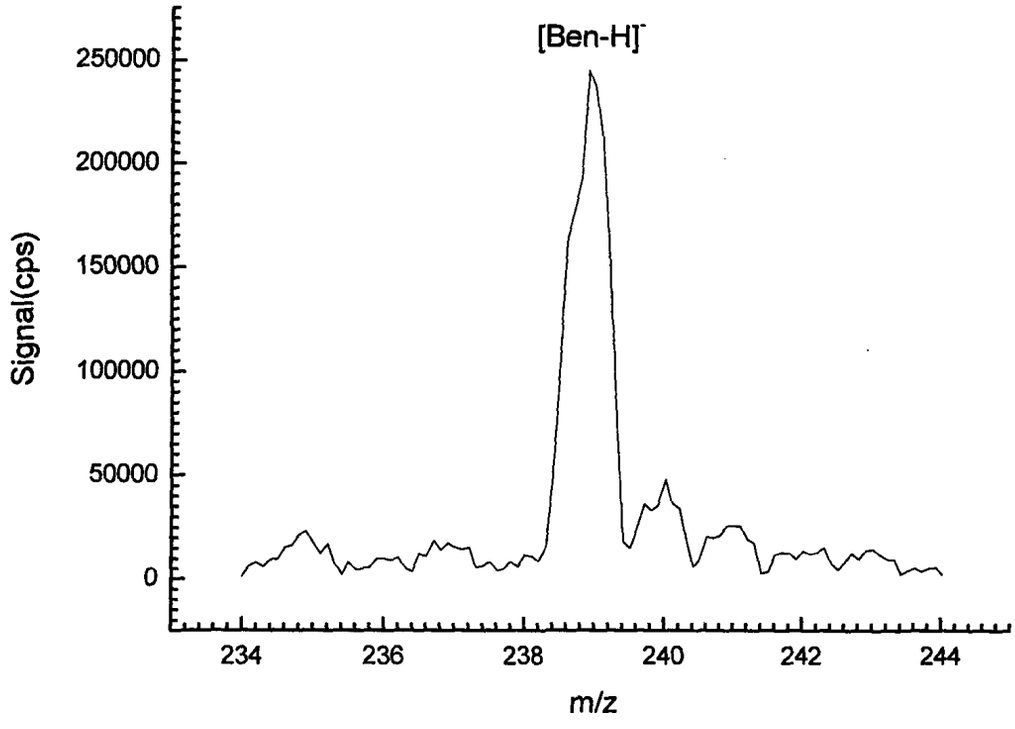

Figure 5.12: Deprotonated Bentazone peak, the signal of ~1.2 × 10^{-14} mole Bentazone in an ablation ring, produced by the sample containing R575+NaOH+Bentazone (1200:10:0.02 in molar ratio)

3. Cationization

Typically, carbohydrates cannot be ionized by protonation or depronation in MALDI mass spectrometry because they usually lack basic or acidic sites. They can however often be ionized by cationization due to the ubiquitous presence of alkali metal cations, such as Na^+ and K^+ from glassware and impurities in the sample[59]. Analyte

cationization rates depend on the cation affinity of the matrix laser absorber[60]. Specifically, analyte cationization will be inefficient if the laser absorber has a higher cation affinity. The signals due to $[R575+Na]^+$ and $[R575+K]^+$ in Fig.5.2 show that R575 can be easily cationized by alkali impurities. Therefore, in these experiments neutral compounds will be cationized using an excess concentration of an alkali source, for example, sodium trifluoroacetate (NaTFA).

Fig. 5.13 shows that a binary matrix of R575+NaTFA can ionize neutral compounds, Lovastatin (Lov) and Erythromycin (Ery) which are not easily cationized by the alkali impurities in a matrix containing R575 due to high alkali affinity of R575. The NaTFA additive first sodiates the R575. The excess NaTFA then ionizes Lov and Ery. A binary matrix of R575+NaTFA (in a molar ratio = 1.2:1) can be used to detect $\sim 6\times10^{-12}$ mol of Erythromycin (Fig.5.14) and $\sim 6\times10^{-10}$ mol of Lovastatin (Fig.5.15).

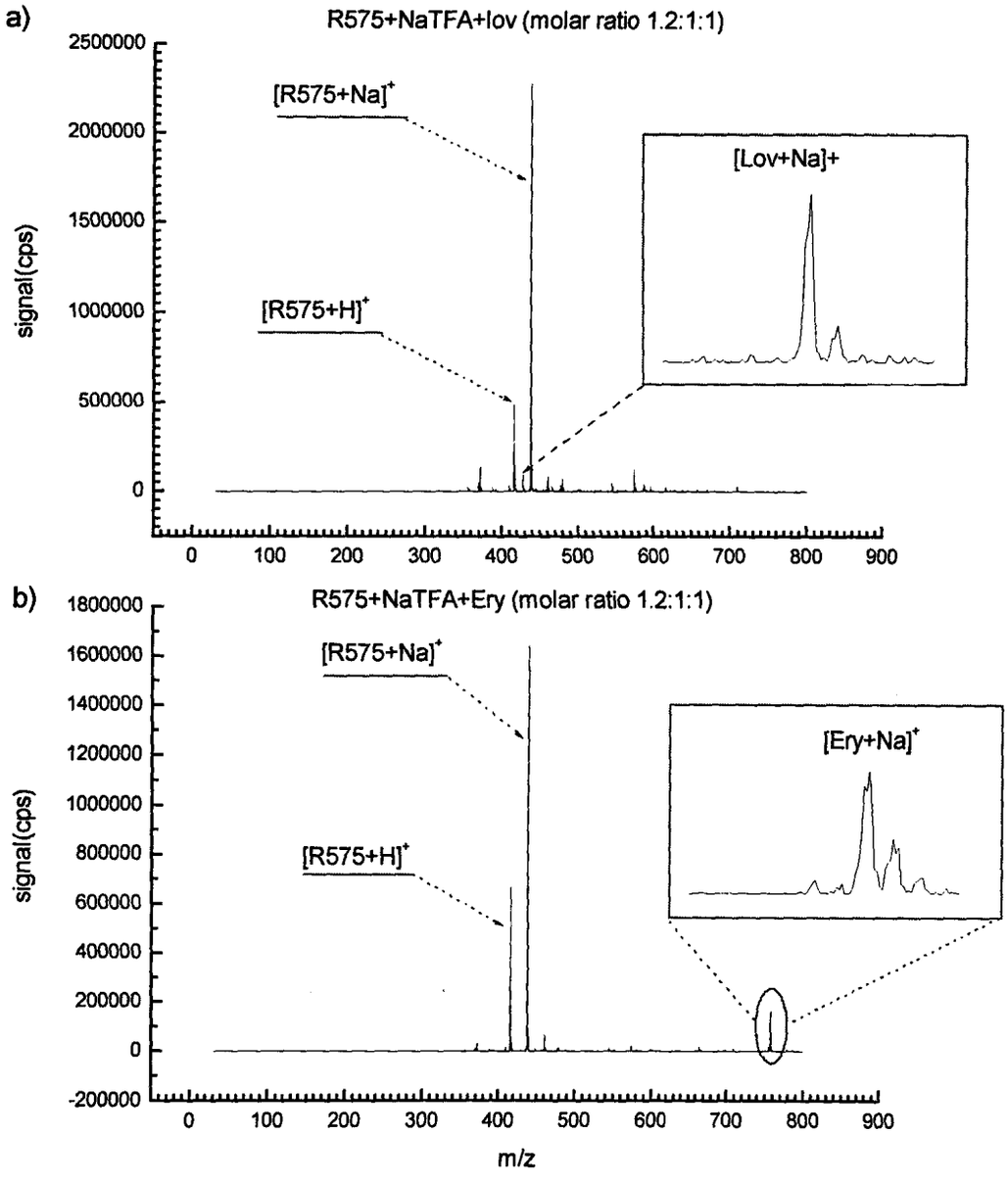

Figure 5.13: Positive ion mode visible-MALDI mass spectra between m/z = 30 and 800 of a sample containing a) R575:NaTFA:Lov (molar ratio = 1.2:1:1) and b) R575:NaTFA:Ery (molar ratio = 1.2:1:1)

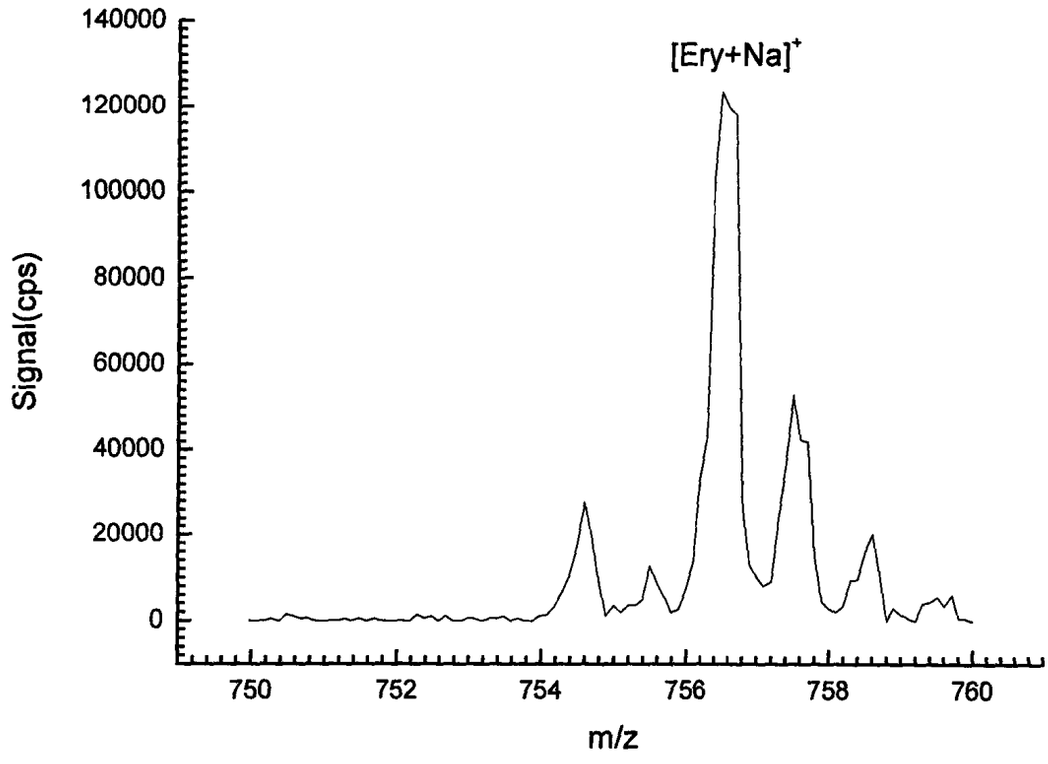

Figure 5.14: Visible-MALDI mass spectrum of ~ 6×10^{-12} mol of sodiated Erythromycin produced by a sample containing R575:NaTFA:Erythromycin (molar ratio = 1.2:1:1). The smaller lower mass peaks are attributed to impurities in the Erythromycin sample (purity ~ 95%).

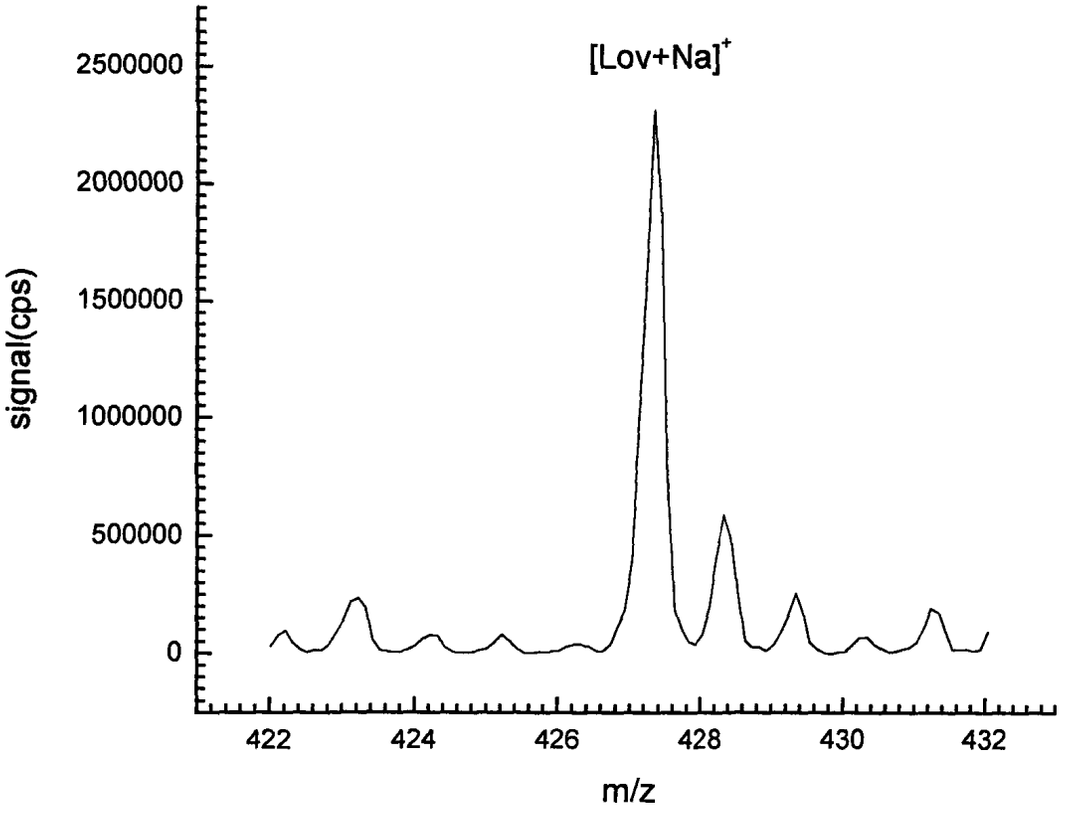

Figure 5.15: Visible-MALDI mass spectrum of ~ 6×10^{-10} mol of sodiated Lovastatin produced by a sample containing R575:NaTFA:Lovastatin (molar ratio = 1.2:1:1).

4.Laser fluence study

The experimental method used to study the dependence of the MALDI analyte signal intensity as a function of laser fluence has been reported elsewhere[38]. The log-log plots for the analyte (Dal) and matrix R575 (HCl) signals are shown in Fig. 5.16. The slopes found for the matrix and analyte are ~4 and 3, respectively. These slopes are lower than those found for Coumarin dyes[38] as a matrix for visible MALDI, and for conventional matrices under UV illumination[61, 62]. Thermal desorption and ionization[63]

are highly dependent on laser fluence[62, 63]. Many models for MALDI assume that the absorbed laser energy is converted to heat which leads to desorption. In this context a lower slope in the power plot for R575 means that the ionization process requires more photons than other matrices. One reason for this may be rapid radiative relaxation of R575 after it has been pumped to its S_1 excited state[10] by the 532 nm laser irradiation. Thus, more energy is required to achieve sufficient heating of the matrix for desorption and ionization. At the same time, R575 produces few chemical fragments as a result of this efficient relaxation pathway.

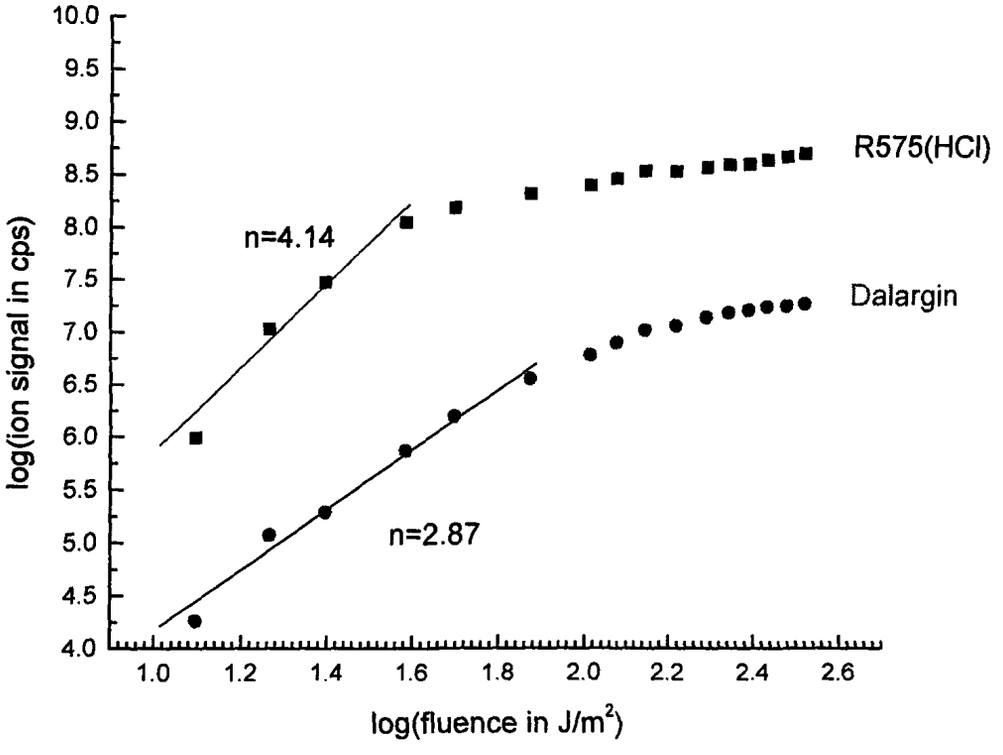

Figure 5.16: Log-log plot of the ion signals of $[R575+H]^+$ and $[Dal+H]^+$ versus laser fluence from 12 to ~ 269 J/m^2 at 532 nm.

5.3. Conclusions

R575 combined with an acid such as HCl or CHCA, or a base such as NaOH has been shown in this work to be an efficient visible-MALDI matrix under 532 nm laser irradiation. This amphoteric matrix can be used to detect small molecular weight basic and acidic compounds in positive and negative ion modes, respectively. The main advantages of using R575 are that it efficiently absorbs 532 nm light, and can serve as a good proton donor or acceptor. R575 as laser absorber combined with NaTFA as a sodium donor can also ionize small neutral compounds by cationizaiton. The study here suggests that the MALDI mechanism at low fluences is thermal in nature similar to that found for UV and IR-MALDI. However, higher fluences are required when using R575 as a matrix most likely due to efficient radiative relaxation. Although the upper mass range of analytes that can be desorbed and ionized using R575 visible-MALDI remains unknown due to the limited mass range of quadrupole mass spectrometer, R575 produces very few chemical fragments, making it a strong candidate for low molecular weight compound analyses. It is anticipated that a better detection limit value for each analyte could be obtained using a TOF mass spectrometer.

Chapter 6: Summary, conclusions and future studies

1. Summary and conclusions

The previous chapters have explored the viability of visible-MALDI using a 532 nm laser source and a triple quadrupole MALDI mass spectrometer.

One class of compounds tried as visible MALDI matrices, the pyrromethene laser dyes, were found to fragment extensively under 532 nm laser irradiation. On the other hand, Rhodamine laser dyes exhibit less fragmentation and could be used to ionize test analytes by protonation. The chloride salts of the Rhodamine laser dyes were found to be more stable under 532 nm laser irradiation than the same compounds with ClO_4^- and BF_4^- anions. This is an interesting phenomenon which merits more consideration because the reason for these differences remains unclear.

Rhodamine (R) 575 proved to be an effective a laser absorber in three kinds of binary matrices: an acidic binary matrix (R575+HCl or R575+CHCA) to ionize basic analytes, a basic binary matrix (R575+NaOH) to ionize acidic analytes, and a cationization binary matrix (R575+NaTFA) to ionize neutral analytes.

The laser fluence study described in Chapter 5 indicates that a MALDI matrix that uses R575 as laser absorber requires a higher fluence before ionization is observed than other more conventional matrices, presumably due to efficient relaxation of of the dye after being pumped to its S_1 excited state. This effect may also explain why R575 exhibits less fragmentation under 532 nm laser irradiation.

2. Future studies

The commercial laser dye R575 contains impurities to the 1% level which may interfere negatively with the R575 desorption and ionization processes. Some effort should be made in the future to purify the R575 to determine if this helps its properties as a matrix or laser absorber under MALDI condition.

Athough R610.Cl and R575 at low concentration (2 mM) are suitable for low molecular analyte analysis, it is not clear whether they can desorb and ionize heavier molecules (m/z > 3000). If not, this should be investigated starting with the influence of the matrix concentration on desorption of large molecules. Experiments are being planned to use a TOF instrument at MDS Analytical Technologies to assess the use of R575 for heavier analytes.

Other organic dyes with chemical structures similar to that of R575 should be tested with 532 nm irradiation to understand why R575+HCl makes such a good binary matrix. It was concluded in chapter 5 that R575 as laser dye undergoes efficient electronic relaxation after being pumped to its S_1 excited state. A fundamental study of R575's photochemistry could confirm this hypothesis. It would be interesting to compare this photochemistry with for example Coumarin laser dyes as MALDI matrices using the 480 nm laser which exhibits a completely different slope in its log-log signal-fluence plot [36].

From a more global perspective much more fundamental work remains to be done to understand the MALDI mechanism both in the visible and in the UV and IR.

References

[1] Tanaka, K. *Angew. Chem. -Int. Edit.* **2003**, *42*, 3860-3870.

[2] Fenn, J. B. *Angew. Chem. -Int. Edit.* **2003**, *42*, 3871-3894.

[3] Karas, M.; Bachmann, D.; Bahr, U. and Hillenkamp, F. *Int. J. Mass Spectrom. Ion Processes* **1987**, *78*, 53-68.

[4] Knochenmuss, R. *Analyst* **2006**, *131*, 966-986.

[5] Gusev, A. I.; Wilkinson, W. R.; Proctor, A.; Hercules, D. M. *Anal. Chem.* **1995**, *67*, 1034-1041.

[6] Canas, B.; Pineiro, C.; Calvo, E.; Lopez-Ferrer, D.; Manuel Gallardo, J. *J. Chromatogr. A* **2007**, *1153*, 235-258.

[7] Sauer, S. *J. Biochem. Biophys. Methods* **2007**, *70*, 311-318.

[8] Karas, M.; Hillenkamp, F. *Anal. Chem.* **1988**, *60*, 2299-2301.

[9] Leisner, A.; Rohlfing, A.; Rohling, U.; Dreisewerd, K.; Hillenkamp, F. *J. Pys. Chem. B* **2005**, *109*, 11661-11666.

[10] Menzel, C.; Dreisewerd, K.; Berkenkamp, S.; Hillenkamp, F. *J. Am. Soc. Mass Spectrom.* **2002**, *13*, 975-984.

[11] Hillenkamp, F.; Karas, M. In *The MALDI Process and Method;* Hillenkamp, F., Peter-Katalinic, J., Eds.; MALDI MS- A practical Guide to Instrumentation, Methods and Applications; 2007; pp 10.

[12] Knochenmuss, R. *J. Mass Spectrom.* **2002**, *37*, 867-877.

[13] Knochenmuss, R. *Anal. Chem.* **2003**, *75*, 2199-2207.

[14] Karas, M.; Gluckmann, M.; Schafer, J. *J. Mass Spectrom.* **2000**, *35*, 1-12.

[15] Knochenmuss, R.; Zenobi, R. *Chem. Rev.* **2003**, *103*, 441-452.

[16] Zhigilei, L. V.; Garrison, B. J. *Appl. Phys. Lett.* **1999**, *74*, 1341-1343

[17] Karbach, V.; Knochenmuss, R. *Rapid Commun. Mass Spectrom.* **1998**, *12*, 968-974.

[18] Hoteling, A. J.; Nichols, W. F.; Giesen, D. J.; Lenhard, J. R.; Knochenmuss, R. *Eur. J. Mass Spectrom.* **2006**, *12*, 345-358.

[19] Setz, P. D.; Knochenmuss, R. *J Phys Chem A* **2005**, *109*, 4030-4037.

[20] Knochenmuss, R.; Vertes, A. *J Phys Chem B* **2000**, *104*, 5406-5410.

[21] Knochenmuss, R.; Dubois, F.; Dale, M. J.; Zenobi, R. *Rapid Commun. Mass Spectrom.* **1996**, *10*, 871-877.

[22] Kruger, R.; Pfenninger, A.; Fournier, I.; Gluckmann, M.; Karas, M. *Anal. Chem.* **2001**, *73*, 5812-5821.

[23] Quist, A. P.; Huthfehre, T.; Sundqvist, B. U. R. *Rapid Commun. Mass Spectrom.* **1994**, *8*, 149-154.

[24] Niu, S. F.; Zhang, W. Z.; Chait, B. T. *J. Am. Soc. Mass Spectrom.* **1998**, *9*, 1-7.

[25] Siegel, M. M.; Tabei, K.; Tsao, R. S.; Pastel, M. J.; Pandey, R. K.; Berkenkamp, S.; Hillenkamp, F.; de Vries, M. S. *J. Mass Spectrom.* **1999**, *34*, 661-669.

[26] Berkenkamp, S.; Kirpekar, F.; Hillenkamp, F. *Science* **1998**, *281*, 260-262.

[27] Towers, M.; Cramer, R. *Spectroscopy* **2007**, *22*, 29-+.

[28] Strupat, K.; Karas, M.; Hillenkamp, F. *Int. J. Mass Spectrom. Ion Process.* **1991**, *111*, 89-102.

[29] Beavis, R. C.; Chait, B. T. *Rapid commun. Mass spectrom.* **1989**, *3*, 432.

[30] Beavis, R. C.; Chaudhary, T.; Chait, B. T. *Org. Mass Spectrom.* **1992**, *27*, 156-168.

[31] Caldwell, K. L.; Murray, K. K. *Appl. Surf. Sci.* **1998**, *127*, 242-247.

[32] Romano, L. J.; and Levis, R. J. *Am. Chem. Soc.* **1991**, *113*, 9665-9667.

[33] Tang, K.; Allman, S. L.; Jones, R. B.; Chen, C. H. *Org. Mass Spectrom.* **1992**, *27*, 1389-1392.

[34] Cornett, D. S.; Duncan, M. A.; Amster, I. J. *Anal. Chem.* **1993**, *65*, 2608-2613.

[35] Smith, C. J.; Chang, S. Y.; Yeung, E. S. *J. Mass Spectrom.* **1995**, *30*, 1765-1767.

[36] Chen, L. C.; Asakawa, D.; Hori, H.; Hiraoka, K. *Rapid commun. Mass spectrom.* **2007**, *21*, 4129-4134.

[37] Chen, L. C.; Mori, K.; Hori, H.; Hiraoka, K. *Int. J. Mass Spectrom.* **2009**, *279*, 41-46.

[38] Hu, X. K.; Lacey, D.; Li, J.; Yang, C.; Loboda, A. V.; Lipson, R. H. *Int. J. Mass Spectrom.* **2008**, *278*, 69-74.

[39] Karas, M.; Hillenkamp, F. *Anal. Chem.* **1988**, *60*, 2299-2301.

[40] Pyrromethene 567. *http://www.exciton.com/pdfs/p567.pdf.*

[41] Pyrromethene 597. *http://www.exciton.com/pdfs/p597.pdf.*

[42] Rhodamine 610. *http://www.exciton.com/pdfs/r610.pdf.*

[43] Rhodamine 590. *http://www.exciton.com/pdfs/r590.pdf.*

[44] Rhodamine 575. *http://www.exciton.com/pdfs/r575.pdf.*

[45] Reference source: SciFinder Scholar, data calculated using Advanced Chemistry Development (ACD/Labs) software V8.14 for Solaris (1994-2007 ACD/Labs)

[46] Guimont, S.; Perrin-Ganier, C.; Real, B.; Schiavon, M. *Agron. Sustain. Dev.* **2005**, *25*, 323-329.

[47] Arbeloa, F. L.; Banuelos, J.; Martinez, V.; Arbeloa, T.; Arbeloa, I. P. *Int. Rev. Phys. Chem.* **2005**, *24*, 339-374.

[48] Jones, G.; Kumar, S.; Klueva, O.; Pacheco, D. *J Phys Chem A* **2003**, *107*, 8429-8434.

[49] Michael J. MacCoss , 0.3.

[50] Isotope Distribution Calculator and Mass Spec Plotter. http://www2.sisweb.com/mstools/isotope.htm.

[51] Mackey, M. S.; Sisk, W. N. *Dyes and Pigments* **2001**, *51*, 79-85.

[52] Yariv, E.; Reisfeld, R. *Opt. Mater.* **1999**, *13*, 49-54.

[53] Drexhage, K. H. In *Structure and properties of Laser Dyes;* Schäfer, F. P., Ed.; Dye Laser; Springer-Verlag: Berlin ; New York, 1990; pp 144.

[54] Maeda, M. In *Laser dyes :properties of organic compounds for dye lasers;* Academic Press: New York ; Toronto, 1984; pp 335.

[55] Chemical structure of Rhodamine B base. *http://www.sigmaaldrich.com/catalog/ProductDetail.do?N4=234141|ALDRICH&N5=SEARCH_CONCAT_PNO|BRAND*

[56] Namazian, M.; Zakery, M.; Noorbala, M. R.; Coote, M. L. *Chem. Phys. Lett.* **2008**, *451*, 163-168.

[57] Schaiberger, A. M.; Moss, J. A. *J. Am. Soc. Mass Spectrom.* **2008**, *19*, 614-619.

[58] Sodium bentazon. *http://www.alanwood.net/pesticides/derivatives/bentazone-sodium.html.*

[59] North, S.; Okafo, G.; Birrell, H.; Haskins, N.; Camilleri, P. *Rapid commun. Mass spectrom.* **1997**, *11*, 1635-1642.

[60] Chinthaka, S. D. M.; Chu, Y.; Rannulu, N.S. and Rodgers, M.T. *J. Pys. Chem. A* **2006**, *110*, 1426-1437.

[61] Dreisewerd, K.; Schurenberg, M.; Karas, M.; Hillenkamp, F. *Int. J. Mass Spectom. Ion Process.* **1995**, *141*, 127-148.

[62] Westmacott, G.; Ens, W.; Hillenkamp, F.; Dreisewerd, K.; Schurenberg, M. *Int. J. Mass Spectrom.* **2002**, *221*, 67-81.

[63] Zenobi, R.; Knochenmuss, R. *Mass Spectrom. Rev.* **1998**, *17*, 337-366.